Rational Design and Synthesis of Squaraine Dye-Based Near-Infrared Fluorescent Probes for Biosensing

DISSERTATION

FOR THE DEGREE OF

DOCTOR OF PHILOSOPHY

SHEKHAR GUPTA

Ph.D. SUPERVISOR

Professor. Tamaki Kato

Department of Biological Functions Engineering

Kyushu Institute of Technology

Graduate School of Life Science and Systems Engineering

Dedicated to

My Parents and Teachers

ACKNOWLEDGEMENTS

First and foremost, I am grateful to my supervisor, **Prof. Tamaki Kato**, for believing in me and accepting me into his distinguished doctorate program. He has always been interested in all aspects of my studies. His unwavering effort in developing me, even in the smallest of my tasks, is something for which I am eternally grateful.

I would like to extend my heartfelt appreciation to **Prof. Shyam S. Pandey** for his pivotal assistance in securing my recommendation and acceptance to work under **Prof. Tamaki Kato**. His extensive expertise and experience have furnished me with invaluable foundation and support to conduct research; without his assistance, this undertaking would have been unattainable.

I would like to extend my sincere gratitude to **Prof. Shigeori Takenaka** and **Prof. Toshinari Maeda** for their evaluation and valuable feedback on my PhD research. Your insights have significantly contributed to enhancing the quality and depth of my work.

I take this opportunity to thank **Prof. Shuichi Nagamatsu** and **Prof. Hikima Tomohiro** of Kyushu Institute of Technology (Iizuka campus) for their assistance in the fluorescence microscopic measurements.

I would like to extend my sincere gratitude to the **Kyushu Institute of Technology** for facilitating my research endeavors and assisting me in fulfilling the requisite requirements for my graduation. The financial assistance granted by the **Japan Educational Exchanges and Services (JEES)** for my sojourn in Japan is for which I am extremely grateful.

I express my profound gratitude to **Dr. Maryala Sai Kiran** for his assistance in facilitating my enrollment at Kyushu Institute of Technology and for his consistent support and motivation.

I would like to extend my sincere appreciation to the **current and former members** of the laboratory for their gracious cooperation and for upholding the laboratory's decorum, which is indispensable for the successful completion of our work.

I am very grateful to my father **Mr. Makurdhan Gupta**, mother **Mrs. Tara Gupta**, uncle **Mr. Hiralal Gupta**, Aunt **Mrs. Lalita Gupta** and sisters **Neha Gupta**, **Khushi Gupta,** and **Arushi**

Gupta and the entire family for their unwavering love and moral support. I am also thankful to **Nilima Mam** for her motherly love and guidance.

Finally, I owe my academic success to my beloved **Bhagawan Sri Satya Sai Baba**, who has always blessed me as a friend, philosopher, and guide.

ABSTRACT

Biosensors, which convert biological responses into electrical signals, play a vital role in addressing this demand. They offer high specificity and independence from physical parameters such as pH and temperature, while also being environmentally friendly. The development of biosensors, including enzyme sensors, immune sensors, microbial sensors, and ion channel sensors, is a rapidly growing sector that is being actively promoted worldwide. The advantages of fluorescence-based detection technologies include their high sensitivity, selectivity, and ease of use. In addition, a range of fluorescent materials and sensing mechanisms can be employed in the systematic development of these techniques, thereby showcasing the adaptability of these approaches in detecting diverse targets with exceptional sensitivity and selectivity. Fluorescent biosensors are crucial for drug and cancer research.

Photoinduced electron transfer (PET) and Förster Resonance Energy Transfer (FRET) processes play crucial roles in the detection of target biomolecules, such as bio-analytes and ions. These processes are utilized in various sensing platforms to achieve high sensitivity and selectivity in target detection. By considering the interplay between aggregation-caused quenching (ACQ), PET, and FRET processes, sensor design can be optimized to achieve robust and reliable detection of target biomolecules and ions. Integrating these mechanisms in sensor development allows for the creation of highly sensitive and selective platforms that are capable of overcoming challenges associated with fluorescence quenching and aggregation, ultimately advancing the field of bioanalytical and ion sensing.

Using NIR fluorescent and quenchers in FRET biosensors enhances sensitivity for in vitro and in vivo imaging. Alignment of dye absorption and fluorescence emission wavelengths is key for optimal sensitivity. Adjustments to the enzyme active site peptide sequence ensure the quenching and fluorescent groups are within the Förster radius. Protein and peptide-based biosensors can be easily produced using synthetic chemistry techniques followed by enzymatic labeling with synthetic fluorophores. The assembly of near-infrared FRET biosensors requires the development of NIR dyes, namely fluorescent and quenching groups, as well as the design of an enzyme recognition site in proteases. The present thesis presents an insight into the design and synthesis of far-red sensitive squaraine dyes with different wavelengths. In this study, we developed novel

squaraine-based far-red sensitive fluorescent peptide probes for chymotrypsin assays exploiting the intramolecular interaction between identical fluorophores as the homo-FRET mechanism.

Table of Contents

CHAPTER 1 : INTRODUCTION

1. Bio-Detection

The terms "bio-detection" and "bio-sensing" broadly describe methods for identifying biological materials either in vivo or in vitro. To put it simply, a bio-detection device, as defined by the IUPAC, uses specialized biochemical interactions mediated by proteins produced by immune systems, isolated enzymes, cells, or tissues to detect biological analytes, typically through the use of electrochemical, thermal, and optical signals.

The two main parts of a bio-detection device are typically a transducer and a bio-recognition unit. The bio-recognition unit aids in the biosensor's unique specificity of binding to a target analyte, while the transducer converts the bioreceptor-analyte interactions into electrochemical, thermal, magnetic, or optical signals. The analytes can be any of a wide variety of biological entities, such as the genetic components of viruses or bacteria, antibodies made by the immune systems of infected living organisms, peptides, or other biological elements. Analytes can also be simple molecules like sugars [1] (such as glucose, fructose, etc.), pollutants [2] (such as heavy ions like lead [3], mercury [4], and arsenic [5]) in water, or toxic substances found in food [6] and crops [7].

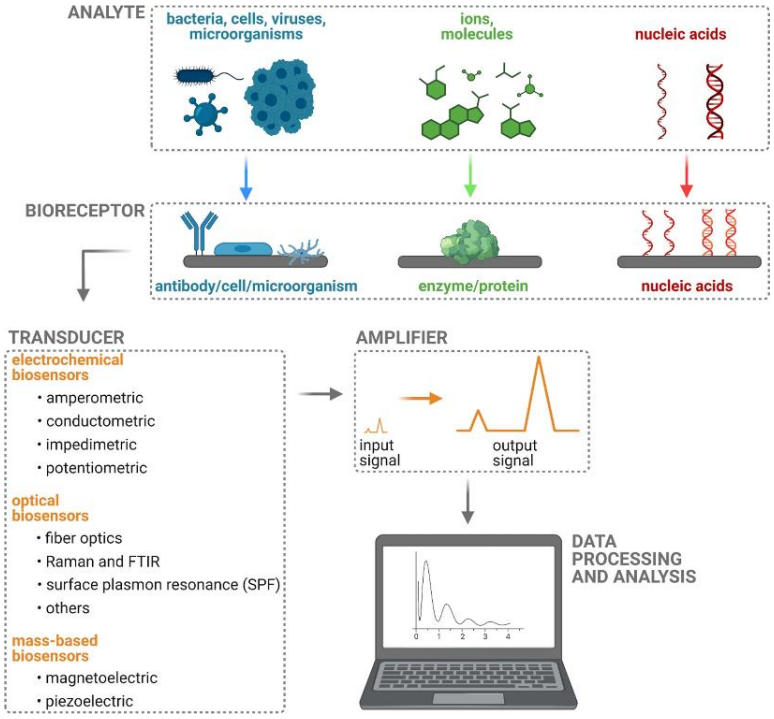

Figure 1. *The diagram illustrates the various phases of a typical biosensing process and the distinct components of a biosensor platform.*

The enzyme-linked immunosorbent assay (ELISA) [8] is a commonly used biochemical detection technique in clinical and industrial settings. It utilizes specific enzymatic reactions to produce a physical change, such as a colorimetric change, in the traditional assay format when the target analyte is present in the sample. However, in recent times, many unique characteristics of materials, including fluorescence [9,10], surface plasmon resonances (SPR) [11–13], and dielectric cavity resonances[14–16], are being utilized to convert and enhance detection signals. Label-free detection techniques increasingly attract attention due to their simplicity, user-friendliness, and frequently enhanced sensitivity.

1.1 Immunology-Based Biosensors

Immunological detection methods for protease employ the antigen-antibody reaction to accurately measure the amount of a specific protease in complex samples obtained from living organisms. These methods are effective because the antigen-antibody reaction is both specific and sensitive. The Western blot and enzyme-linked immunosorbent assay (ELISA) techniques are commonly employed to assess proteins, including proteases[17].

Western blotting, a technique developed by Burnette in 1981, combines the sodium dodecyl sulfate-polyacrylamide gel electrophoresis (SDS-PAGE) method with antigen-antibody interaction[18]. Sixteen Once electrophoresis is finished, a duplicate of the separated proteins can be transferred onto an absorbent material like polyvinylidene fluoride (PVDF) or nitrocellulose (**Figure 2**) [19]. Afterward, the primary antibody attaches to a particular band on the blot, and the secondary antibody, which is linked to an enzyme like alkaline phosphatase or horse radish peroxidase, attaches to the main antibody. Ultimately, the color of a particular band is created and assessed to identify the target protease.

ELISA, which was reported by Engvall and Perlmann in 1971, is a technique in which the specificity of antibodies is combined with the sensitivity of simple enzyme assays by using antibodies or antigens coupled to an enzyme that can be readily assayed[20]. Although many variants of ELISA test procedures have been developed to date, sandwich-ELISA is the most common kind. In sandwich-ELISA, the amount of target protease (antigen) between two layers of antibodies which consist of immobilized or labeled antibodies respectively is measured (**Figure 3**) [8,21].

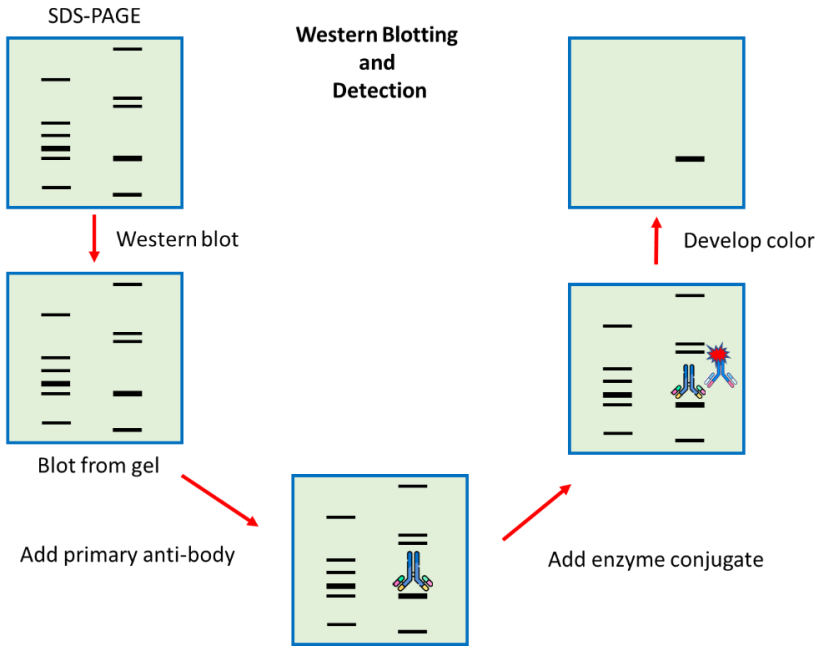

Figure 2. *Illustration depicting the process of western blotting and the subsequent detection technique.*

An antigen-specific antibody is immobilized on the well of the microplate. Antigen binds to immobilized antibody when adding antigen. Next, an enzyme-labeled antibody is added, and bound to the antigen-conjugated immobilized antibody. Finally, the chromogenic or fluorogenic substrates for the detection of labeled enzymes are added, and the colored product is measured to detect the target protease.

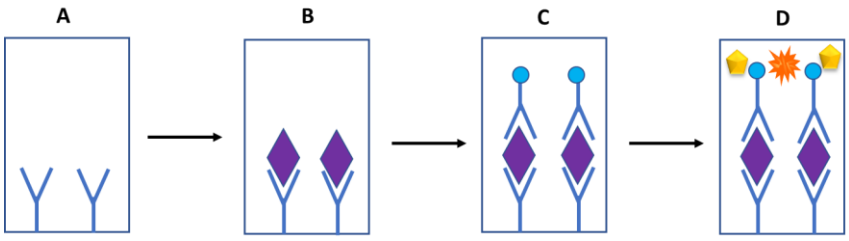

Figure 3. *Illustration depicting the step-by-step procedure of sandwich-ELISA.*

Immunological approaches are not suitable for detecting protease activity as they are designed to measure the quantity of protease rather than its activity [22]. Measuring protease activity is important because ailments states are directly linked to the level of protease activity, rather than the amount of protease present.

1.2 Chromogenic-Based Biosensors

Chromogenic substrates used for protease assay consist of a substrate peptide and a dye. The absorbance of these substrates at a certain wavelength is altered before and after an enzymatic breakdown. Peptide-p-nitroanilide (pNA) is a frequently employed chromogenic substrate in the measurement of protease activity [23]. When the peptide-pNA, which lacks color, is broken by a protease, it releases p-nitroaniline, which is yellow in color. Therefore, the detection of protease activity can be achieved by quantifying the absorbance of unbound p-nitroaniline at a wavelength of 405 nm.

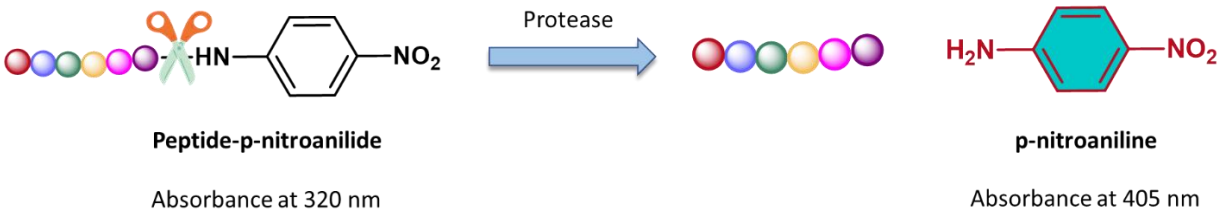

Figure 4. *Schematic representation of the detection of protease activity using peptide-pNA.*

Specific peptide-pNA can effectively detect several protease activities, including trypsin, subtilisin, and chymotrypsin [24–26]. Nevertheless, when it comes to protease assay, the fluorometric method is more desirable than the colorimetric method due to its higher sensitivity. The use of fluorescent probes and dyes allows for precise and highly sensitive detection of protease activities, enabling the quantification of enzymatic reactions with exceptional accuracy. This higher sensitivity is crucial for capturing subtle changes in protease activity, which may have significant implications for understanding cellular processes and disease mechanisms.

1.3 Fluorescence-Based Biosensors

Optical biosensors, including fluorescent biosensors, have become indispensable tools in medical diagnostics and biotechnology. These sensors utilize light to detect and quantify specific analytes,

offering high sensitivity and real-time monitoring capabilities. Fluorescent biosensors, in particular, rely on the emission of fluorescent signals in response to target molecules, providing a highly sensitive and specific method for detecting biomarkers. The integration of optical biosensors, especially fluorescent biosensors, into point-of-care testing devices has revolutionized rapid diagnostic testing by enabling quick and accurate detection of various analytes. With their ability to detect multiple targets simultaneously and their potential for miniaturization and portability, optical biosensors, including fluorescent biosensors, hold great promise for advancing personalized medicine and improving healthcare outcomes [27].

Among the various mechanisms utilized in fluorescent biosensors, two commonly used strategies are Photoinduced Electron Transfer (PET) and Fluorescence Resonance Energy Transfer (FRET). These mechanisms involve distinct molecular interactions that modulate the fluorescence signal, making them versatile tools for biosensing applications. PET and FRET are considered two of the best mechanisms for developing fluorescent biosensors due to their sensitivity, selectivity, and versatility in detecting a wide range of analytes and molecular interactions. These mechanisms offer unique advantages that can be tailored to specific biosensing applications, making them valuable tools in biomedical research, diagnostics, and other fields.

1.3.1 Photoinduced Electron Transfer

Photoinduced Electron Transfer (PET) is a widely used mechanism in fluorescent biosensors due to its ability to quench fluorescence through electron transfer processes. In PET-based biosensors, the fluorophore undergoes a change in its electronic state upon interaction with an electron acceptor molecule, leading to fluorescence quenching. This quenching phenomenon can be harnessed for the sensitive detection of various analytes in biological samples.

For a fluorophore, fluorescence occurs when an electron that has been stimulated in the lowest unoccupied molecular orbital (LUMO) returns to the highest occupied molecular orbital (HOMO) by radiative decay (**Figure 5a**). When a receptor is conjugated to a spacer and its HOMO energy level is positioned between the HOMO and LUMO energy levels of the fluorophore, PET (photoinduced electron transfer) can occur upon excitation. This involves the transfer of an electron from the HOMO of the receptor to the HOMO of the fluorophore, leading to the quenching of fluorescence (**Figure 5b**). When a target is present, the receptor binds to it, causing the receptor's

highest occupied molecular orbital (HOMO) energy level to decrease below that of the fluorophore. As a result, the process of PET is suppressed and the fluorescence is restored (**Figure 5c**). To generate a less efficient PET quenching process, one can increase the distance between the fluorophore and the receptor. The efficiency of PET is dependent on the distance between the HOMO energy levels of the fluorophore and receptor, following a proportional relationship of $e^{-\beta d}$ (where d represents the distance). This results in a more effective radiative decay process, leading to enhanced fluorescence intensity (**Figure 5d**)[28].

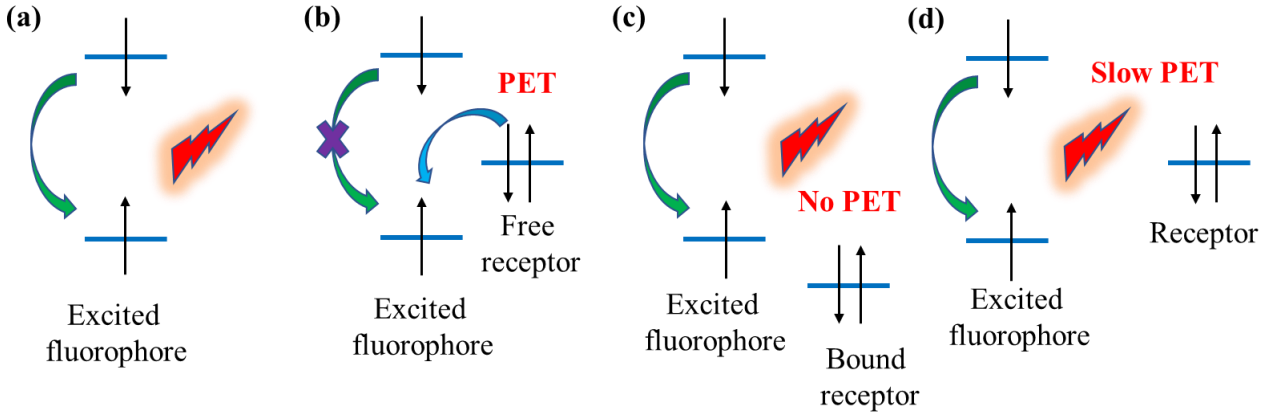

Figure 5. *Mechanism of PET.*

PET-based probes have successfully identified a range of targets, including ions, small molecules, DNA, and proteins[29,30]. The probes for small active compounds, such as thiols, and enzymes are often intended to exploit their respective reactive or catalytic activity. An alternative design technique is employed for targets that do not demonstrate such activity, which relies on the conformational change of the probe upon binding to the target. Qu, Kim, Bhuniya, and associates have created a probe, a two-photon a-PeT-based instrument, to identify tyrosinase (TYR) activity (**Figure 6.**). The probe employs BODIPY as the fluorophore and electron acceptor, while catechol serves as the recognition group and electron donor[31]. When TYR is not present, the a-PeT reaction that occurs between catechol and BODIPY causes the fluorescence to be suppressed. Nevertheless, when TYR is present, the hydroxyl (-OH) groups of the catechol undergo oxidation to form o-quinone, which hinders the a-PeT process. As a result, there is a significant 12.5-fold increase in fluorescence at a wavelength of 450 nm. In addition, the probe has excellent stability

across a variety of pH levels found in the body and may be used to detect the natural activity of TYR utilizing single or two-photon cell imaging.

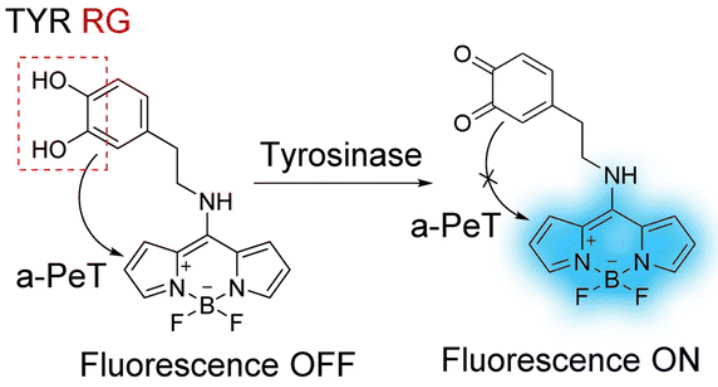

Figure 6. *The response mechanism of the probe for TYR is due to a-PET mechanism [31].*

Zhang and his colleagues have created six fluorescent probes using o-phenylenediamine (OPD) with various leaving groups[32]. Their goal is to selectively detect glutathione (GSH). In this case, the p-aminobenzene acted as the electron donor, while the OPD served as the electron acceptor. Without any glutathione (GSH) present, the p-aminophenyl group suppresses the fluorescence of OPD by an alpha-polarization electron transfer (a-PeT) mechanism (**Figure 7.**). Nevertheless, when GSH is present, the probe experiences a distinct recognition reaction with GSH, preventing the a-PeT process and causing the fluorescence to activate. The probe demonstrated remarkable capability by selectively detecting GSH at a detection limit of 23 nM, even in the presence of several amino acids.

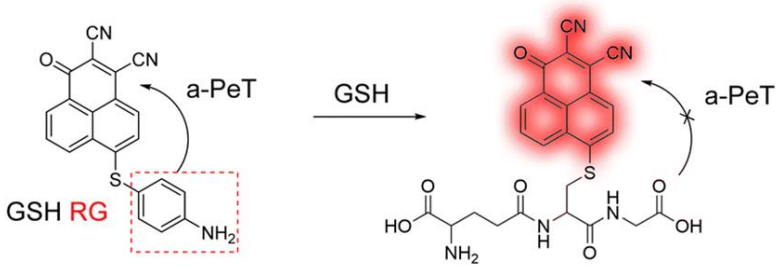

Figure 7. *Schematic illustration of probe fluorescence activation mechanism in the presence of GSH [32].*

Fan et al. have presented a theranostic prodrug that is activated by aminopeptidase N (APN) for use in fluorescence-based cancer detection and tumor therapy[33]. Hexamethylenediamine

connects the two groups in the probe, which uses an electron-donating melphalan analog as the recognition group for APN and an electron-accepting NB as the fluorophore (**Figure 8**). The weak fluorescence of the probe at 680 nm is first caused by an a-PeT interaction between the melphalan and NB fluorophore. Upon activation by APN, the amide bond undergoes hydrolysis, hence inhibiting the a-PeT process and allowing for an increase in fluorescence at 680 nm. Simultaneously, the non-toxic prodrug undergoes conversion into the extremely toxic-free melphalan, which can induce cell death. The fluorescence intensity of the probe shows a strong linear connection with the concentration of APN within the range of 0–7 ng mL^{-1}. The detection limit, computed to be 0.75 ng mL^{-1}, is the lowest concentration of APN that can be reliably detected.

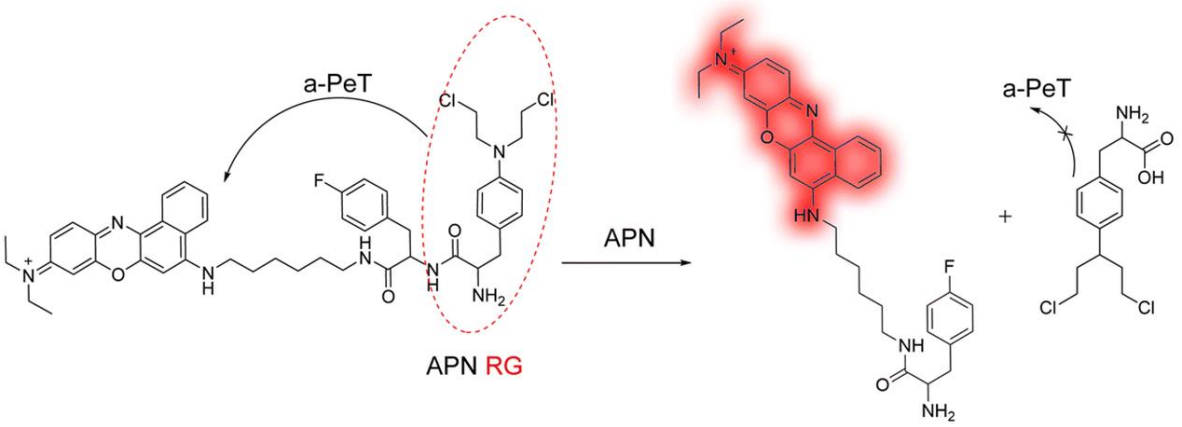

Figure 8. *Schematic illustration of the response mechanism of the probe for APN. The probe is activated by APN, resulting in enhanced fluorescence [33].*

More specifically, computational tools will enhance our understanding of the comparative electron density and energy disparities among various fluorophores and recognition groups. This will enable the creation of PeT-based systems with enhanced performance that will apply to a broader array of uses. We anticipate that in the future, it will be possible to precisely control the PeT process, which will allow for the development of fluorescent prodrugs based on PeT that has a better therapeutic impact and fewer side effects for cancer patients. This thesis work focuses on synthesizing and characterizing novel squaraine dyes tailored for PET processes to enhance fluorescence intensity. These fluorophores are then incorporated into the design of the squaraine dye-based biosensor to demonstrate their application in fluorescence biosensing, particularly in interactions with bovine serum albumin (BSA). The study aims to elucidate the PET mechanisms

involved in enhancing fluorescence and its potential for sensitive and selective detection in biological samples.

1.3.2. Förster Resonance Energy Transfer

Biosensors based on Förster resonance energy transfer (FRET) are being developed to specifically detect biomolecules or alterations in the microenvironment. The transfer of energy from an excited donor fluorophore molecule to a neighboring acceptor fluorophore molecule via FRET is a non-radiative process. FRET biosensors are characterized by their exceptional sensitivity and adaptability. They can detect a diverse array of biomolecules and environmental alterations, making them suitable for various applications. These include the detection of protein-protein interactions, monitoring pH fluctuations, and measuring enzyme activity, among others [34–36]. FRET is an essential technique in biosensors as it enables the precise and sensitive detection of biomolecules without requiring direct labeling or alteration of the biomolecule. This enables the identification of subtle alterations in the surroundings, such as the existence of a certain biomolecule, without requiring the direct labeling or alteration of said biomolecule. FRET biosensors exhibit a high degree of specificity, enabling them to selectively identify a particular biomolecule or environmental alteration while remaining unaffected by the presence of other molecules or changes. To accomplish this selectivity, the biosensor is designed with a strong affinity for the target biomolecule, and the donor and acceptor molecules are engineered to be in close proximity to each other. The sensitivity of FRET biosensors is remarkably high, typically in the picomolar range. This enables them to detect extremely small quantities of biomolecules, a crucial capability for early disease detection and identifying trace amounts of environmental toxins.

FRET operates on the fundamental concept of energy transfer from a donor molecule to an acceptor molecule through dipole-dipole interaction and non-radiative energy transfer via time-space. The transfer of energy takes place primarily when the molecules acting as donors and acceptors are in close proximity, usually within a range of 1-10 nm, and when their electronic energy levels are closely aligned. The donor fluorophore molecule is initially activated by absorbing a photon of light with a sufficient frequency ($E = h\upsilon$) at a certain wavelength. When in an excited state, the molecule can transmit a portion of its energy to the acceptor molecule, provided that they are near each other. This energy transfer results in a reduction in the fluorescence emission from the donor molecule and an increase in the fluorescence emission from

the acceptor molecule. The efficiency of energy transfer relies on the interplay between the distance separating the donor and acceptor molecules, their spectrum overlaps, and the relative orientation of the molecules. **Figure 9.** depicts a Jablonski diagram illustrating the process of Förster resonance energy transfer (FRET) in a donor-acceptor pair. The visual depiction illustrates the transfer of energy and fluorescence processes in FRET. The diagram depicts the energy levels and interchanges between them for a molecule that donates and receives energy. Upon absorption of light, the donor molecule undergoes excitation to the first excited singlet state (S_1). From this point, it has two possible pathways to follow. It can either transition back to the ground state (S_0) by emitting light spontaneously, resulting in fluorescence, or it can transfer its energy to the acceptor molecule by FRET. Förster resonance energy transfer (FRET) involves the transfer of energy from the donor molecule in its excited state (S_1) to the acceptor molecule in its ground state (S_0), which is then stimulated to its first excited singlet state (S_1). Following the transfer, the donor molecule reverts to its ground state (S_0) without producing any fluorescence. The acceptor molecule undergoes fluorescence to transition back to the ground state (S_0). The Jablonski diagram below elucidates the FRET efficiency, which primarily relies on the spectral overlap between the donor and acceptor fluorophores, the distance between them, and the orientation of the fluorophore molecules[37–40].

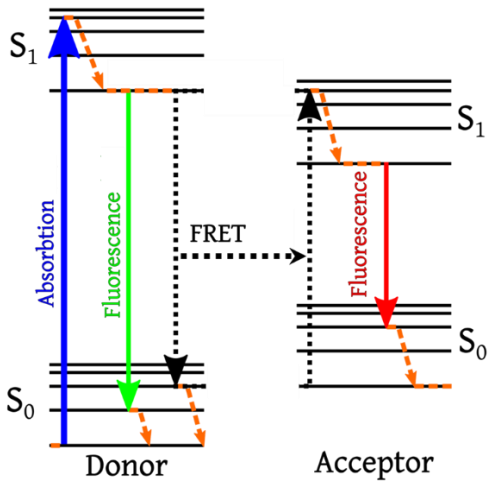

Figure 9. *The Jablonski diagram illustrates the energy transfer process between a donor and acceptor pair in Förster resonance energy transfer (FRET).*

Spectral overlap in FRET refers to the degree of overlap between the emission spectrum of a donor molecule and the absorption spectrum of an acceptor molecule. Increased spectral overlapping

results in a higher transfer of energy from the donor to the acceptor. The spectral overlap is determined by the wavelengths of light emitted by the donor and absorbed by the acceptor, as well as the distance between the molecules. Efficient Förster resonance energy transfer (FRET) necessitates a significant level of spectral overlap, which can be accomplished by carefully choosing donor and acceptor molecules that possess complementary emission and absorption spectra. **Figure 10.** displays the spectrum of the emission of the donor fluorophore overlapping with the absorption of the acceptor fluorophore. The overlap integral J(λ) for energy transfer is represented by equation (1).

$$J(\lambda) = \frac{\int_0^\infty F_D(\lambda)\, \varepsilon\, \lambda^4\, d\lambda}{\int_0^\infty F_D(\lambda)\, d\lambda} \qquad (1)$$

The symbol J(λ) represents the spectral overlap integral between the emission spectrum of the donor and the absorption spectrum of the acceptor, measured in units of M^{-1} cm^{-1} nm^4. The symbol ε represents the extinction coefficient of the acceptor, measured in units of M^{-1} cm^{-1}. F_D represents the fluorescence intensity of the donor within the wavelength range from λ to λ + dλ [41].

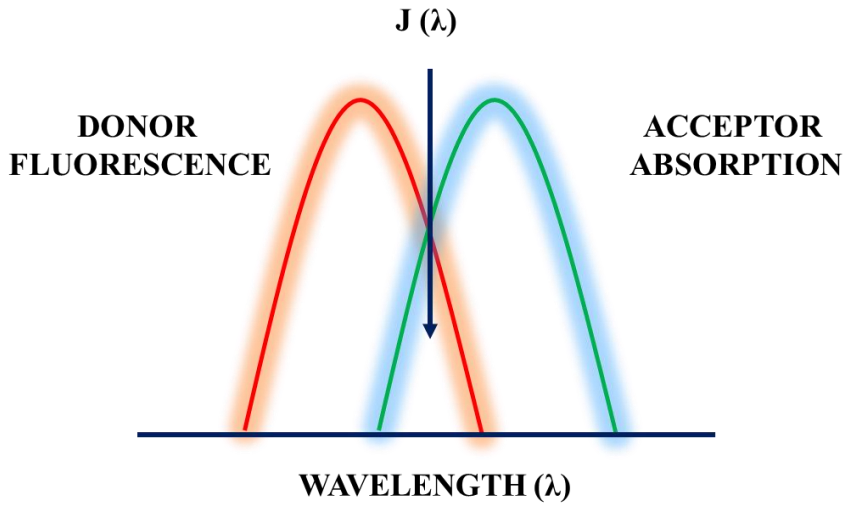

Figure 10. *Overlap integral between the fluorescence of the donor and the absorption of the acceptor.*

The Förster radius (R_0) is a critical parameter in FRET, denoting the maximum separation between a donor and acceptor molecule for efficient energy transfer. It signifies the distance at which the transfer efficiency is half its maximum value, relying on spectral overlap between donor emission

and acceptor absorption spectra, along with their transition dipole moments. The following relation can be used to estimate the value of the R_0 from the overlap integral value.

$$R_0 = 0.211[\kappa^2 \eta^{-4} \varphi_D J(\lambda)]^{1/6} \quad (2)$$

Where φ_D is the donor's quantum efficiency, η is the medium's refractive index, and κ^2 (= 2/3) is the orientational factor.

Goswami et al. successfully developed a probe, that consists of a donor based on quinoline–benzothiazole and an acceptor based on rhodamine[41]. They then demonstrated how this probe can be used for sensing Cd^{2+} ions, as depicted in **Figure 11.** When excited at 360 nm, compound 2 exhibited a robust emission at 470 nm, which was attributed to the emission of the quinoline–benzothiazole fluorophore. Nevertheless, there was no emission peak observed at approximately 585 nm, indicating that the rhodamine component was primarily in its spirolactam form, as proposed by the authors. With the introduction of Cd^{2+} a distinct absorption peak emerged at 565 nm. It was interpreted as a sign that the spirolactam of the rhodamine part underwent ring opening, enabling FRET from the quinoline–benzothiazole to the rhodamine part, resulting in a shift in emission to 585 nm. There was a clear correlation between the emission intensity ratio (I_{585}/I_{470}) and the concentration of Cd^{2+} (ranging from 0 to 9.5 μM).

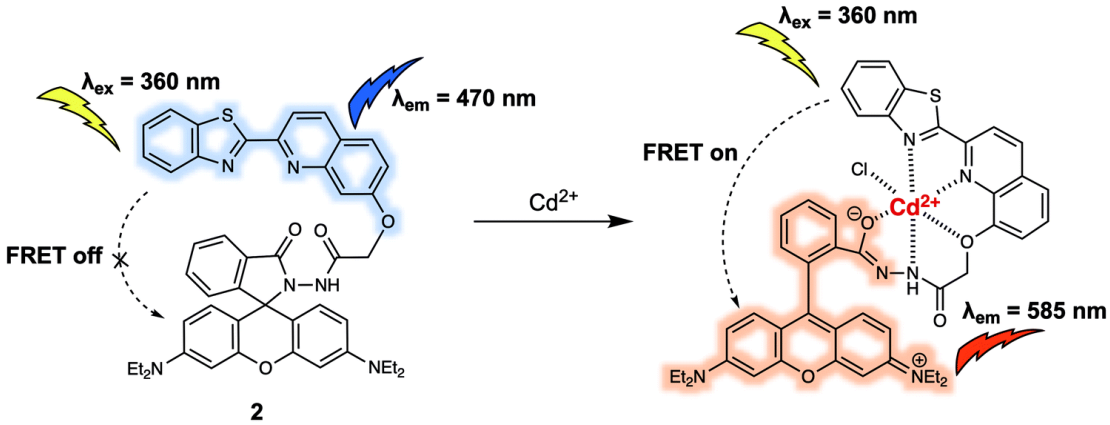

Figure 11. *A FRET probe was used for the ratiometric detection of Cd^{2+}. It is based on the combination of quinoline-benzothiazole and rhodamine as energy donor and acceptor [41].*

One advantage of FRET-based small-molecule probes is that they can be designed and prepared more easily compared to their green fluorescent protein (GFP) counterparts. This is especially

beneficial for creating systems that can function as fluorescent substrates for enzymes. Schultz et al. developed a FRET-based probe that is targeted to the cell membrane to track the activity of matrix metalloproteinase 12 (MMP-12) [42]. The probe (**Figure 12**) was developed by attaching a coumarin343/TAMRA FRET pair to a short peptide that is sensitive to MMP-12. This probe demonstrated a strong preference for MMP-12 compared to other matrix metalloproteases. When excited at 450 nm, the emission of 27 is observed at 575 nm, which corresponds to the acceptor (TAMRA) due to FRET. The probe exhibits an emission at a wavelength of 575 nm when it is excited at 450 nm. This emission is attributed to the acceptor molecule (TAMRA) due to FRET. Upon exposure to MMP-12 in a laboratory setting, a novel emission at a wavelength of 490 nm was detected, and there was a 4.5-fold enhancement in the ratio of the intensity at 490 nm to that at 575 nm. The activity of MMP-12 in RAW264.7 macrophages can be observed via real-time ratiometric imaging.

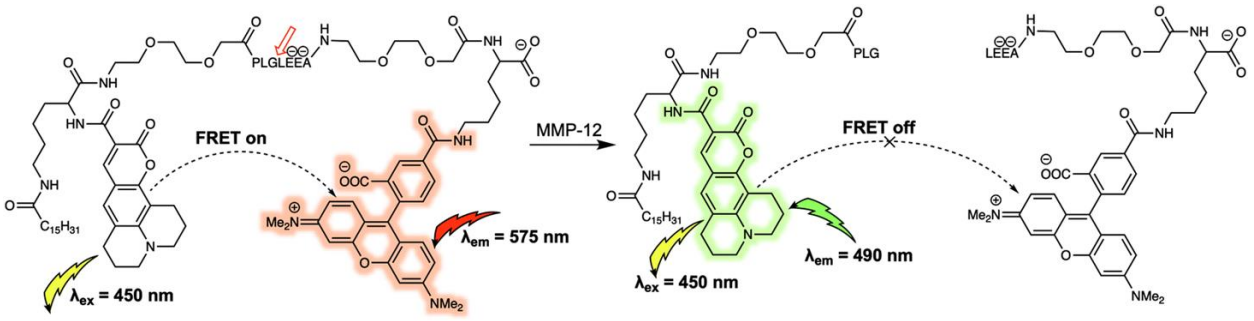

Figure 12. *The structure of the probe utilized in the detection of MMP-12. The cleavage occurs between glycine and leucine [42].*

Typically, the performance of FRET-based biosensors that utilize visible fluorescent molecules is affected by the auto-fluorescence found in clinical samples such as blood, serum, or other body fluids. This results in a low signal-to-noise (SN) ratio and makes it difficult to achieve high sensitivity. Using a FRET biosensor that utilizes near-infrared (NIR) fluorescent and quencher molecules, it is possible to detect the resulting fluorescence signals from the body at a distance of several 10 cm from a detector outside the body, with a high signal-to-noise ratio (high sensitivity). This indicates that it is highly suitable for in vivo pathological imaging. For optimal sensitivity of the biosensor using NIR-FRET, the wavelengths of the dye absorption and fluorescence emission

must align perfectly. To ensure the optimal functioning of the enzyme, it is important to carefully modify the peptide sequence of the active site. This will ensure that the quenching group and the fluorescent group are positioned within the appropriate range, known as the Forster radius. Using a biosensor that utilizes a near-infrared (NIR) probe offers several benefits. One of the main advantages is its high sensitivity, which is not easily affected by the auto-fluorescence of water or biomolecules. Additionally, NIR rays have excellent tissue penetrability, making them ideal for this application. By manipulating the peptide sequence, one can precisely regulate the absorption wavelength for the enzyme by altering the fluorescent and quenching groups in different wavelength ranges. In the development of a NIR-FRET biosensor, it is necessary to develop NIR dyes (fluorescent group and quenching group) and design an enzyme recognition site. This thesis provides valuable insights into the synthesis and characterization of NIR dyes with different wavelengths. Furthermore, efforts have been made to evaluate the unique amino acid sequences associated with specific enzymes and incorporate them into a prototype near-infrared (NIR) probe to demonstrate their effectiveness in fluorescence biosensing. In my thesis, I have synthesized a squaraine-based probe for detecting chymotrypsin using a homo-FRET mechanism. This innovative approach allows for the precise detection and monitoring of chymotrypsin activity, showcasing the potential of utilizing enzyme-specific amino acid sequences in developing advanced biosensing technologies. By integrating these sequences into NIR probes, we can enhance the sensitivity and specificity of enzyme detection, opening up new possibilities for applications in various fields such as biomedical research and diagnostics.

1.4 Fluorophores Used for Biosensors

To ensure the specificity of fluorescent probes for molecular targets in complex environments, a systematic and scientifically guided approach is essential. The initial step in this process involves selecting an appropriate reporter or fluorophore, which plays a critical role in the overall biosensing system. Fluorophores are categorized based on their sensing properties and emission wavelengths, with various classes available for designing biosensors. Several fluorophores **(Figure 13.)** can serve as the foundation for the biosensor design technique. The majority of these dyes have emissions in the visible range of the spectrum.

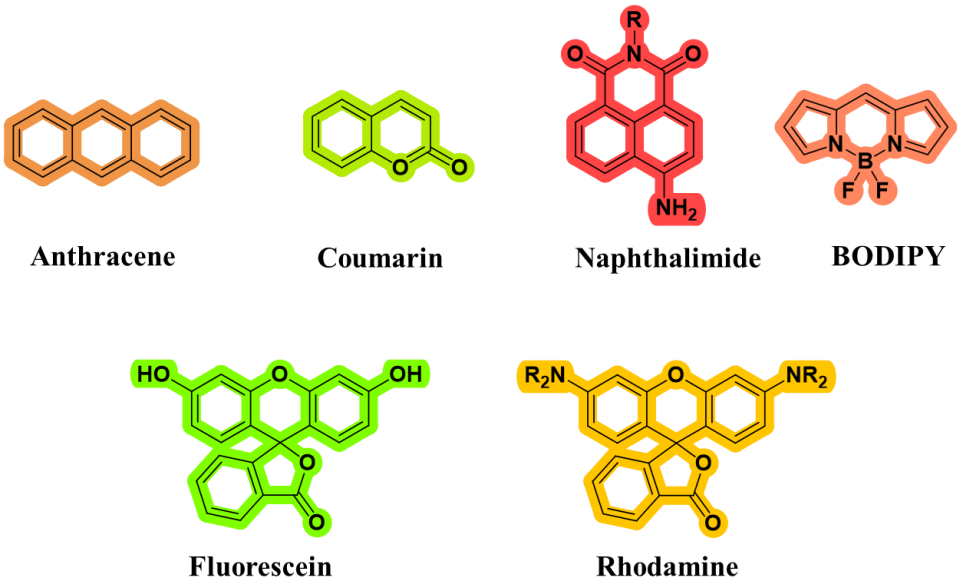

Figure 13. *Structures of various fluorophores.*

Near-infrared (NIR) dyes are often preferred over visible dyes in biosensing applications due to several key advantages that they offer. While there are numerous visible dyes available for molecular detection, but there are many limitations upon usage of visible dyes in bioimaging and biosensing applications. NIR dyes provide unique benefits that make them particularly well-suited for certain types of biosensing systems. One of the main reasons why NIR dyes are favored over visible dyes is their ability to penetrate deeper into biological tissues. The longer wavelengths of NIR light can pass through tissues more effectively than visible light, allowing for non-invasive imaging and detection of molecular targets within living organisms. This deeper tissue penetration is crucial for applications such as in vivo imaging, where visible dyes may be limited by their inability to reach target molecules located deep within the body[43] (**Figure 14**). Additionally, NIR dyes exhibit reduced background autofluorescence compared to visible dyes, leading to improved signal-to-noise ratios in biosensing applications. This lower background interference enhances the sensitivity and specificity of molecular detection, enabling researchers to accurately identify and quantify target molecules in complex biological environments. Furthermore, NIR dyes offer enhanced photostability and resistance to photobleaching, making them more durable and reliable for long-term imaging and sensing applications[44]. This increased stability ensures consistent performance over extended periods, which is essential for maintaining the accuracy and reliability of biosensing systems.

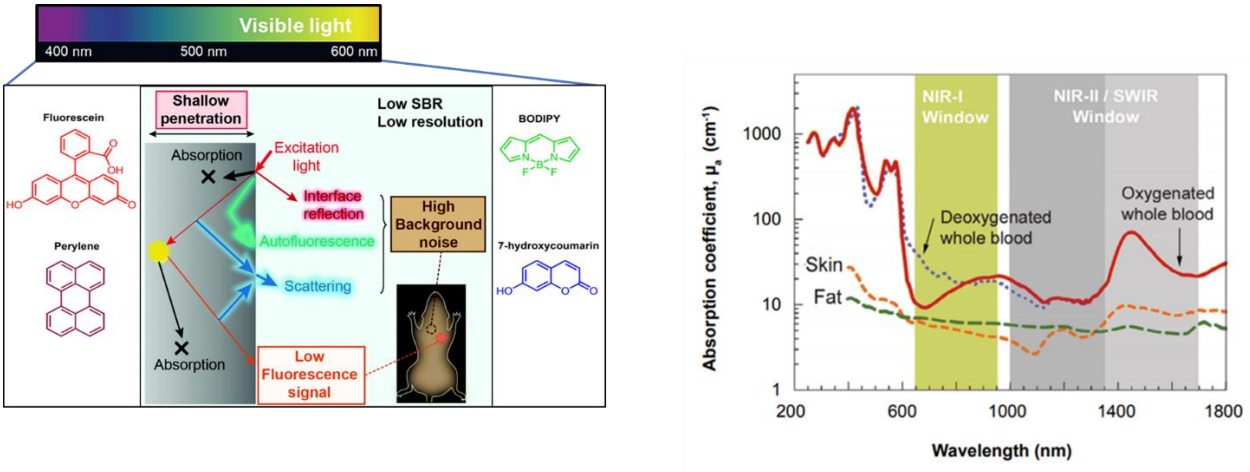

Figure 14. *Issues with visible fluorophores(left). The NIR-I and NIR-II spectral regions exhibit high optical transparency in biological tissues and fluids (right).*

1.4.1 Squaraine Dyes

The squaraine dye is named after its core component, known as "squaric acid," which was initially introduced by Schmidt in 1980. The primary structure of squaraine dyes is composed of a core electron-deficient four-membered ring, flanked by electron-donating groups on both sides. Essentially, it is a type of dye called polymethine Donor-Π-Acceptor (D-A-D) dye that achieves stability by resonance. The presence of a zwitterionic structure contributes to a significant dipole moment of the dye. Squaraine dyes are classified as far-red sensitizers because of their exceptional physio-chemical characteristics, including excellent photoconductivity, strong absorption in the range of 600 to 750 nm, and a high molar absorption coefficient [45]. In addition, squaraine dye often demonstrates a minimal stokes shift of 15-20 nm, indicating its high degree of structural rigidity.

Squaraine dyes can be classified into two distinct categories: symmetrical and unsymmetrical. The symmetrical squaraine dyes consist of donor units that are the same on both sides, whereas the unsymmetrical dyes consist of two separate donor groups. Usually, the donor units are attached to the first and third positions of the squaraine unit because they have more desired optical characteristics that cause a shift towards the red end of the spectrum, compared to the 1,2 regioisomer [46]. The fundamental process of synthesizing an unsymmetrical squaraine dye involves first forming the semi-squaraine and then condensing the second donor unit with the semi-squaraine to produce the unsymmetrical squaraine dye. Before the second condensation, the

squaric acid must be changed with a hydroxyl group. This modification enhances the reactivity of semi-squaraine during the condensation reaction. Acid or base hydrolysis might be used to perform this procedure.

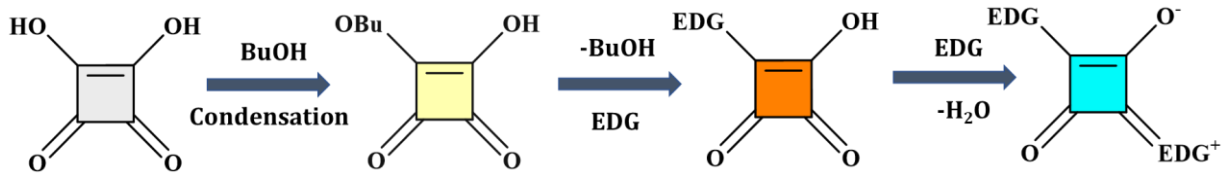

Figure 15. *Synthetic strategy employed in the synthesis of squaraine dye.*

The squaraine dyes have a higher tendency to aggregate because of their rigid and planar structure. They display both H aggregation and J aggregation. The planar structure of squaraine dye often leads to the occurrence of H aggregation. When aggregates form, they cause a shift towards shorter wavelengths, resulting in a blue shift in the lower wavelength region. The overlapping of squaraine dye molecules leads to the formation of J aggregate. The J aggregate absorbs at a higher wavelength compared to the monomer, resulting in a bathochromic shift[47].

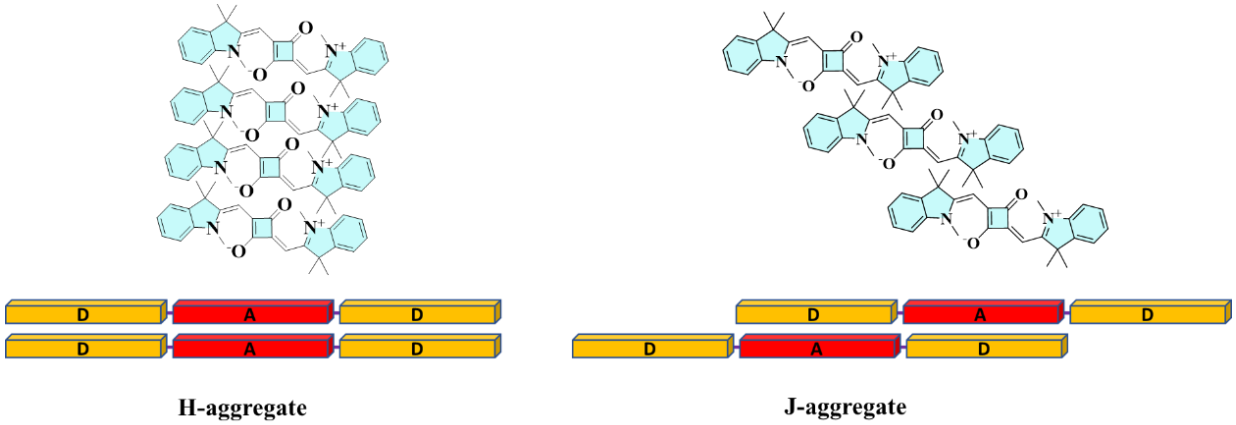

Figure 16. *Formation of H aggregate and J aggregates in squaraine monomer dye.*

The application of squaraine dyes for protein sensing and labeling is mostly investigated using model proteins such as bovine serum albumin (BSA), human serum albumin (HSA), ovalbumin, and avidin. Suzuki and Yokoyama employed a straightforward approach by utilizing simple squaraine dye as a sensor for BSA protein [48]. When BSA is added, squaraine forms noncovalent interactions with proteins, causing a noticeable change in color from orange to deep purple. Squaraine exhibited a reliable concentration response to different proteins, making it a more

favorable option compared to other protein detection materials currently on the market. The author additionally found that the squaraine-BSA complex exhibited excellent stability towards various nonprotein compounds. Oswald et al. synthesized squaraine dyes with succinimide groups and covalently bonded them to serum albumin using succinidyl esters. Chemical binding enhanced the fluorescence quantum yield of the final complexes from 0.15 to 0.6-0.7, allowing for fluorescence measurement in whole blood with a detection minimum of twice that of cyanine chromophores[49]. Klymchenko and colleagues recently developed a dye using a squaraine dimer [50]. This dye does not emit light in water due to the aggregation of squaraine molecules, but it emits strongly in the far-red region when used in organic solvents, as depicted in **Figure 17**.

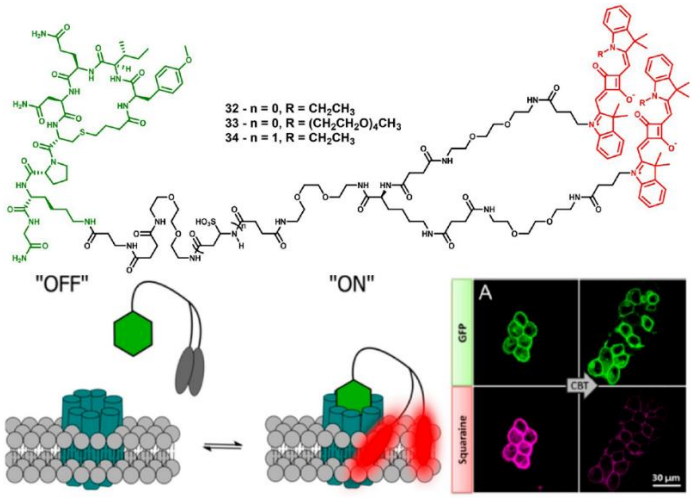

Figure 17. *The image displays the structures of squaraine dimers (colored red) linked to Lys8-CBT (colored green) at the top. The bottom left shows the mechanism of action of polarity sensors based on dimers. The bottom right shows in vitro imaging of the probe in GFP−OTR cells. The introduction of a competing CBT leads to a considerable reduction in fluorescence emitted by the probe. Adapted with permission from* [50]. *Copyright 2015 American Chemical Society.*

Carbetocin, a ligand of the oxytocin G protein-coupled receptor, was used for grafting. An intense receptor-specific signal was detected when this probe was bound to the specific serum and membrane. In the context of biosensing applications, particularly for in vivo and in vitro molecular detection, the choice of squaraine dyes with specific characteristics is crucial to ensure optimal performance. An essential criterion for squaraine dyes used in biosensing is their requirement to have little aggregation and exceptional water solubility. The aggregation of dye molecules can result in self-quenching, causing a decrease in fluorescence intensity and changes in spectral

characteristics. These effects can have a major impact on the sensitivity and accuracy of biosensing tests. Minimizing aggregation is crucial in maintaining the integrity of squaraine dyes, which are renowned for their robust absorption and emission properties, to optimize their detection capabilities. In addition, it is crucial to have high water solubility to maintain the stability and ability to be absorbed by biological systems of squaraine dyes. One of the squaraine dyes designed and synthesized for this investigation is a distinct amine-functionalized squaraine dye, while the other is flanked with fluorescein isothiocyanate (FITC). Another squaraine dye contains a benzo[e]indole group with a long alkyl chain. These dyes exhibit absorption and emission properties in the range of 650 to 674 nm, making them suitable for fluorescence-based applications. For the specific application of sensing protein in phosphate buffer solution (PBS), this squaraine dye was utilized to investigate its interaction with bovine serum albumin (BSA), a commonly used model protein. The dye's ability to bind to BSA and induce fluorescence changes upon protein binding was studied to evaluate its potential as a fluorescent probe for protein detection. Furthermore, this squaraine dye was also incorporated into a FRET-based probe for the detection of chymotrypsin activity using a homo-FRET mechanism. In this setup, the dye serves as the donor fluorophore, while the enzyme-substrate or cleavage site acts as the acceptor fluorophore. Upon enzymatic hydrolysis by chymotrypsin, the proximity-induced FRET effect leads to a fluorescence enhancement signal, indicating enzyme activity. By combining the unique spectral properties of the squaraine dye with the specificity of chymotrypsin recognition and cleavage, this FRET-based probe offers a sensitive and selective method for detecting enzyme activity. The long alkyl chain and benzo[e]indole group in the squaraine dye contribute to its stability, solubility, and interaction with biomolecules, enhancing its performance as a fluorescent probe in biological systems.

1.5 The Aim and Motivation of this Research

Fluorescent biosensors, particularly those utilizing near-infrared (NIR) technology, have emerged as promising tools in advanced biomedical applications due to their unique advantages, including enhanced tissue penetration, reduced background interference from biological autofluorescence, and multiplexing capabilities that allow for simultaneous detection of multiple analytes. Recent developments have focused on expanding NIR biosensors into the NIR-I and NIR-II window, which further improves imaging depth and sensitivity. Novel fluorophores, including new NIR fluorescent proteins, organic dyes, and inorganic nanoparticles, are being developed to enhance

sensor design and functionality. However, challenges remain, such as limitations in single analyte detection, sensitivity to interfering agents, the need for prior analyte processing, and throughput constraints. Ongoing research aims to create sensitive high-throughput detection methods compatible with advanced imaging processes, positioning NIR fluorescent biosensors as vital tools for medical diagnostics, environmental monitoring, and biological research.

Fluorescence detection is known for its high sensitivity compared to other detection methods, and when combined with microarray technology, high-throughput detection capabilities can be achieved. By leveraging the advantages of fluorescence-based sensing and incorporating them into biosensor development, the aim is to enhance the sensitivity, specificity, and throughput of enzyme detection. This approach holds promise for advancing the field of biosensing and enabling the development of more efficient and reliable diagnostic tools for various applications in healthcare, environmental monitoring, food analysis, and beyond.

The focus of the current thesis is on fluorescence-based sensing through the design and development of novel sensitive fluorescent probes for the detection of target enzymes. Fluorescence detection offers higher sensitivity compared to optical detection methods, and when combined with microarray technology, high-throughput detection capabilities can be achieved. NIR dyes have been preferred due to their features such as the potential for in-vitro/in-vivo bio-imaging, good tissue penetration depth, reduced noise from biological auto-fluorescence, direct use in biological fluids, and the ability for multi-color and multi-target detection. Attempts have been undertaken to create and produce near-infrared fluorescent dye molecules that can be adjusted in terms of wavelength to develop biological probes. Before employing FRET, these dyes were examined for their interactions with BSA, a versatile protein model, to evaluate their biocompatibility. The research also encompasses the investigation of the PET process and dual emission in a new substance, exhibiting emissions in both the visible and near-infrared (NIR) ranges. In addition, a quencher and fluorophore based on squaraine dye was synthesized. The SQ-122 PC probe was developed using solid-phase peptide synthesis to detect chymotrypsin activity. It utilizes homo-FRET to achieve high sensitivity and selectivity. The objective of this research endeavor is to enhance the field of biosensing by employing fluorescence-based sensing techniques and creating novel fluorescent probes for the detection of enzymes. These probes will have enhanced sensitivity, specificity, and the potential for use in high-throughput applications.

1.6 References

1. van Wijck, K.; van Eijk, H.M.H.; Buurman, W.A.; Dejong, C.H.C.; Lenaerts, K. Novel Analytical Approach to a Multi-Sugar Whole Gut Permeability Assay. *J. Chromatogr. B* **2011**, *879*, 2794–2801, doi:https://doi.org/10.1016/j.jchromb.2011.08.002.

2. Denisov, I.; Lukyanenko, K.; Yakimov, A.; Kukhtevich, I.; Esimbekova, E.; Belobrov, P. Disposable Luciferase-Based Microfluidic Chip for Rapid Assay of Water Pollution. *Luminescence* **2018**, *33*, 1054–1061, doi:https://doi.org/10.1002/bio.3508.

3. Vijitvarasan, P.; Oaew, S.; Surareungchai, W. Paper-Based Scanometric Assay for Lead Ion Detection Using DNAzyme. *Anal. Chim. Acta* **2015**, *896*, 152–159, doi:https://doi.org/10.1016/j.aca.2015.09.011.

4. Gu, Z.; Zhao, M.; Sheng, Y.; Bentolila, L.A.; Tang, Y. Detection of Mercury Ion by Infrared Fluorescent Protein and Its Hydrogel-Based Paper Assay. *Anal. Chem.* **2011**, *83*, 2324–2329, doi:10.1021/ac103236g.

5. Kalluri, J.R.; Arbneshi, T.; Afrin Khan, S.; Neely, A.; Candice, P.; Varisli, B.; Washington, M.; McAfee, S.; Robinson, B.; Banerjee, S.; et al. Use of Gold Nanoparticles in a Simple Colorimetric and Ultrasensitive Dynamic Light Scattering Assay: Selective Detection of Arsenic in Groundwater. *Angew. Chemie Int. Ed.* **2009**, *48*, 9668–9671, doi:https://doi.org/10.1002/anie.200903958.

6. Geißler, D.; Hildebrandt, N. Recent Developments in Förster Resonance Energy Transfer (FRET) Diagnostics Using Quantum Dots. *Anal. Bioanal. Chem.* **2016**, *408*, 4475–4483, doi:10.1007/s00216-016-9434-y.

7. Arola, H.O.; Tullila, A.; Kiljunen, H.; Campbell, K.; Siitari, H.; Nevanen, T.K. Specific Noncompetitive Immunoassay for HT-2 Mycotoxin Detection. *Anal. Chem.* **2016**, *88*, 2446–2452, doi:10.1021/acs.analchem.5b04591.

8. Lequin, R.M. Enzyme Immunoassay (EIA)/Enzyme-Linked Immunosorbent Assay (ELISA). *Clin. Chem.* **2005**, *51*, 2415–2418, doi:10.1373/clinchem.2005.051532.

9. Liao, J.; Song, Y.; Liu, Y. A New Trend to Determine Biochemical Parameters by

Quantitative FRET Assays. *Acta Pharmacol. Sin.* **2015**, *36*, 1408–1415, doi:10.1038/aps.2015.82.

10. Takkinen, K.; Žvirblienė, A. Recent Advances in Homogenous Immunoassays Based on Resonance Energy Transfer. *Curr. Opin. Biotechnol.* **2019**, *55*, 16–22, doi:https://doi.org/10.1016/j.copbio.2018.07.003.

11. Mitchell, J. Small Molecule Immunosensing Using Surface Plasmon Resonance. *Sensors* **2010**, *10*, 7323–7346, doi:10.3390/s100807323.

12. Haes, A.J.; Hall, W.P.; Chang, L.; Klein, W.L.; Van Duyne, R.P. A Localized Surface Plasmon Resonance Biosensor: First Steps toward an Assay for Alzheimer's Disease. *Nano Lett.* **2004**, *4*, 1029–1034, doi:10.1021/nl049670j.

13. Giannetti, A.M.; Koch, B.D.; Browner, M.F. Surface Plasmon Resonance Based Assay for the Detection and Characterization of Promiscuous Inhibitors. *J. Med. Chem.* **2008**, *51*, 574–580, doi:10.1021/jm700952v.

14. Vollmer, F.; Arnold, S. Whispering-Gallery-Mode Biosensing: Label-Free Detection down to Single Molecules. *Nat. Methods* **2008**, *5*, 591–596, doi:10.1038/nmeth.1221.

15. Chakravarty, S.; Lai, W.-C.; Zou, Y.; Drabkin, H.A.; Gemmill, R.M.; Simon, G.R.; Chin, S.H.; Chen, R.T. Multiplexed Specific Label-Free Detection of NCI-H358 Lung Cancer Cell Line Lysates with Silicon Based Photonic Crystal Microcavity Biosensors. *Biosens. Bioelectron.* **2013**, *43*, 50–55, doi:https://doi.org/10.1016/j.bios.2012.11.012.

16. Santiago-Cordoba, M.A.; Boriskina, S. V; Vollmer, F.; Demirel, M.C. Nanoparticle-Based Protein Detection by Optical Shift of a Resonant Microcavity. *Appl. Phys. Lett.* **2011**, *99*, 73701, doi:10.1063/1.3599706.

17. Jiang, Z.; Jiang, X.; Li, C.; Xue, H.; Zhang, X. Development of an IgY Antibody-Based Immunoassay for the Screening of the CYP2E1 Inhibitor/Enhancer from Herbal Medicines. *Front. Pharmacol.* **2016**, *7*, 502, doi:10.3389/fphar.2016.00502.

18. Burnette, W.N. "Western Blotting": Electrophoretic Transfer of Proteins from Sodium Dodecyl Sulfate-Polyacrylamide Gels to Unmodified Nitrocellulose and Radiographic Detection with Antibody and Radioiodinated Protein A. *Anal. Biochem.* **1981**, *112*, 195–203,

doi:https://doi.org/10.1016/0003-2697(81)90281-5.

19. MacPhee, D.J. Methodological Considerations for Improving Western Blot Analysis. *J. Pharmacol. Toxicol. Methods* **2010**, *61*, 171–177, doi:https://doi.org/10.1016/j.vascn.2009.12.001.

20. Engvall, E.; Perlmann, P. Enzyme-Linked Immunosorbent Assay (ELISA) Quantitative Assay of Immunoglobulin G. *Immunochemistry* **1971**, *8*, 871–874, doi:https://doi.org/10.1016/0019-2791(71)90454-X.

21. Lazcka, O.; Campo, F.J. Del; Muñoz, F.X. Pathogen Detection: A Perspective of Traditional Methods and Biosensors. *Biosens. Bioelectron.* **2007**, *22*, 1205–1217, doi:https://doi.org/10.1016/j.bios.2006.06.036.

22. Creasy, B.M.; Hartmann, C.B.; White, F.K.H.; McCoy, K.L. New Assay Using Fluorogenic Substrates and Immunofluorescence Staining to Measure Cysteine Cathepsin Activity in Live Cell Subpopulations. *Cytom. Part A J. Int. Soc. Anal. Cytol.* **2007**, *71*, 114–123, doi:10.1002/cyto.a.20365.

23. Altmeppen, H.C.; Prox, J.; Puig, B.; Dohler, F.; Falker, C.; Krasemann, S.; Glatzel, M. Roles of Endoproteolytic α-Cleavage and Shedding of the Prion Protein in Neurodegeneration. *FEBS J.* **2013**, *280*, 4338–4347, doi:10.1111/febs.12196.

24. Lesner, A.; Brzozowski, K.; Kupryszewski, G.; Rolka, K. Design, Chemical Synthesis and Kinetic Studies of Trypsin Chromogenic Substrates Based on the Proteinase Binding Loop of Cucurbita Maxima Trypsin Inhibitor (CMTI-III). *Biochem. Biophys. Res. Commun.* **2000**, *269*, 81–84, doi:10.1006/bbrc.2000.2257.

25. Pozsgay, M.; Gáspár, R.; Elödi, P.; Bajusz, S. Investigations on New Tripeptidyl-p-Nitroanilide Substrates for Subtilisins. *FEBS Lett.* **1977**, *74*, 67–70, doi:https://doi.org/10.1016/0014-5793(77)80754-0.

26. Stepanov, V.M.; EYu, T.; Voyushina, T.L.; MYu, G. Subtilisin and Alpha-Chymotrypsin Catalyzed Synthesis of Peptides Containing Arginine and Lysine p-Nitroanilides as C-Terminal Moieties. *Bioorg. Med. Chem.* **1995**, *3*, 479–485, doi:10.1016/0968-0896(95)00073-p.

27. Johnsson, K. Visualizing Biochemical Activities in Living Cells. *Nat. Chem. Biol.* **2009**, *5*,

63–65, doi:10.1038/nchembio0209-63.

28. Wong, J.K.-H.; Todd, M.H.; Rutledge, P.J. Recent Advances in Macrocyclic Fluorescent Probes for Ion Sensing. *Molecules* **2017**, *22*, doi:10.3390/molecules22020200.

29. Kobayashi, H.; Ogawa, M.; Alford, R.; Choyke, P.L.; Urano, Y. New Strategies for Fluorescent Probe Design in Medical Diagnostic Imaging. *Chem. Rev.* **2010**, *110*, 2620–2640, doi:10.1021/cr900263j.

30. Dias, G.G.; King, A.; de Moliner, F.; Vendrell, M.; da Silva Júnior, E.N. Quinone-Based Fluorophores for Imaging Biological Processes. *Chem. Soc. Rev.* **2018**, *47*, 12–27, doi:10.1039/C7CS00553A.

31. Naidu Bobba, K.; Won, M.; Shim, I.; Velusamy, N.; Yang, Z.; Qu, J.; Kim, J.S.; Bhuniya, S. A BODIPY-Based Two-Photon Fluorescent Probe Validates Tyrosinase Activity in Live Cells. *Chem. Commun.* **2017**, *53*, 11213–11216, doi:10.1039/C7CC05043G.

32. Zhang, X.; Wang, Z.; Guo, Z.; He, N.; Liu, P.; Xia, D.; Yan, X.; Zhang, Z. A Novel Turn-on Fluorescent Probe for Selective Sensing and Imaging of Glutathione in Live Cells and Organisms. *Analyst* **2019**, *144*, 3260–3266, doi:10.1039/C9AN00115H.

33. Xiao, M.; Sun, W.; Fan, J.; Cao, J.; Li, Y.; Shao, K.; Li, M.; Li, X.; Kang, Y.; Zhang, W.; et al. Aminopeptidase-N-Activated Theranostic Prodrug for NIR Tracking of Local Tumor Chemotherapy. *Adv. Funct. Mater.* **2018**, *28*, 1805128, doi:https://doi.org/10.1002/adfm.201805128.

34. Ahmad, A.I.; Ghasemi, J.B. New FRET Primers for Quantitative Real-Time PCR. *Anal. Bioanal. Chem.* **2007**, *387*, 2737–2743, doi:10.1007/s00216-007-1123-4.

35. Nath-Chowdhury, M.; Sangaralingam, M.; Bastien, P.; Ravel, C.; Pratlong, F.; Mendez, J.; Libman, M.; Ndao, M. Real-Time PCR Using FRET Technology for Old World Cutaneous Leishmaniasis Species Differentiation. *Parasit. Vectors* **2016**, *9*, 255, doi:10.1186/s13071-016-1531-4.

36. Didenko, V. V DNA Probes Using Fluorescence Resonance Energy Transfer (FRET): Designs and Applications. *Biotechniques* **2001**, *31*, 1106–1121, doi:10.2144/01315rv02.

37. Forster, T. Energiewanderung Und Fluoreszenz. *Naturwissenschaften* **1946**, *33*, 166–175, doi:10.1007/BF00585226.

38. VAN MUNSTER, E.B.; KREMERS, G.J.; ADJOBO-HERMANS, M.J.W.; GADELLA JR, T.W.J. Fluorescence Resonance Energy Transfer (FRET) Measurement by Gradual Acceptor Photobleaching. *J. Microsc.* **2005**, *218*, 253–262, doi:https://doi.org/10.1111/j.1365-2818.2005.01483.x.

39. Cano-Raya, C.; Fernández-Ramos, M.D.; Capitán-Vallvey, L.F. Fluorescence Resonance Energy Transfer Disposable Sensor for Copper(II). *Anal. Chim. Acta* **2006**, *555*, 299–307, doi:https://doi.org/10.1016/j.aca.2005.09.011.

40. Sekar, R.B.; Periasamy, A. Fluorescence Resonance Energy Transfer (FRET) Microscopy Imaging of Live Cell Protein Localizations . *J. Cell Biol.* **2003**, *160*, 629–633, doi:10.1083/jcb.200210140.

41. Rowland, C.E.; Brown, C.W.; Medintz, I.L.; Delehanty, J.B. Intracellular FRET-Based Probes: A Review. *Methods Appl. Fluoresc.* **2015**, *3*, 42006, doi:10.1088/2050-6120/3/4/042006.

42. Aich, K.; Goswami, S.; Das, S.; Mukhopadhyay, C. Das; Quah, C.K.; Fun, H.-K. Cd2+ Triggered the FRET "ON": A New Molecular Switch for the Ratiometric Detection of Cd2+ with Live-Cell Imaging and Bound X-Ray Structure. *Inorg. Chem.* **2015**, *54*, 7309–7315, doi:10.1021/acs.inorgchem.5b00784.

43. Cobos-Correa, A.; Trojanek, J.B.; Diemer, S.; Mall, M.A.; Schultz, C. Membrane-Bound FRET Probe Visualizes MMP12 Activity in Pulmonary Inflammation. *Nat. Chem. Biol.* **2009**, *5*, 628–630, doi:10.1038/nchembio.196.

44. Zhang, X.; Bloch, S.; Akers, W.; Achilefu, S. Near-Infrared Molecular Probes for in Vivo Imaging. *Curr. Protoc. Cytom.* **2012**, *Chapter 12*, Unit12.27, doi:10.1002/0471142956.cy1227s60.

45. Yan, K.; Hu, Z.; Yu, P.; He, Z.; Chen, Y.; Chen, J.; Sun, H.; Wang, S.; Zhang, F. Ultra-Photostable Small-Molecule Dyes Facilitate near-Infrared Biophotonics. *Nat. Commun.* **2024**, *15*, 2593, doi:10.1038/s41467-024-46853-0.

46. Mayerhöffer, U.; Fimmel, B.; Würthner, F. Bright Near-Infrared Fluorophores Based on

Squaraines by Unexpected Halogen Effects. *Angew. Chemie Int. Ed.* **2012**, *51*, 164–167, doi:https://doi.org/10.1002/anie.201107176.

47. Lima, E.; Reis, L. V 'Lights, Squaraines, Action!'–The Role of Squaraine Dyes in Photodynamic Therapy. *Future Med. Chem.* **2022**, *14*, 1375–1402.

48. Chen, G.; Sasabe, H.; Sasaki, Y.; Katagiri, H.; Wang, X.-F.; Sano, T.; Hong, Z.; Yang, Y.; Kido, J. A Series of Squaraine Dyes: Effects of Side Chain and the Number of Hydroxyl Groups on Material Properties and Photovoltaic Performance. *Chem. Mater.* **2014**, *26*, 1356–1364, doi:10.1021/cm4034929.

49. Oswald, B.; Patsenker, L.; Duschl, J.; Szmacinski, H.; Wolfbeis, O.S.; Terpetschnig, E. Synthesis, Spectral Properties, and Detection Limits of Reactive Squaraine Dyes, a New Class of Diode Laser Compatible Fluorescent Protein Labels. *Bioconjug. Chem.* **1999**, *10*, 925–931, doi:10.1021/bc9801023.

50. Karpenko, I.A.; Collot, M.; Richert, L.; Valencia, C.; Villa, P.; Mély, Y.; Hibert, M.; Bonnet, D.; Klymchenko, A.S. Fluorogenic Squaraine Dimers with Polarity-Sensitive Folding As Bright Far-Red Probes for Background-Free Bioimaging. *J. Am. Chem. Soc.* **2015**, *137*, 405–412, doi:10.1021/ja5111267.

CHAPTER 2 : INSTRUMENTATION AND CHARACTERIZATION

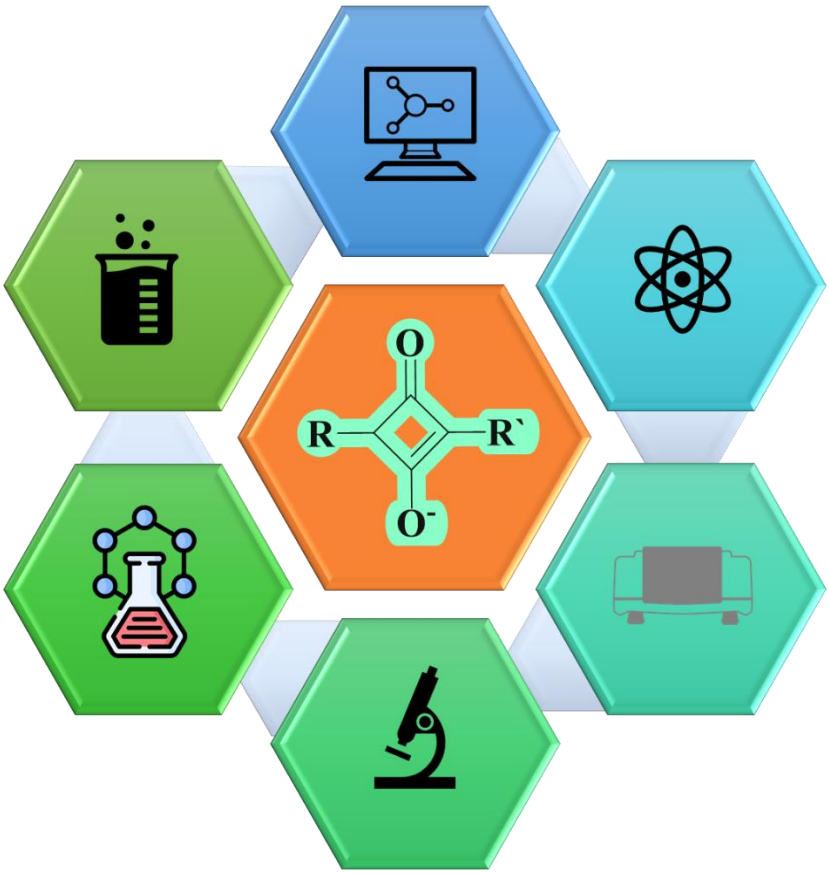

2.1 Fluorescence Spectroscopy

Fluorescence spectroscopy is an electromagnetic spectroscopy technique used to analyze the fluorescence emitted by a material. Typically, an ultraviolet laser beam is employed to stimulate electrons and induce them to release light. Molecules possess various energy levels, which can be described in different states. Fluorescence primarily focuses on vibrational and electronic states[1]. When a species absorbs a photon, it becomes excited and moves from its ground state to one of the various vibrational states in higher energy levels. The molecule gradually loses its energy as it interacts with other molecules, eventually reaching its lowest state of excited energy level. The visualization of this process can be represented using a Jablonski diagram, as depicted in **Figure 1(a)**. The molecule then transitions to one of the various vibrational levels of the ground electronic states by releasing a photon. The emitted photon will have varying energies and frequencies. By carefully examining the various frequencies of emitted light and their corresponding intensities, one can accurately ascertain the distinct vibrational levels of the structure. For emission measurement, the excitation wavelength remains constant while the detection wavelength is altered.

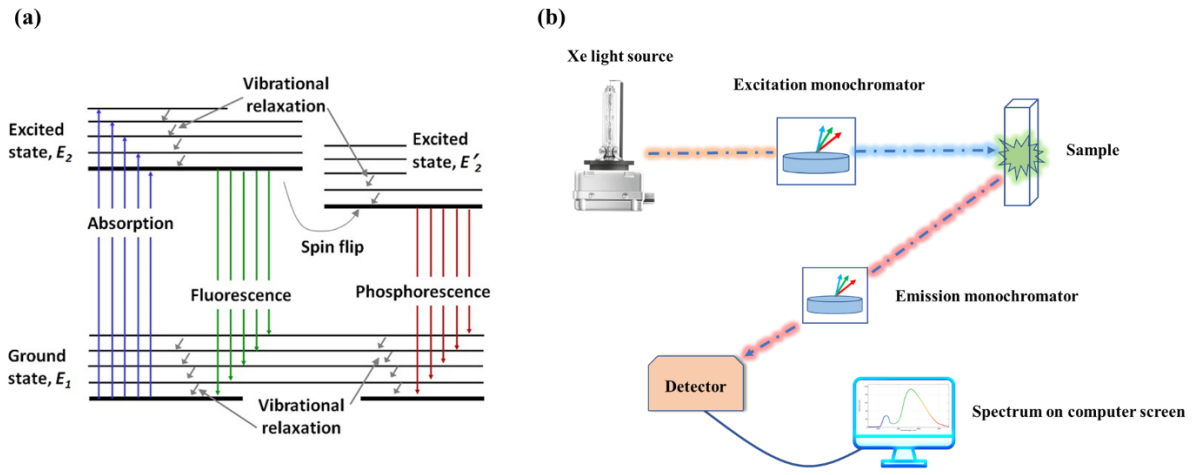

Figure 1. *(a) Jablonski diagram (b) Working principle of a fluorescence spectrometer*

Fluorescence spectroscopy involves the transmission of excitation light from a source through a monochromator or filter to the sample, where it is absorbed and causes molecules to fluorescence. A second monochromator or filter then filters the emitted fluorescent light before it reaches a detector at a right angle to the incident light beam (**Figure 1. (b)**). Excitation can come from a variety of light sources, including xenon arc lamps, mercury-vapor lamps, lasers, and LED lights. Monochromators are essential for transmitting light at specific wavelengths with precise control. Detectors in fluorescence spectroscopy can be single-channeled, capable of measuring the intensity of one wavelength, or multi-channeled, which can detect the intensities of multiple wavelengths.

In the present thesis, fluorescence spectroscopy is employed to evaluate the quantum yield of far-red sensitive symmetrical and unsymmetrical squaraine dyes. Fluorescence spectroscopy is commonly employed to analyze the binding interactions between dyes and BSA, serving as a protein model. Moreover, it is also used for measuring the fluorescence signal due to the FRET mechanism in our designed probe. In this current thesis, the JASCO FP-6600 model fluorescence spectrophotometer is utilized, as depicted in **Figure 2**.

Figure 2. *The fluorescence spectrophotometer used during my work***.**

2.2 Electronic Absorption Spectroscopy

Electronic absorption spectroscopy is named as such because it quantifies the transition of an electron from a lower energy atomic orbital to a higher energy atomic orbital upon absorbing a photon. The radiation absorption, often in the UV-vis and Near Infrared range, is quantified by wavelength. The molecule becomes energized when it absorbs a photon with the same energy as its band gap. The efficiency of a molecule in absorbing radiation is measured by its molar extinction coefficient. The molar absorption coefficient of a substance can be determined by measuring its absorbance. The molar absorption coefficient is a quantitative metric that describes the degree to which a chemical species absorbs light at a specific wavelength. The absorbance is calculated using the following equation:

$$\mathbf{A = \log I_0 / I} \qquad (1)$$

Where I_0 represents the incident light intensity and I represent the transmitted light intensity.

$$\mathbf{A = \varepsilon c l} \qquad (2)$$

OR $\quad \boldsymbol{\varepsilon = A/cl}$

In this context, the variables A, ε, c, and l represent the absorbance, molar extinction coefficient, concentration, and length of the cell, respectively. Figure 3. illustrates the working mechanism of the UV Spectrophotometer. When light strikes the sample, it can either be reflected, transmitted, or absorbed. Absorbance is the difference between the intensity of incident light (I_0) and the intensity of transmitted light (I). The light that is taken in can be described using either transmittance or absorbance. The sample is illuminated with light, and the intensity of the light that passes through is measured. This measurement is used to plot the absorbance of the sample as a function of the wavelength of the light.

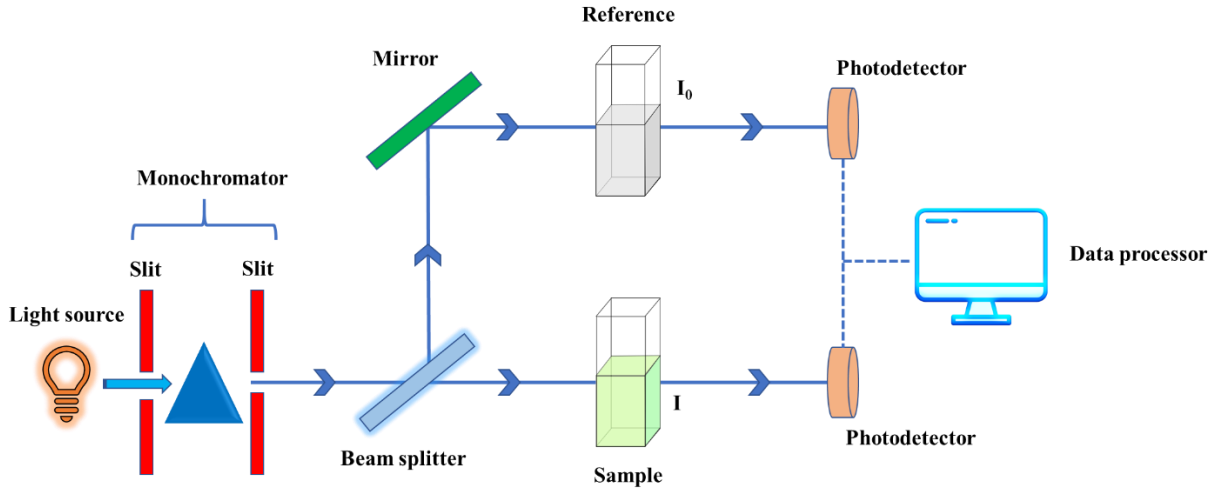

Figure 3. *The working mechanism of a UV-Vis spectrophotometer*

The detection of a compound is based on the presence of an absorbance band at a specific wavelength. This is because the absorption peak is unique to a specific compound and is therefore used to determine the substance's composition. The use of absorbance studies for material characterization is extensively researched. The spectrophotometer used during the present investigation is the JASCO V-570, as depicted in **Figure 4**.

Figure 4. *The UV-visible spectrometer employed in this study*

2.3 Nuclear Magnetic Resonance Spectroscopy (NMR)

Each nucleus possesses a certain quantity of charge and a spin of 1/2, resulting in a distinct magnetic moment. When the nuclei are subjected to an external magnetic field, the degenerate energy is divided into several energy levels ($\Delta E = hv$), a phenomenon referred to as the Zeeman Effect[2]. The energy transfer occurs at a specific frequency, and when the spin relaxes, it emits the same frequency, which is used to obtain the NMR spectrum. Some significant NMR-active nuclei include those with an odd spin, such as ^{1}H, ^{13}C, ^{15}N, ^{19}F, and ^{31}P. Nevertheless, the most commonly utilized is ^{1}H. Nuclear Magnetic Resonance (NMR) is a crucial technique for determining the molecular structure, identifying functional groups, and determining the precise positions of atoms inside the molecule. Typically, tetramethyl silane (TMS) is used as the reference in NMR data collection since it contains protons that are all identical. The chemical shift (δ) of the nuclei is quantified in parts per million (ppm) relative to the zero value of the reference[3]. The samples are dissolved in deuterated solvents such as $CDCl_3$, d-6 DMSO, and D_2O to prevent interference from the solvent signals.

2.3.1 ^{1}H-NMR

Nuclear magnetic resonance (NMR) is a technique used to investigate the 1H nuclei in a molecule to quantify the number of hydrogen atoms present, as well as to some extent, identify the functional groups. The chemical shift (δ) values for ^{1}H-NMR range from -4 to 14 ppm. The expected outcome is a single peak for a single proton. However, the peak experiences splitting as a result of its chemical surroundings, caused by spin-spin coupling. First-order coupling in NMR spectroscopy occurs when the coupling constant (J) remains consistent for all protons involved [4]. This yields a predictable pattern of peaks, where the number of peaks formed equals (n+1), with 'n' representing the number of neighboring protons. For instance, when 'n' is zero, the peak appears as a singlet (s). With 'n' as one, it forms a doublet (d), and for 'n' equal to two, a triplet (t) emerges, and so forth. Conversely, non-first-order coupling arises when the J value varies among the protons. Consequently, the resultant signal manifests as a multiplet. Here, non-equivalent protons mutually influence one another's splitting, leading to the formation of doublet of doublet

(dd) peaks. This distinction is pivotal in NMR analysis, offering insights into the structural and chemical environment of molecules under study[5].

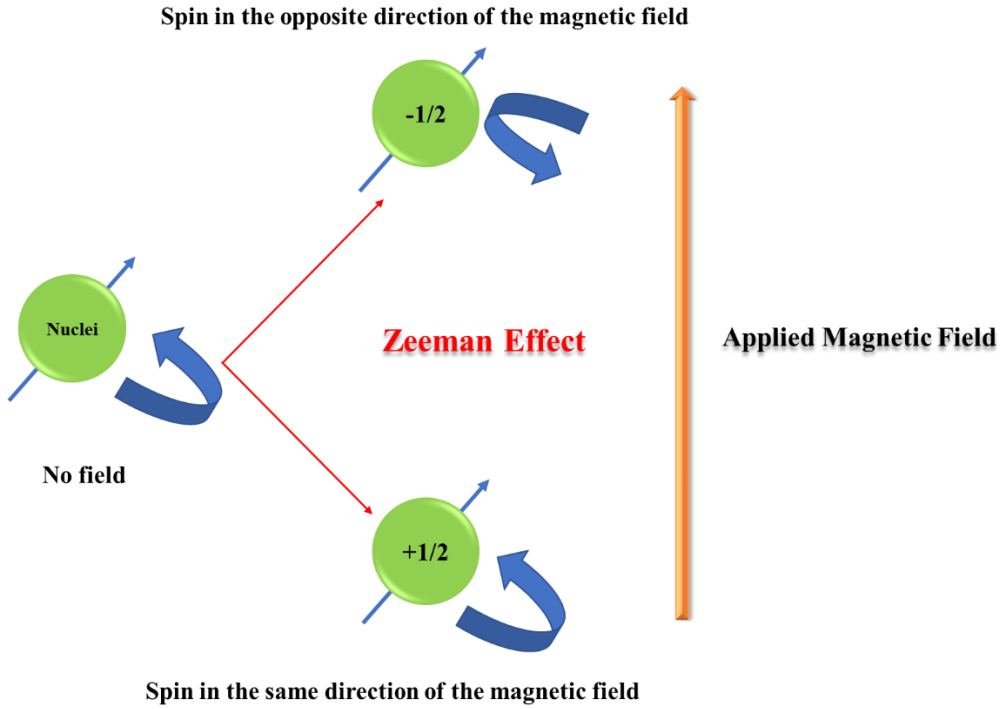

Figure 5. *The presence of a magnetic field causes the atomic nucleus to undergo spin splitting, resulting in the formation of peaks in the NMR analysis*

2.3.2 ^{13}C-NMR

In the realm of nuclear magnetic resonance (NMR) spectroscopy, ^{13}C-NMR serves as the carbon counterpart to the well-established proton NMR (H-NMR). Unlike ^{1}H-NMR, ^{13}C-NMR selectively detects carbon atoms containing the ^{13}C isotope, which possesses a non-zero spin, while not detecting the more abundant ^{12}C with a net zero spin. However, due to its lower natural abundance constituting merely 1.1% and inherent lower sensitivity compared to H-NMR, ^{13}C-NMR demands larger sample sizes, typically around 15 mg dissolved in the requisite solvent, and a substantial number of scans. The chemical shift (δ) values in ^{13}C-NMR spectra typically range from 20 to 220 parts per million (ppm). Notably, in contrast to H-NMR, ^{13}C-NMR lacks peak splitting arising from neighboring carbon atoms, owing to the scarcity of the ^{13}C isotope,

thereby enabling each peak to correspond to a distinct carbon atom. These nuances underline the importance of ^{13}C-NMR in elucidating the structural and chemical composition of organic molecules in scientific research and analysis.

NMR samples were prepared by dissolving 15 mg of the sample in the appropriate deuterated solvent in sealed tubes. We then recorded NMR spectra using a JEOL JNM-A500 Nuclear Magnetic Resonance Spectrometer, which operated at frequencies of 500 MHz for ^{1}H NMR and 125 MHz for ^{13}C-NMR, respectively. It is worth noting that in rare instances, small peaks may emerge at the shoulders of ^{1}H NMR spectra. These peaks, known as carbon satellites, occur when ^{1}H protons are coupled with ^{13}C nuclei rather than proton-proton coupling. However, we typically disregard these carbon satellites for analytical purposes, ensuring accurate interpretation of the NMR data.

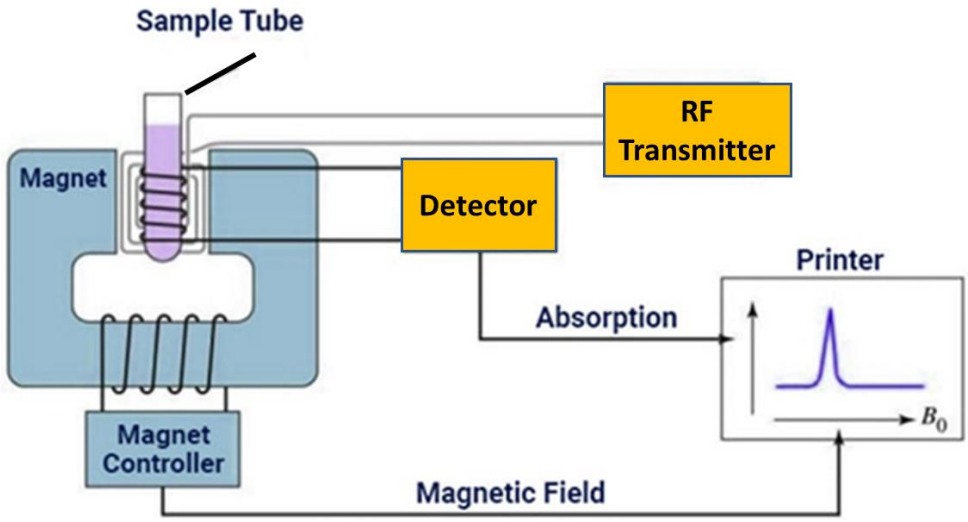

Figure 5. *The NMR spectroscopy scheme and its necessary components*

2.4 Mass Spectrometer

Mass spectroscopy is a crucial analytical technique that determines the mass of a specific compound. Initially, the sample undergoes ionization through bombardment, leading to the

formation of ionized species. Subsequently, these ions migrate within the spectrometer according to the principles of mass-to-charge ratio, with lighter species exhibiting faster movement compared to their heavier counterparts. During their migration, the ions experience deflection, influenced by magnetic or electric fields. Ultimately, a detector within the spectrometer captures the ions based on their mass-to-charge ratio. The resulting spectra manifest as sharp peaks, providing insights into the mass distribution of the analyzed compound. Various methodologies exist for measuring sample mass, including matrix-assisted laser desorption/ionization (MALDI) for small molecules and fast atom bombardment (FAB) mass spectrometry for complex molecules. These techniques, integral to scientific inquiry, facilitate precise and comprehensive analysis of molecular structures and compositions.

2.4.1 Matrix-Assisted Laser Desorption Ionization Time of Flight (MALDI-TOF Mass)

TOF-Mass, an alternative soft ionization technique distinct from ESI-mass spectrometry, exhibits the notable feature of generating significantly fewer multiply-charged ions. This method is particularly well-suited for the analysis of delicate biomolecules, including peptides, proteins, sugars, and DNA, as well as large organic molecules like polymers and macromolecules[6]. These biomolecules are prone to fragmentation when subjected to conventional ionization methods. Figure 6. illustrates the schematic working principle of TOF-Mass, showcasing its ability to accurately analyze molecular structures while minimizing fragmentation. This technique holds great promise for advancing research across various fields by enabling the comprehensive analysis of complex molecular compositions with enhanced sensitivity and precision.

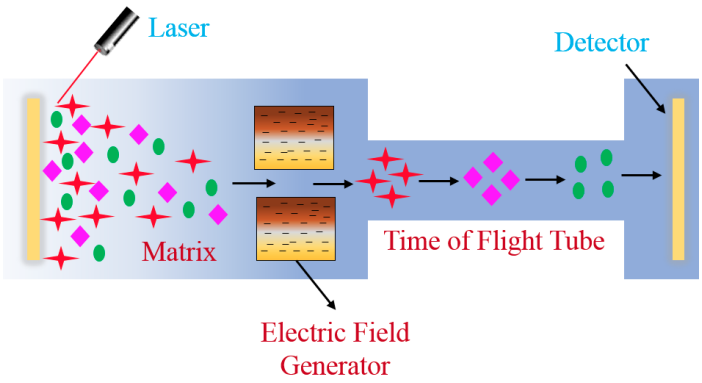

Figure 6. *The principle involved in time-of-flight (TOF) mass spectrometry*

In the analysis of compounds using TOF-mass spectrometry, the samples were combined with a matrix compound. This matrix comprises crystallized molecules of three commonly utilized types, including 3,5-dimethoxy-4-hydroxycinnamic acid, α-cyano-4-hydroxycinnamic acid (α-CHCA), and 2,5-dihydroxybenzoic acid (DHB) (Figure 7.) [7]. A solution of the matrix is prepared by dissolving it in a mixture of purified water and organic solvents such as acetonitrile or ethanol. Subsequently, the matrix solution is mixed with the analyte sample, and the resulting solution is then deposited onto a MALDI plate. Upon deposition, the solvent evaporates, leaving behind the recrystallized matrix. The co-crystallization of the matrix and analyte is pivotal, as it significantly influences the quality of the obtained mass spectrum. However, certain molecules possessing a π-conjugated system, such as naphthalene, can also serve as electron acceptors and be utilized as the matrix. This approach is particularly relevant when studying molecules with π-conjugated systems. As the dyes synthesized in the present thesis exhibit a π-conjugated system, MALDI-TOF mass spectrometry is employed to analyze some of these dye molecules.

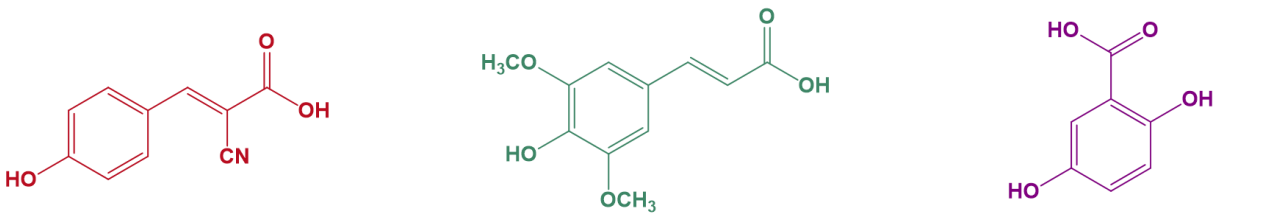

α-cyano-4-hydroxycinnamic acid **3,5-dimethoxy-4-hydroxycinnamic acid** **2,5-dihydroxybenzoic acid**

Figure 7. *Molecular structure of the matrix*

The current thesis uses the Bruker Microflex-KI time-of-flight (TOF) mass spectrometer, as illustrated in Figure 8. This apparatus utilizes ultraviolet (UV) lasers, specifically nitrogen lasers and ND: YAG lasers. During the operation, the laser beam focuses on the matrix crystals located within the dried-droplet location. When the laser energy is absorbed, the matrix goes through desorption and ionization. The resulting heated cloud consists of both neutral and ionized matrix molecules, Nano-droplets, as well as molecules that have gained or lost a proton. The ions detected after ionization may consist of molecules with additional or missing ions, such as $[M+H]^+$ for the

addition of a proton, $[M+Na]^+$ for the addition of a sodium ion, and $[M-H]^+$ for the removal of a proton. The specific ionization results are contingent upon various elements, such as the composition of the matrix, the intensity of the laser, and the applied voltage. The Time-of-Flight (TOF) measurement is highly compatible with this ionization technique due to the pulsed laser's operation in distinct shots. In addition, the TOF instrument has an ion mirror that employs an electric field to reflect ions, resulting in a twofold increase in the ion flight path and improved resolution. This complete configuration allows for accurate and detailed mass analysis while studying molecular compositions.

2.4.2 Electrospray Ionization (ESI-Mass)

The method of electrospray ionization (ESI) is utilized, in which a high voltage is given to the sample to create an aerosol, resulting in the formation of ions. ESI stands out from other atmospheric pressure ionization methods due to its highly efficient production of ions with multiple charges. ESI is acknowledged as a gentle ionization technique since it causes minimum fragmentation, resulting in constant observation of molecular ion peaks[8]. The groundbreaking research on electrospray ionization (ESI) was reported by Masamichi Yamashita and John Fenn in 1984. **Figure 10.** illustrates the schematic depiction of the operational principle of ESI-mass spectrometry. This approach is highly useful in scientific study as it enables the accurate determination of molecule compositions while minimizing sample deterioration.

In the ionization process, the analyte of interest is dissolved in a liquid and then dispersed into fine aerosol through electrospray [9]. Ion formation occurs as solvent evaporation takes place, with commonly used organic solvents such as methanol and acetonitrile facilitating this process. The aerosol is introduced into the initial vacuum stage of the spectrophotometer via a capillary, where it encounters a potential difference of approximately 3000V. Additionally, heating is

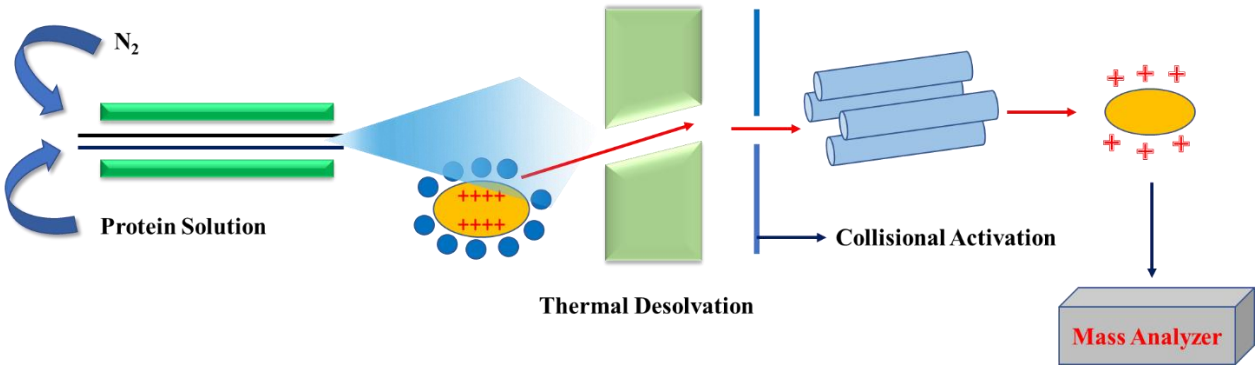

Figure 10. *Working principle of ESI-Mass*

applied to aid in further solvent evaporation. In the context of this thesis, methanol serves as the solvent of choice for analyzing the mass of dyes.

2.5 Fluorescence Microscopy

The fluorescence microscope is a fundamental tool in contemporary biological research, providing unparalleled resolution and sensitivity for observing specimens that have been labeled with fluorescent markers [10,11]. This microscope utilizes the principle of fluorescence and is powered by an excitation light source, usually a high-intensity lamp or laser that emits light across a wide range of wavelengths, from ultraviolet (UV) to visible light[12]. Excitation wavelengths commonly vary from 300 to 700 nanometers (nm), which aligns with the absorption spectra of different fluorophores [13]. The objective lens carefully collects the emitted fluorescent light and filters it to remove any remaining excitation light, ensuring accurate detection of the fluorescent signal [14] (**Figure 11**). This allows for the production of high-resolution fluorescence images, which are caught by sophisticated camera systems or photodetectors.

An important advantage of the fluorescence microscope is its capacity to selectively observe particular molecules or cellular structures inside complex biological materials [15]. This ability is enabled by fluorescent markers, such as fluorescent dyes or genetically engineered fluorescent proteins, which can be accurately directed to specific molecules or cellular compartments of interest. Furthermore, fluorescence microscopy allows for the direct and immediate monitoring of

dynamic events occurring within living cells. This is made possible by the ability to constantly stimulate and capture images of fluorophores over some time [11].

Advancements in technology have led to the development of specialized imaging techniques including confocal microscopy, multiphoton microscopy, and super-resolution microscopy. These techniques provide improved spatial resolution and imaging depth compared to traditional fluorescence microscopy. These advanced approaches show potential for understanding intricate biological events with exceptional levels of precision.

To summarize, the fluorescence microscope is a very effective instrument that has significantly transformed our comprehension of cellular organization and operation, leading to progress in biomedical investigation and enhancing our understanding of health and illness.

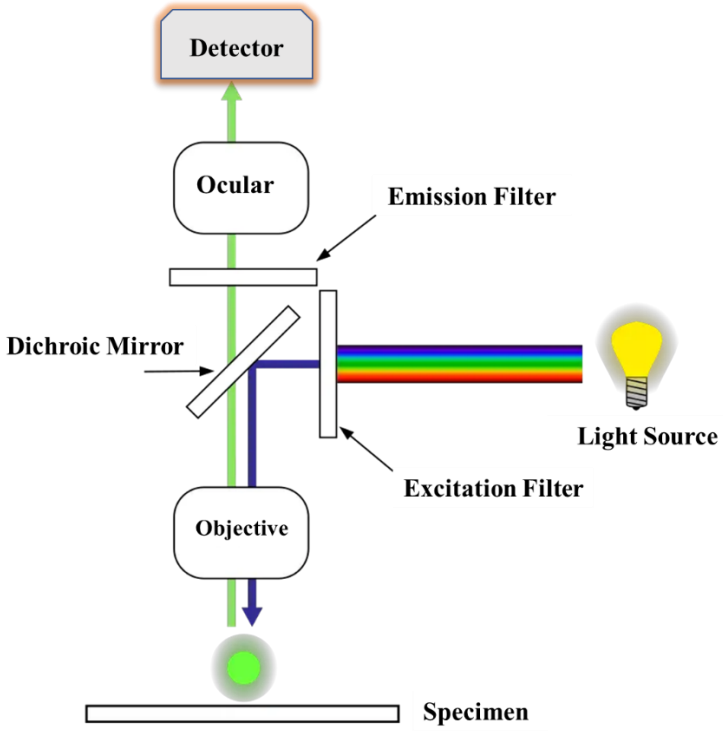

Figure 11. *The basic setup of a fluorescence microscope*

Different methods for fluorescence microscopy have been developed to enhance image contrast and spatial resolution. The three primary categories of fluorescence microscopy are widefield microscopy, confocal microscopy, and total internal reflection fluorescence microscopy.

2.5.1 Widefield microscopy

Wide-field (WF) Fluorescence Microscopy is a commonly used fluorescence microscope in the field of cell biology. With this microscope, a beam of light is used to illuminate the entire specimen simultaneously, causing the fluorophore to become excited. All the fluorescence emitted by specimens can be viewed at the same time, enabling easy and quick imaging. When observing a specimen with multiple probabilities, it is possible to view all the fluorescence simultaneously. Thanks to the ability to view all parts of the specimen simultaneously, it enables a rapid selection of fluorescent cells for imaging.

2.5.2 Confocal microscopy

WF microscope is limited by thin specimens. Imaging is hampered by an increase in out-of-focus light as specimen thickness increases. Confocal microscopy can remove out-of-focus light from pictures and provide high-resolution viewing of thick specimens. A confocal microscope may achieve a maximum resolution of around 200 nm. The primary distinction between confocal microscopy and other methods in the illumination and detection area. When it comes to immunofluorescence, the confocal microscope is a very useful tool for reducing background glare [16].

2.5.3 Total Internal Refraction Microscopy

Total Internal Refraction Microscopy (TIRFM) relies on the activation of fluorophores through the evanescent wave or field generated by the internally refracted laser beam. Total internal refraction (TIRF) is an optical phenomenon where light reflects instead of refracting when it moves from a medium with a high refractive index to one with a low refractive index. This reflection occurs when the incident angle exceeds the critical angle. This phenomenon is governed by Snell's Law. When it comes to TIRF, the reflected light transforms an electromagnetic field at the interface. This then leads to the formation of an evanescent field through the media of low refractive index, with its amplitude decaying exponentially. Thus, the evanescent field's penetration depth is limited to approximately 100 nm. In a typical experimental setup, the fluorophores near the interface can

be excited by the evanescent field when they have the capacity for electronic transition with or close to the wavelength of the laser beam.

The Nikon Eclipse Ti2 is a highly advanced and versatile fluorescence microscope that is widely used in various biological studies. With its cutting-edge modular design, the Nikon Eclipse Ti2 provides unparalleled flexibility and adaptability to suit a diverse array of applications. With cutting-edge imaging capabilities, such as motorized stage movement, autofocus, and high-speed camera systems, the Ti2 allows for accurate and efficient data acquisition. In addition, its ability to work with different fluorescence imaging techniques, like confocal microscopy and total internal reflection fluorescence (TIRF) microscopy, makes it even more valuable for a wide range of research applications.

In the course of my current thesis, I have employed the Nikon Eclipse Ti2 fluorescence microscope to investigate the dynamic fluorescence changes that arise during the enzymatic hydrolysis of a probe utilizing Förster Resonance Energy Transfer (FRET). The Nikon Eclipse Ti2 has emerged as an indispensable asset in this endeavor, facilitating high-resolution fluorescence imaging of the probe and its interactions with the enzyme. Moreover, the versatility and advanced features of the Nikon Eclipse Ti2 have proven instrumental in conducting intricate fluorescence experiments, underscoring its significance as a sophisticated tool in contemporary biological research. The findings obtained through the utilization of the Nikon Eclipse Ti2 fluorescence microscope contribute to our understanding of enzymatic processes and highlight its pivotal role in advancing knowledge in the field of molecular biology.

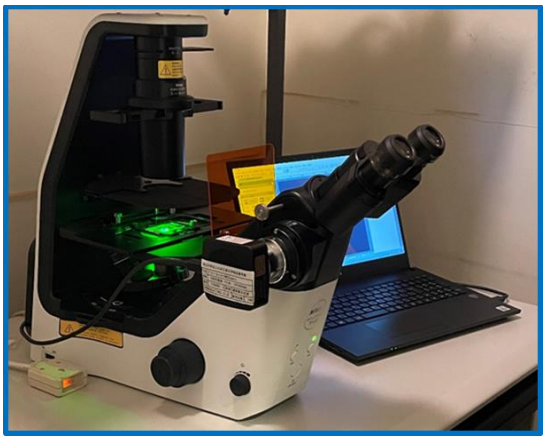

Figure 11. *Fluorescence microscopy (Nikon Eclipse Ti2) used in my study*

2.6 Cyclic Voltammetry (CV)

Cyclic voltammetry (CV) is a widely used electrochemical technique that enables the study of the reduction and oxidation processes of molecular species. CV is also extremely useful for studying electron transfer-initiated chemical reactions, including catalysis[17]. The working electrode's potential varies over time in cyclic voltammetry. The term "cyclic" refers to the way it slopes down in the opposite direction to return to the initial potential after reaching the peak potential. The scan rate represented by V/s, is the rate at which voltage changes with time. Working, reference, and counter electrodes must be dipped in the analyte solution including a supporting electrolyte to set up a cyclic voltammetry apparatus.

Working electrode: The working electrode serves as the site where the analyte undergoes oxidation or reduction processes. Typically comprised of inert metals such as platinum, gold, and silver, or materials like glassy carbon, this electrode interface plays a crucial role in facilitating electrochemical reactions during experimentation.

Reference electrode: Reference electrode maintains a relatively stable potential, making it a reference point for assessing the potentials of other working and counter electrodes. Commonly utilized reference electrodes include the Ag/AgCl/KCl electrode, standard Calomel electrode (Hg/HgCl/KCl), and Standard Hydrogen Electrode (SHE), among others.

Counter electrode: The counter electrode plays a crucial function in either supplying or accepting electrons to ensure the continuity of the circuit, depending on the electrochemical reaction occurring at the working electrode. Essentially, it assures that if oxidation happens at the working electrode, its corresponding opposite reaction occurs at the counter electrode, and vice versa. To avoid a bottleneck in electron kinetics at the counter electrode, it is common for its surface area to be larger than that of the working electrode. The counter electrode is typically made of platinum, gold, or silver.

Supporting electrolyte: The supporting electrolyte typically consists of an ionic salt with elevated conductivity, introduced into the electrolytic solution alongside the analyte. Its principal role is to augment the conductivity of the analyte and to mitigate the occurrence of the so-called IR drop, which could potentially shift peaks. This aspect is particularly critical as it directly influences the determination of the HOMO-LUMO level in our study.

To carry out cyclic voltammetry on the analyte (particularly, dyes in this research), it was dissolved in dimethyl formamide (DMF) with tetra butyl ammonium hexafluorophosphate (0.1M) as the supporting electrolyte. The CV measurements were performed using a scan rate of 10mV/s. A high concentration of the supporting electrolyte was used since the dye being studied had lesser conductivity. The initial peak apparent on the CV curve corresponds to the first oxidation state of the molecule, which can be used to estimate the energy level of the Highest Occupied Molecular Orbital (HOMO). In contrast, the corresponding peak of the material indicates the energy level of the Lowest Unoccupied Molecular Orbital (LUMO). Before performing the cyclic voltammetry analysis on the dyes, the device was calibrated using ferrocene as the reference standard.

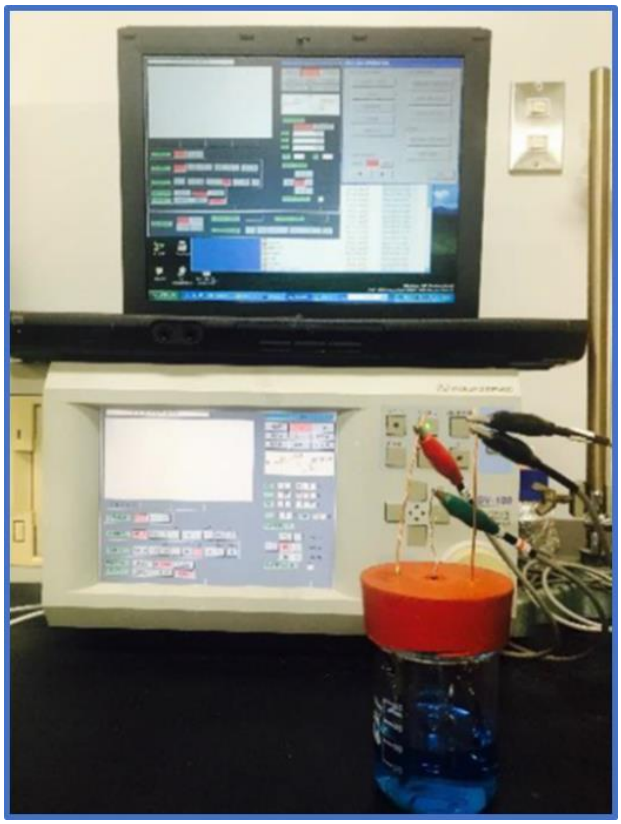

Figure 12. *The CV measuring apparatus is arranged beside the electrochemical cell*

2.7. High-Performance Liquid Chromatography (HPLC)

High Performance Liquid Chromatography (HPLC), is a sophisticated analytical equipment used to separate dissolved chemicals in a solution[18]. The system consists of a pressurized sample input, a column containing a stationary phase, a pump for dispersing solvents as the mobile phase, and a detector [19]. The specimen is introduced and then traverses the column. The operational mechanism of HPLC involves introducing analytes into the mobile phase flow and carrying them onto the column that contains the stationary phase. The analytes that do not interact with the stationary phase pass through the column and are the first to elute from it. The analytes that exhibit strong interactions with the stationary phase are retained on the column and are not observed further. The analytes that lie within the range between these two extremes are the ones that remain in the column for a certain period. Each analyte has a distinct duration of time. Therefore, after the column, the various constituents of the analyte sample can be isolated and identified. The operational principle of HPLC is illustrated in Figure 13.

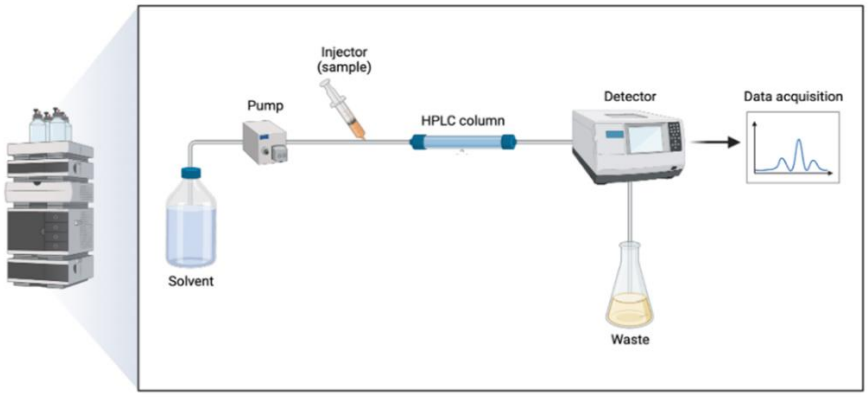

Figure 13. *Schematic working principle of HPLC*

The separation of components in a liquid mixture is achieved by utilizing their varying interactions with the stationary phase, leading to distinct flow rates for each component[20]. The mobile phase facilitates the mobility of various components of the mixture. The interactions

between the sample and column are determined by the adsorbent material of the column. The components in a mixture can be separated based on their adsorption properties using different types of columns. Alumina or silica columns are used for separation based on differences in adsorption [21], while solid columns functionalized with sulfonic acid are used for ion exchange separation [22]. Size-exclusion separation is achieved using columns made of porous silica or polymeric particles.

The High-Performance Liquid Chromatography (HPLC) utilized in this present thesis is depicted in Figure 14. The synthesized squaraine dyes, dye peptide conjugates and dye intermediates in this thesis were evaluated using high-performance liquid chromatography (HITACHI) with a chromolith analytical column (RP – 18e, φ 4.6 mm × 100 mm) and Xterra MS C8-5µm column (4.6 × 150 mm; made by Waters), Integrator D – 5700, UV-Vis detector L – 7420, and pump L - 7100.

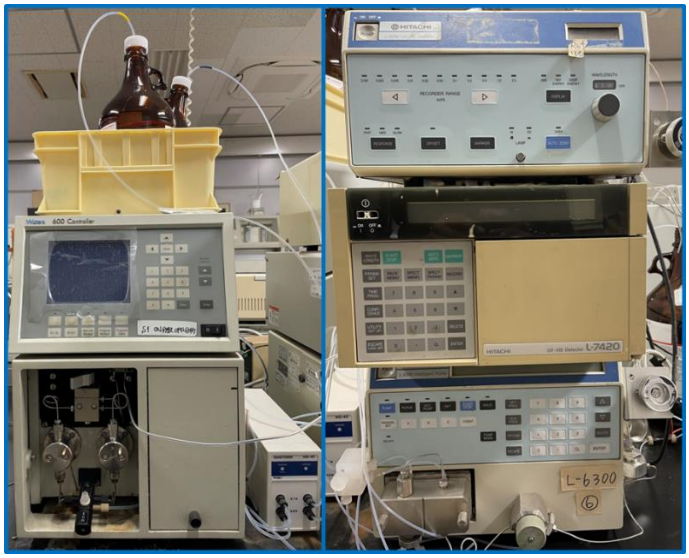

Figure 14. *HPLC used during our study*

2.8 Incubator

An incubator within laboratory settings serves as a meticulously controlled habitat tailored to foster the proliferation of microbiological or cellular cultures. Its primary function revolves around the maintenance of optimal environmental parameters including temperature, humidity, and often CO_2 and oxygen concentrations. Analogous to a protective enclosure crafted from stainless steel, it shields its inhabitants from external disruptions, guaranteeing an environment conducive to their growth and reproductive processes. Enzyme kinetics, protein folding, and other biological operations often demand specific temperatures for maximum performance. Incubators facilitate the execution of these reactions with specific parameters, guaranteeing consistent results and precision.

In my current thesis, the EYELA SLI-400 incubator is used for enzymatic hydrolysis of the probe SQ-122 PC.

Figure 15. *Incubator used in our work*

2.9 Gaussian Structure Optimization

It has been determined that the electron, an atomic particle, exhibits a dual nature, meaning it displays characteristics of both a particle and a wave. The particle character of an object is substantiated by its mass and charge, yet it also demonstrates a diffraction pattern akin to that of a wave. Wave functions can explain the characteristics of electrons. Schrodinger was the first to document these wave functions and their associated equations, which are referred to as "Schrodinger's wave equation for a particle in 1D". This equation characterizes the variations in wave function concerning time and spatial position caused by quantum phenomena.

Gaussian is a popular computational chemistry software package that is widely used for performing density functional theory (DFT) calculations. DFT is a quantum mechanical modeling method used to study the electronic structure of molecules and solids. DFT is a quantum mechanical approach that aims to directly compute the electron density, eliminating the need to first determine the wave function. This sets it apart from the semi-empirical and ab initio techniques. In the context of Density Functional Theory (DFT), the task of determining the wave function of a system is substituted with the analogous task of determining the electron density. The computation was performed using the G09 software package, with the structure being inputted using the Gauss view software. Subsequently, the input program was utilized for quantum computation employing TDDFT. The calculation was performed utilizing LSDA (Linear Spin Density Approximation) and the 6311G basis set. The computation was performed in the singlet state, employing default spin and without considering solvation effects. The calculation utilized 1000 MB of CPU memory.

3. References

1. Romani, A.; Clementi, C.; Miliani, C.; Favaro, G. Fluorescence Spectroscopy: A Powerful Technique for the Noninvasive Characterization of Artwork. *Acc. Chem. Res.* **2010**, *43*, 837–846, doi:10.1021/ar900291y.

2. Pyykkö, P. Theory of NMR Parameters. From Ramsey to Relativity, 1953 to 1983. In *Calculation of NMR and EPR Parameters*; 2004; pp. 7–19 ISBN 9783527601677.

3. Diehl, B. Chapter 1 - Principles in NMR Spectroscopy. In; Holzgrabe, U., Wawer, I., Diehl, B.B.T.-N.M.R.S. in P.A., Eds.; Elsevier: Amsterdam, 2008; pp. 1–41 ISBN 978-0-444-53173-5.

4. Wong, K.C. Review of NMR Spectroscopy: Basic Principles, Concepts and Applications in Chemistry. *J. Chem. Educ.* **2014**, *91*, 1103–1104, doi:10.1021/ed500324w.

5. Zia, K.; Siddiqui, T.; Ali, S.; Farooq, I.; Zafar, M.S.; Khurshid, Z. Nuclear Magnetic Resonance Spectroscopy for Medical and Dental Applications: A Comprehensive Review. *Eur. J. Dent.* **2019**, *13*, 124–128, doi:10.1055/s-0039-1688654.

6. Singhal, N.; Kumar, M.; Kanaujia, P.K.; Virdi, J.S. MALDI-TOF Mass Spectrometry: An Emerging Technology for Microbial Identification and Diagnosis. *Front. Microbiol.* **2015**, *6*.

7. Leopold, J.; Popkova, Y.; Engel, K.M.; Schiller, J. Recent Developments of Useful MALDI Matrices for the Mass Spectrometric Characterization of Lipids. *Biomolecules* **2018**, *8*, doi:10.3390/biom8040173.

8. Ho, C.S.; Lam, C.W.K.; Chan, M.H.M.; Cheung, R.C.K.; Law, L.K.; Lit, L.C.W.; Ng, K.F.; Suen, M.W.M.; Tai, H.L. Electrospray Ionisation Mass Spectrometry: Principles and Clinical Applications. *Clin. Biochem. Rev.* **2003**, *24*, 3–12.

9. Prabhu, G.R.D.; Williams, E.R.; Wilm, M.; Urban, P.L. Mass Spectrometry Using Electrospray Ionization. *Nat. Rev. Methods Prim.* **2023**, *3*, 23, doi:10.1038/s43586-023-00203-4.

10. Schermelleh, L.; Heintzmann, R.; Leonhardt, H. A Guide to Super-Resolution

Fluorescence Microscopy. *J. Cell Biol.* **2010**, *190*, 165–175, doi:10.1083/jcb.201002018.

11. Hell, S.W. Far-Field Optical Nanoscopy. *Science (80-.).* **2007**, *316*, 1153–1158, doi:10.1126/science.1137395.

12. Fluorescence Microscopy. In *Molecular Fluorescence*; 2012; pp. 327–348 ISBN 9783527650002.

13. Xu, C.; Webb, W.W. Measurement of Two-Photon Excitation Cross Sections of Molecular Fluorophores with Data from 690 to 1050 Nm. *J. Opt. Soc. Am. B* **1996**, *13*, 481–491, doi:10.1364/JOSAB.13.000481.

14. Lippincott-Schwartz, J.; Patterson, G.H. Development and Use of Fluorescent Protein Markers in Living Cells. *Science* **2003**, *300*, 87–91, doi:10.1126/science.1082520.

15. Shaner, N.C.; Steinbach, P.A.; Tsien, R.Y. A Guide to Choosing Fluorescent Proteins. *Nat. Methods* **2005**, *2*, 905–909, doi:10.1038/nmeth819.

16. Amos, W.B.; White, J.G.; Fordham, M. Use of Confocal Imaging in the Study of Biological Structures. *Appl. Opt.* **1987**, *26*, 3239–3243, doi:10.1364/AO.26.003239.

17. Elgrishi, N.; Rountree, K.J.; McCarthy, B.D.; Rountree, E.S.; Eisenhart, T.T.; Dempsey, J.L. A Practical Beginner's Guide to Cyclic Voltammetry. *J. Chem. Educ.* **2018**, *95*, 197–206, doi:10.1021/acs.jchemed.7b00361.

18. Erni, F.; Frei, R.W. Two-Dimensional Column Liquid Chromatographic Technique for Resolution of Complex Mixtures. *J. Chromatogr. A* **1978**, *149*, 561–569, doi:https://doi.org/10.1016/S0021-9673(00)81011-0.

19. Zapata, M.; Rodríguez, F.; Garrido, J. Separation of Chlorophylls and Carotenoids from Marine Phytoplankton: A New HPLC Method Using a Reversed Phase C8 Column and Pyridine-Containing Mobile Phases. *Mar. Ecol. Prog. Ser.* **2000**, *195*, 29–45, doi:10.3354/meps195029.

20. Rodrigues, A.E.; Zuping, L.; Loureiro, J.M. Residence Time Distribution of Inert and Linearly Adsorbed Species in a Fixed Bed Containing "Large-Pore" Supports: Applications in Separation Engineering. *Chem. Eng. Sci.* **1991**, *46*, 2765–2773,

doi:https://doi.org/10.1016/0009-2509(91)85145-N.

21. Heinemann, G.; Köhler, J.; Schomburg, G. New Polymer Coated Anion-Exchange HPLC-Phases: Immobilization of Poly (2-Hydroxy, 3N-Ethylenediamino) Butadiene on Silica and Alumina. *Chromatographia* **1987**, *23*, 435–441, doi:10.1007/BF02311821.

22. Viklund, C.; Svec, F.; Fréchet, J.M.; Irgum, K. Fast Ion-Exchange HPLC of Proteins Using Porous Poly(Glycidyl Methacrylate-Co-Ethylene Dimethacrylate) Monoliths Grafted with Poly(2-Acrylamido-2-Methyl-1-Propanesulfonic Acid). *Biotechnol. Prog.* **1997**, *13*, 597–600, doi:10.1021/bp9700667.

CHAPTER 3 : Design and Synthesis of Novel Squaraine Dye with Highly Enhanced Far-Red Fluorescence and its Interaction with a Model Protein

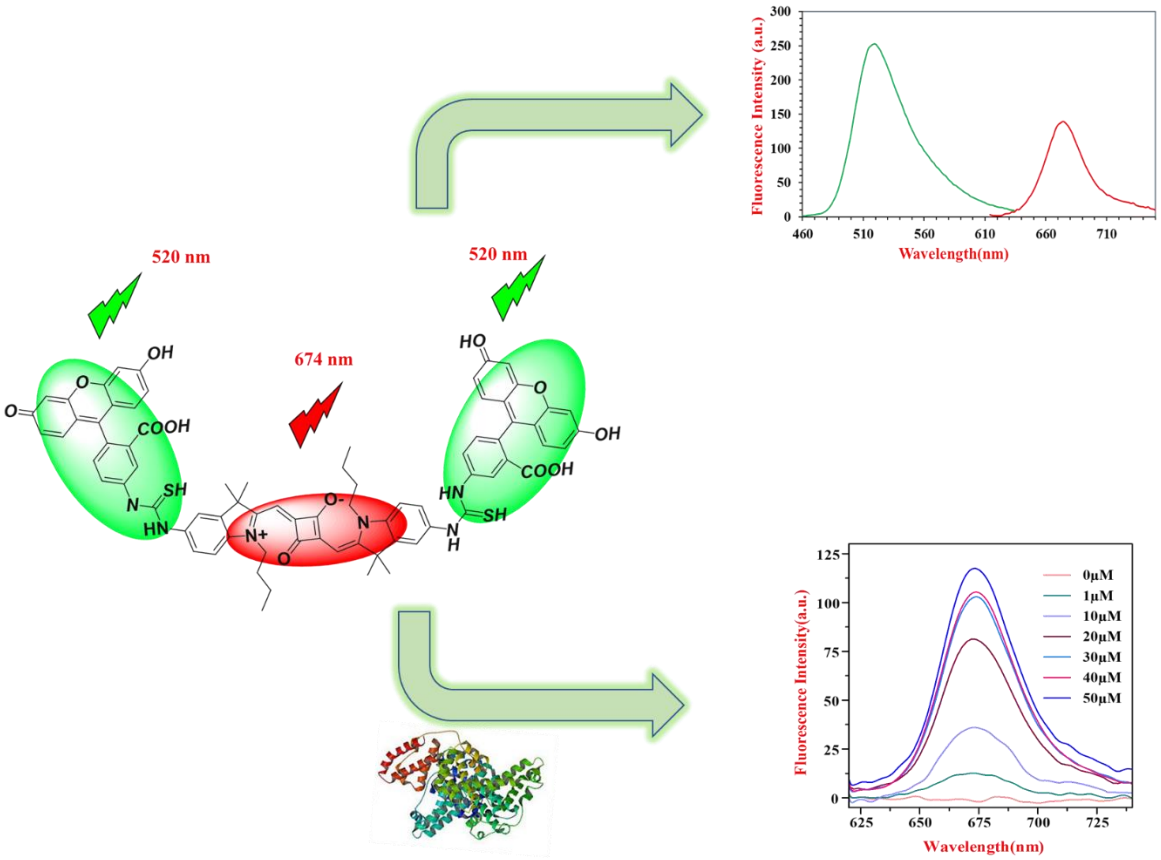

Abstract: Fluorescent probes have multiple applications that utilize photoinduced electron transfer (PET) to mitigate fluorescence. A novel symmetrical squaraine (SQ) dye, modified with an amine group, and a conjugate of fluorescein isothiocyanate (FITC) with SQ, are designed and synthesized. Subsequently, the compounds' structures and photophysical properties are analyzed and characterized. The symmetrical SQ dye exhibits complete fluorescence suppression in polar solvents, which is caused by the main pathway of photoinduced electron transfer (PET) leading to quenching. However, when the FITC-SQ-FITC dye combination is used, it decreases the aggregation of both SQ and FITC components. This leads to a remarkable 47-fold increase in the intensity of far-red fluorescence at 674 nm. The notable enhancement in the intensity of far-red fluorescence can be ascribed to the synergistic impact of mitigating aggregation-induced quenching (ACQ) and photoinduced electron transfer (PET). The newly developed FITC–SQ–FITC dye conjugate eliminates the far-red fluorescence in phosphate buffer saline (PBS) because of strong dye aggregation, as confirmed by spectral absorption studies. When in PBS, it forms a significant interaction with bovine serum albumin (BSA) ($Ka = 1.1 \times 10^4\ M^{-1}$), which is utilized as a model protein. This interaction disrupts the aggregation of the dye by BSA and leads to an increase in far-red fluorescence associated with SQ. The increase in fluorescence is directly proportional to the concentration of BSA. The fluorescence at 674 nm increased significantly by a factor of 117 when the concentration of BSA was increased by 25 times. This indicates that the proposed FITC-SQ-FITC is a highly effective probe for studying dye-protein interactions in the far-red range.

3.1 Introduction

Electronic excitation energy transfer (EET) is a commonly employed mechanism for labeling biological molecules [1]. Molecular cascading using a range of dyes as donor (D) and acceptor (A) has become increasingly popular in EET operations. The successful exploitation of spectral overlap in energy transfer systems has allowed for an artificial increase in the Stokes shift. This is achieved through through space energy transfer [2]. Two different pathways for EET, namely fluorescence resonance energy transfer (FRET) and through bond energy transfer (TBET), have been extensively studied. The distance between the donor and acceptor fluorophore moieties and

the extent of the overlap between their absorption and emission spectra are crucial factor in determining FRET efficiency [3]. Various phenomena, including intermolecular charge transfer (ICT), photoinduced electron transfer (PET), FRET, and TBET, have been extensively utilized in the creation and advancement of innovative chemical and biological sensing molecular probes[4-8]. A wide range of small-molecule fluorophores with different core structures, including BODIPY, fluorescein, rhodamine, cyanine, naphthalimide, and coumarin, have been extensively utilized in the development of PET-based fluorescent probes. The pyrrole ring with an abundance of electrons has been found to effectively suppress the fluorescence of the designed fluorescence component. This is achieved through an enhanced process known as PET, which reduces the background fluorescence and improves the signal-to-noise ratio. This method proves to be more effective compared to the traditional single-atom electron donors like oxygen [5][6], nitrogen, and selenium, ([7][8]) [9]. The mechanism behind PET-based fluorescent probes has been explained using frontier orbital theory [10–13]. The use of fluorescent sensors based on the photoinduced electron transfer (PET) approach has generated significant interest due to their wide range of potential applications [14]. However, the majority of these PET systems function efficiently in the UV-visible range, whereas just a small number of them operate in the near-infrared (NIR) range. A careful examination of the Weller equation [15] reveals that it is challenging to identify a PET system when the energy difference between the highest occupied molecular orbital (HOMO) and the lowest unoccupied molecular orbital (LUMO) is extremely tiny, as is the case with near-infrared (NIR) fluorescent dyes.

Fluorescent dyes that are sensitive to far-red/near-infrared (NIR) light have a multitude of applications in the fields of biomedical research, nanotechnology, and material science. Because of their greatly reduced auto-fluorescence in biological fluids and ability to penetrate deep tissue, these NIR fluorescent probes are extremely appealing for non-invasive in vivo imaging [16]. Fluorescent labels and probes used in biological and pharmaceutical research have sparked significant interest. One particular group of sensitizing dyes, known as squaraine, has caught the attention of researchers. These dyes offer the advantage of adjustable absorption and emission properties, ranging from visible to near-infrared wavelengths. Additionally, they possess high molar absorptivity and moderate quantum yields, making them valuable tools in various

applications [17]. Squaraine dyes offer the advantage of being able to alter their absorption and emission properties across a wide range of wavelengths, including the visible and infrared regions. This makes them highly suitable for applications in fluorescence imaging. Squaraine dyes possess unique chemical and physical properties that make them highly versatile in various applications. These include serving as NIR fluorescent probes, environmental sensors[18], molecular sensors [19], bioimaging tools, and biochemical labeling agents [20]. Indolenine-based squaraines are known for their superior photostability compared to similar compounds like cyanines and other aromatic squaraines [21]. This makes them highly sought after for the development of fluorescent labels and probes. A FRET system has been developed using two naphthalimide donors and a squaraine acceptor. This system functions as a FRET turn-off, which is caused by the decomposition of the acceptor chromophore due to the presence of the analyte [22].

This study focuses on the synthesis of a symmetrical squaraine dye with two fluorescein isothiocyanate donors and squaraine as an acceptor. The resulting dye emits fluorescence in the far-red wavelength region. This dye exhibited a highly effective energy transfer of 94.69%, resulting in emission in the far-red region. In contrast, the Squaraine dye with an amine-functionalized group did not exhibit any fluorescence in the far-red region. However, when it came to the FITC-flanked squaraine dye, the fluorescence emission in the far-red region increased by a staggering 47 times compared to the regular squaraine dye. The significant enhancement in the fluorescence emission of the new squaraine dye has been elucidated by considering the phenomena of aggregation caused by quenching (ACQ) and PET.

3.2 Experimental

3.2.1 Materials and Methods

All the chemicals, solvents, and reagents used for synthesis and photophysical characterization are of high quality and are utilized as they are received without any modifications. The synthesized symmetrical squaraine dyes and dye intermediates were examined using MALDI-TOF/FAB-mass spectroscopy in positive ion monitoring mode and nuclear magnetic resonance spectroscopy (NMR 500 MHz for ^{1}H NMR) to determine their structure. The solution's electronic absorption spectra were measured using a JASCO V-530 UV/VIS spectrophotometer, which is capable of

detecting UV, visible, and near-infrared light. Simultaneously, the fluorescence emission spectrum was captured using a JASCO FP-6600 spectrophotometer, which is a fluorescence emission spectrometer. A three-electrode electrochemical cell was utilized to conduct cyclic voltammetry (CV) to determine the energy level of dyes. The cell consisted of a Pt foil serving as the counter electrode, a Pt wire as the working electrode, and a saturated calomel electrode (SCE) as the reference electrode.

3.2.2 Synthesis of SQ, FITC-SQ-FITC and Dye Intermediates

The FITC-flanked symmetrical SQ dye (FITC–SQ–FITC) and the amine-functionalized SQ dye utilized in this study were produced according to **Scheme 1**.

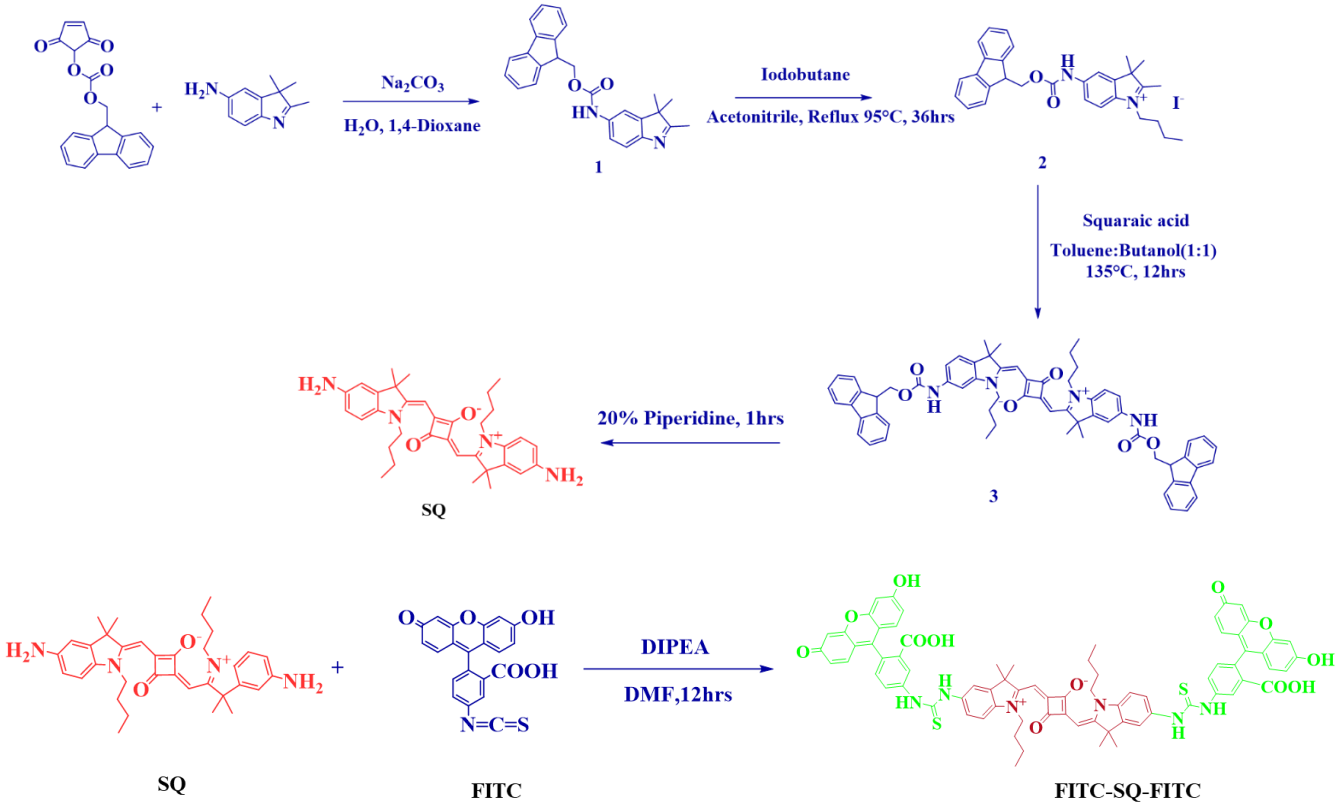

Scheme 1. *Synthesis of the target far-red dye probes.*

3.2.2.1 Synthesis of Compound 1

2,3,3-trimethyl-3H-indol-5-amine (2gm, 11.478mmol, 1 eq.) was added in a solution of Na_2CO_3 (6.082g, 57.39mmol, 5eq) in 20 ml water and 1,4-dioxane (20 mL) and the reaction was cooled to

0 °C. Fmoc-OSu (1.1eq, 12.221mmol) was added to the mixture and stirred overnight from 0°C to room temperature. The resulting mixture was washed with Et_2O (40 mL). The aqueous layer was neutralized with citric acid monohydrate and the desired product was extracted with EtOAc (4 × 25 mL). The combined organic layers were washed with brine, dried over Na_2SO_4, filtered, and concentrated in vacuo. The mass of the compound was 5.197 g giving 58.60% yield. HPLC analysis of the product suggests that the compound was 99% pure. High Resolution-ESI-TOF mass (measured 397.19160 $[M + H]^+$; 396.18378 calculated).

3.2.2.2 Synthesis of Compound 2

In a round bottom flask, one equivalent of (9H-fluoren-9-yl)methyl (2,3,3-trimethyl-3H-indol-5-yl)carbamate (compound 1)(1eq, 12.62mmol, 5g) and 1-Iodobutane (3 eq, 36.86mmol, 4.3 ml) were dissolved in dehydrated acetonitrile and the reaction was refluxed for overnight to give the corresponding alkyl-3H-indolium iodide. After completion of the reaction as monitored by TLC, the solvent was evaporated and the crude product was washed with ample diethyl ether. The crude product (6.12g) was purified by silica gel column chromatography (Methanol: Chloroform). The pure compound after column chromatography weighed 5.3 g and the yield was 21.8%. High Resolution-ESI-TOF mass (measured 453.25420 $[M]^+$;453.25365 calculated).

3.2.2.3 Synthesis of Compound 3

The dye (Fmoc-SQ-Fmoc) was synthesized using two equivalents of 5-((((9H-fluoren-9-yl)methoxy)carbonyl)amino)-1-butyl-2,3,3-trimethyl-3H-indol-1-ium (compound 2) (2.20916mmol, 1.0361g) and squaric acid(1 eq, 1.0458 mmol, 125mg) in 1-butanol: toluene mixture (1:1, v/v). The reaction mixture was subjected to reflux overnight using a Dean–A stark trap. Once the reaction was completed, the mixture was cooled, the solvent was removed by evaporation, and the product was purified using silica gel column chromatography. Chloroform: methanol (9:1) was used as the eluting solvent. The weight of the product was 800 mg. The physical and spectroscopic data of symmetrical Fmoc-SQ-Fmoc dye are as follows; Yield 56 % and HPLC purity 99 %. High Resolution-ESI-TOF mass (measured 982.46693 $[M]^+$; 982.46694 calculated).

3.2.2.4 Synthesis of SQ

Compound 3 (0.7633mmol, 795mg) was taken in a round bottom flask and 20% piperidine in DMF was added to the flask. The reaction mixture was stirred at room temperature for 3 hours. The reaction was monitored using TLC and the solvent was evaporated and the product was purified by alumina oxide column chromatography using chloroform: methanol as the eluting solvent. The weight of the product was 300 mg and the yield was 73%. High Resolution-ESI-TOF mass (measured 538.33078 $[M]^+$; 538.33078 calculated). ^{1}H NMR (DMSO-d6): δ 0.89 -0.92 (t, 6H), 1.31-1.39 (m, 2H), 1.59 (s, 12H), 1.60-1.67 (m, 4H), 5.10 (s, 1H), 5.63(s, 4H), 6.52-6.53(d, 2H), 6.68(d, 2H), 6.95-6.97(d, 2H), 8.26 (s, 2H).

3.2.2.5 Synthesis of FITC-SQ-FITC Dye

Diisopropylethylamine (DIPEA, 69.6 µl, 0.4 mmol, 2 eq) was added to a solution of SQ (100 mg, 0.2mmol, 1eq), and FITC (155.752mg, mmol, 2eq) in dimethylformamide (DMF, 5 ml) in room temperature. The mixture was stirred overnight. The complete conversion was determined using liquid-chromatography–mass spectrometry. After evaporating the solvent under reduced pressure and purifying the residue through silica gel chromatography with chloroform: methanol as the eluting solvent, the resulting product FITC–SQ–FITC, was obtained in 55 % yield. High Resolution-ESI-TOF mass (measured 1357.32 $[M+K]^+$; 1357.51631 calculated). ^{1}H NMR (MeOH-d3): δ 0.84 - 0.88 (t,6H), δ 0.90 - 0.94 (t,6H), δ 1.31-1.39 (m,2H), δ 1.67 (s, 12H), δ 5.83 (s,1H), δ 5.87 (s,1H), δ 6.45-6.53 (m,12H), 7.11-7.16 (m,12H), 7.30-7.31 (d,1H), 7.34-7.35 (d,1H), 7.36-7.37(d,1H), 7.50-7.51 (d,1H), 7.67-7.68 (d,1H), 7.96 (d,1H).

3.3 Results and Discussion

3.3.1 Analysis of the Electronic Absorption and Fluorescence Emission Spectra

The absorption spectra depicted in **Figure 1.** reveal distinct absorption peaks of FITC–SQ–FITC, indicating the coexistence of FITC and SQ components within the designed probe. In methanol, these peaks manifest at absorption maxima (λ_{max}) of 486 and 656 nm, respectively. The absorption band observed at λ_{max} of 656 nm, accompanied by a vibronic shoulder at 610 nm, corresponds to the SQ dye, while the second band at λ_{max} 486 nm corresponds to FITC. Specifically, the SQ

constituent of the probe exhibits a λ_{max} at 670 nm with a vibronic shoulder at 625 nm, yielding an absorbance ratio of the vibronic shoulder to the prominent peak estimated at 0.5. This ratio, indicative of aggregate formation, tends to be more pronounced in the solid state due to enhanced intermolecular interactions. A higher ratio signifies a greater degree of dye aggregation. Examination of the absorption spectrum of FITC–SQ–FITC reveals an absorbance ratio for the vibronic shoulder to the main monomeric dye absorption peak estimated at 0.28, suggesting a lower extent of dye aggregation. This diminished aggregation is attributed to the steric hindrance imposed by two terminal and bulky FITC moieties, which impede dye aggregation.

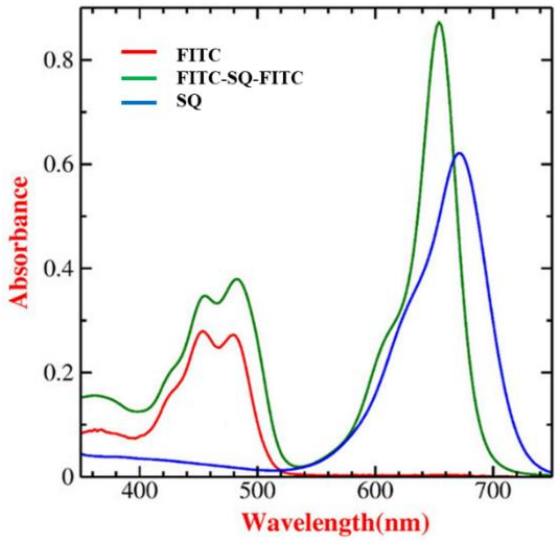

Figure 1. *UV–visible–near-infrared (NIR) electronic absorption spectra of fluorescein isothiocyanate (FITC), FITC– SQ–FITC, and SQ in 10μm methanol solution.*

Considering the absorption maxima of FITC and SQ, which appear at 480 nm and 650 nm respectively, efforts were made to measure the emission spectra of the newly designed FITC–SQ–FITC. This was achieved by exciting the sample at 450 nm and 610 nm, which are below the respective λmax values of FITC and SQ, as depicted in **Figure 2**. Additionally, the optical parameters derived from both absorption and emission spectra are summarized in **Table 1**. Upon excitation at 450 nm, a single emission band was observed with a peak at 520 nm, corresponding to the emission of FITC. It is noteworthy that FITC alone exhibited a broad and intense emission centered at 512 nm. In contrast, when excited at 610 nm, which corresponds to the absorption

wavelength of SQ, no fluorescence was observed from SQ alone, indicating complete quenching. However, under the same conditions, FITC–SQ–FITC demonstrated enhanced fluorescence with emission peaks at 670 nm, which was 47 times higher compared to the emission from SQ when excited at 610 nm.

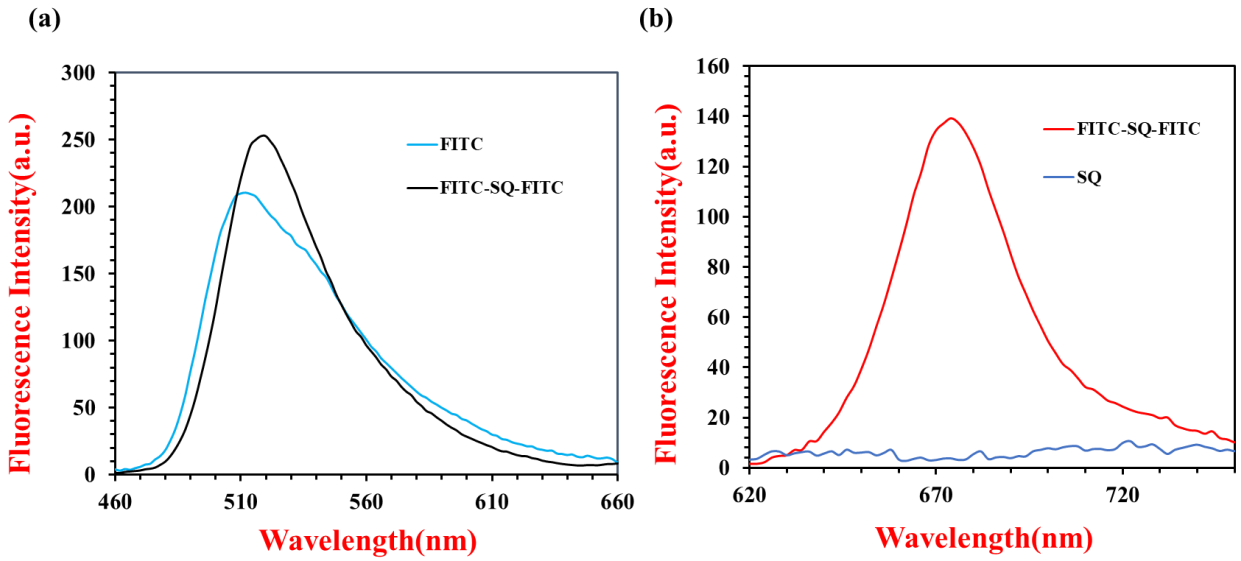

Figure 2. *a) The spectra were measured for FITC and FITC–SQ–FITC in MeOH (10μM), with an excitation wavelength of 450 nm. b) The spectra were measured for FITC–SQ–FITC and SQ in MeOH (10μM), with an excitation wavelength of 610 nm.*

Table 1. *The optical properties of SQ, FITC-SQ-FITC, and FITC in methanol were determined through analysis of absorption and spectrum emission studies.*

Compound	λ_{abs} [a] (nm)	λ_{em} [b] (nm)	Δ[c] (nm)	Φ_F [e]
SQ	674	-	-	0
FITC-SQ-FITC	656, 486	674, 520	20, 34	0.07, 0.32
FITC	482	512	30	0.92

UV/Vis absorption maximum, [b] Fluorescence emission maximum, [c] Stokes shift, calculated as the difference between emission and absorption maxima, [d] The energy transfer efficiency, [e] Fluorescence quantum yield (determined using Rhodamine 6G as reference).

3.3.2 Photoinduced electron transfer (PET) and aggregation caused quenching (ACQ)

The complete fluorescence quenching observed in the amine-substituted symmetrical squaraine dye (SQ) suggests its potential as an effective far-red fluorescence quencher, thereby offering opportunities for designing efficient Förster Resonance Energy Transfer (FRET) systems for the development of far-red-sensitive biological probes. Among various mechanistic pathways, aggregation-caused quenching (ACQ) and intramolecular photoinduced electron transfer (PET) have been widely utilized to elucidate the fluorescence quenching mechanisms in π-conjugated organic dyes.

The highly planar molecular structure of amine-functionalized symmetrical squaraine dye (SQ), attributed to its extended π-conjugation, predisposes it to aggregate formation, as schematically depicted in Figure 3. Previous studies by Kim et al. have highlighted the formation of blue-shifted H-aggregates in squaraine dyes, which have been associated with compromised electron injection compared to their monomeric counterparts [23,24]. Strategies involving the use of derivatives of bulky chenodeoxycholic acid have been employed to mitigate such aggregate formation, leading to improved electron injection and enhanced photoconversion efficiency [25,26].

Conversely, the SQ dye comprises an electron-rich amine group substituted in the indole ring and an electron-deficient central squaraic acid core, offering the potential for efficient intramolecular photoinduced electron transfer (PET), as depicted in Figure 3. Studies utilizing cyanine dye fluorophores have demonstrated that the presence of electron donors with free electron characteristics, such as -OH or -NH_2 groups, in combination with electron-deficient moieties results in strong fluorescence quenching due to PET. Conversely, the substitution of these free donor groups leads to the suppression of PET, resulting in significantly enhanced fluorescence [27,28].

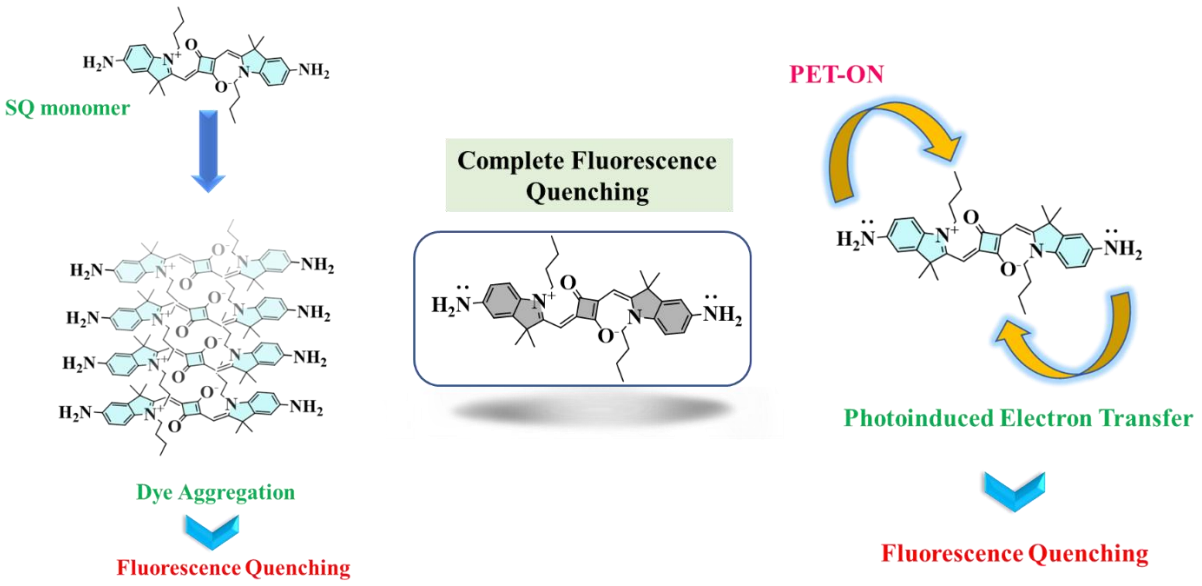

Figure 2. *The diagram illustrates the process of fluorescence quenching in SQ dye, which occurs through the formation of aggregates on the left and by photoinduced electron transfer pathways.*

To determine the primary cause of fluorescence quenching in amine-functionalized symmetrical SQ dye, we first measured and analyzed the absorption and emission spectra of the dye in various solvents such as methanol, chloroform, dimethyl sulfoxide (DMSO), and phosphate buffer saline (PBS) (**Figure 3**). The absorption spectra of a dilute concentration of standard squaraine dyes in a non-polar solvent, where the dyes exist as individual molecules, show a prominent and sharp peak in the near-infrared (NIR) wavelength range. Additionally, a minor vibronic shoulder is observed at a shorter wavelength in the blue-shifted region. Squaraine dyes with polar groups or dissolved in polar solvents exhibit a phenomenon called blue-shifted H-aggregate formation, which is the most prevalent, as well as red-shifted J-aggregate formation [29]. The formation of H-aggregates results in alterations in the absorption spectrum characteristics, including spectral broadening, a modest blue-shift in the primary absorption peak, a prominent blue-shifted vibronic shoulder, and, in extreme circumstances, an extra distinct peak in the lower wavelength area [30,31]. An examination of the absorption spectra of SQ dye depicted in Figure 3(a) indicates that the dye is present in a monomeric state or exhibits minimal aggregation in chloroform. In polar solvents, it exhibits distinct H-aggregation, with the order of aggregation being PBS>>methanol>DMSO>>chloroform. The lower wavelength region of PBS exhibited a significant absorption, which can be explained by the presence of blue-shifted H-aggregates and

the widening of the absorption peak. However, the emission spectra showed a faint fluorescence in chloroform and a total suppression of fluorescence in the other three solvents, while having differing aggregation properties (**Figure 3(b)**). This confirms that the aggregation of dye molecules in the case of SQ dye has a very minor effect on fluorescence through aggregation-caused quenching (ACQ), while photoinduced electron transfer (PET) is the main mechanism responsible for the significant reduction in fluorescence intensity.

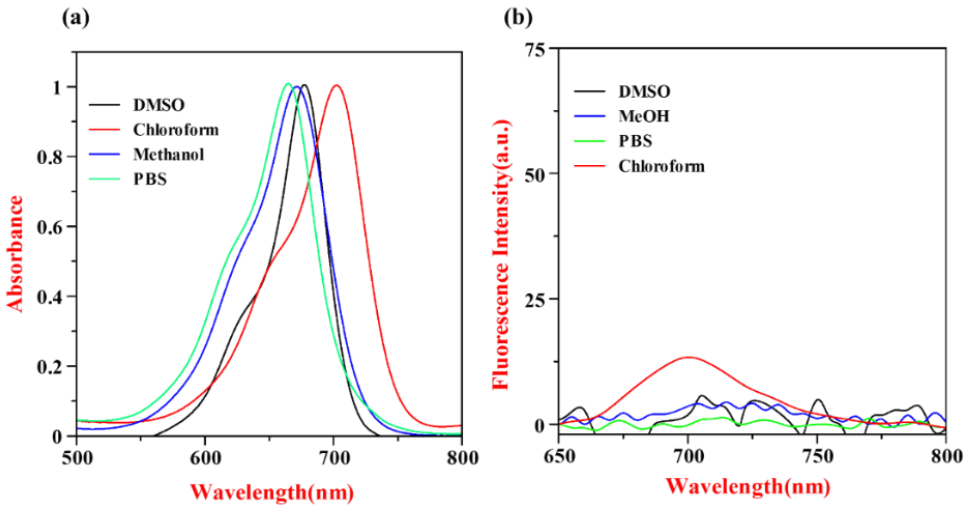

Figure 3. *(a) The normalized electronic absorption and (b) fluorescence emission spectra of the SQ-dye in various polar and non-polar solvents (10μM).*

Overall, the incorporation of amine-substituted symmetrical squaraine dyes offers a promising avenue for the development of efficient FRET-based far-red-sensitive biological probes, leveraging mechanisms such as ACQ and PET to achieve optimal fluorescence quenching and enhanced sensitivity.

There is an immense demand for fluorescence and quenching moieties that are efficient and have significant overlap in their absorption and emission spectra. This is important when developing a highly effective FRET system. The incorporation of the ability to emit light in the far-red wavelength range makes this FRET system very well-suited for effective fluorescence biosensing and bio-imaging applications. Studies have shown that the synthesized SQ dye can effectively act as a quencher of far-red fluorescence by utilizing dominating PET. Hence, the FITC-SQ-FITC far-red fluorescence probe was synthesized through the reaction between FITC and the amine group of the squaraine dye. The existence of spectral absorption characteristics of both FITC and SQ-

dye confirms the presence of both substances, as depicted in **Figure 2**. The absorption spectra of the FITC-SQ-FITC conjugate showed a more prominent absorption peak around 480 nm, which is associated with FITC, compared to FITC alone. On the other hand, the vibronic shoulder at 610 nm, which is associated with SQ, was less pronounced in the conjugate compared to the non-conjugated SQ dye. This suggests that the aggregation of dye molecules in the conjugate was hindered in comparison to the individual FITC and SQ components. The prevention of dye aggregation in the FITC-SQ-FITC conjugate was additionally confirmed through a theoretical molecular orbital calculation using Gaussian16. The calculation revealed that the optimal structure of the conjugate is non-planar, which hinders the formation of face-to-face H-aggregates, similar to SQ. This information is illustrated in **Figure 4**.

The process of conjugating FITC with a free amine group of the SQ dye results in the deactivation of PET, as illustrated in Figure 4. This leads to the emergence of far-red fluorescence caused by the SQ dye. Hence, the combined impact of inhibited ACQ (aggregation-caused quenching) and PET (photoinduced electron transfer) in the FITC-SQ-FITC conjugate results in a significant enhancement in far-red fluorescence (>47 times), as depicted in **Figure 2**. Consequently, this compound serves as an appropriate probe for far-red fluorescence.

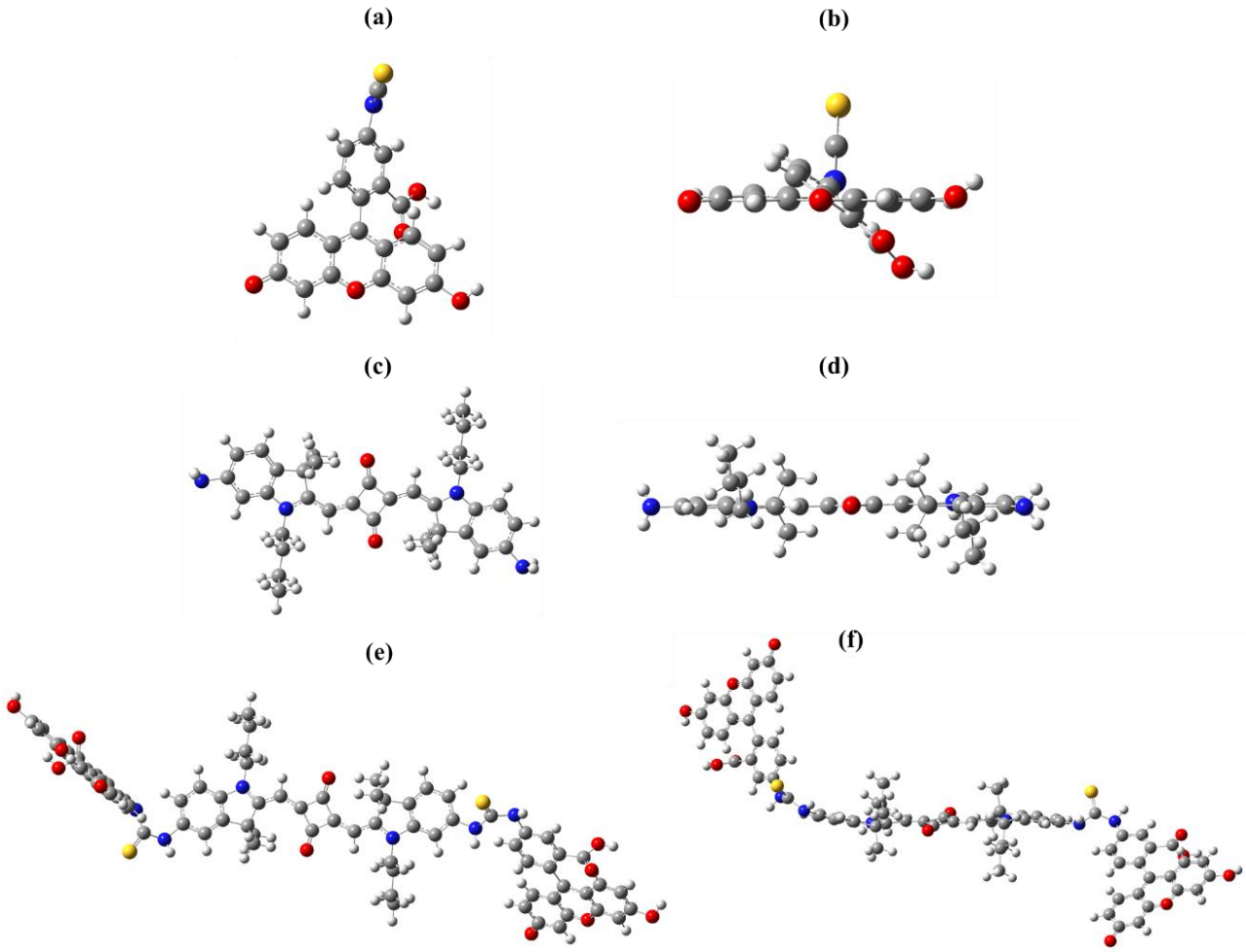

Figure 4. *Optimized structure (a) FITC side view (b) FITC face view (c) SQ side view (d) SQ face view (e) FITC-SQ-FITC side view and (f) FITC-SQ-FITC face view as calculated using Gaussian G16 program.*

3.3.3 Energy band diagram

The final compounds, including FITC, SQ, and FITC-SQ-FITC, were subjected to cyclic voltammetry (CV) measurements. The experiments were conducted at a scan rate of 10 mV/s, using 0.1 M tetrabutylammonium perchlorate as a supporting electrolyte. The HOMO energy was determined by calculating the 1st oxidation potential of the cyclic voltammogram, as depicted in **Figure 5**.

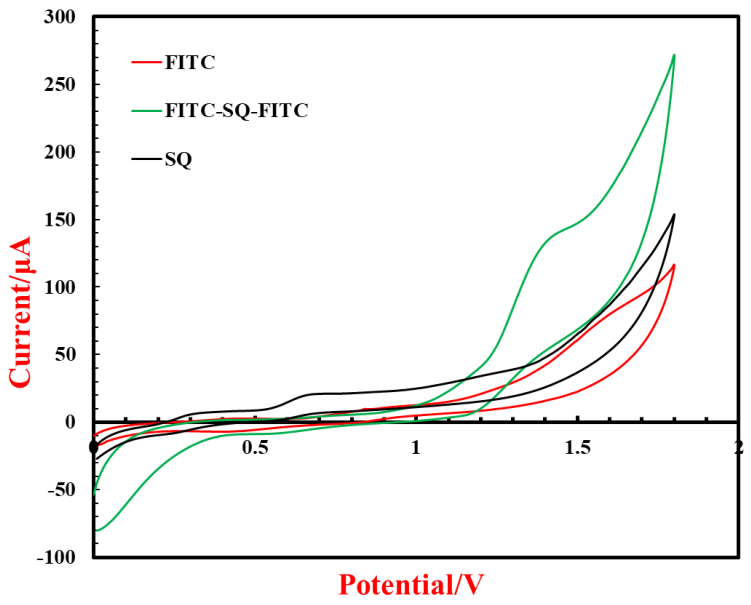

Figure 5. *Cyclic voltammograms of FITC, SQ, and FITC-SQ-FITC in DMF with 0.5 M Bu_4NPF_6 were used as the supporting electrode, and Ag/Ag^+ was used as the reference electrode. Scan rates are 10 mV/s. Ferrocene was used as an internal reference.*

To construct the energy band diagram depicted in **Figure 7**, the Energy of the lowest unoccupied molecular orbital (LUMO) was determined by utilizing the equation LUMO = HOMO + E_g. Here, E_g represents the optical band gap, which was estimated using the equation $E_g = 1240 / \lambda_{onset}$. The λ_{onset} was determined by analyzing the optical absorption edge of the absorption spectra, as depicted in **Figure 1**.

Upon excitation by a suitable light wavelength, the electron from the highest occupied molecular orbital (HOMO) is moved to the lowest unoccupied molecular orbital (LUMO) of the SQ. The receptor is located next to the SQ, and the energy level of the receptor's highest occupied molecular orbital (HOMO) is between the lowest unoccupied molecular orbital (LUMO) and HOMO levels of the SQ. As a result, the electron moves from the HOMO of the receptor to the HOMO of the SQ, preventing the electron in the LUMO of the SQ from going back to the HOMO. This leads to the occurrence of the photoinduced electron transfer (PET) effect, which suppresses the emitted fluorescence from the fluorophore. When the receptor binds to FITC, the HOMO energy of the receptor decreases and becomes lower than the HOMO energy level of the SQ. Consequently, the PET process gets blocked, resulting in a resurgence of fluorescence (**Figure 6**).

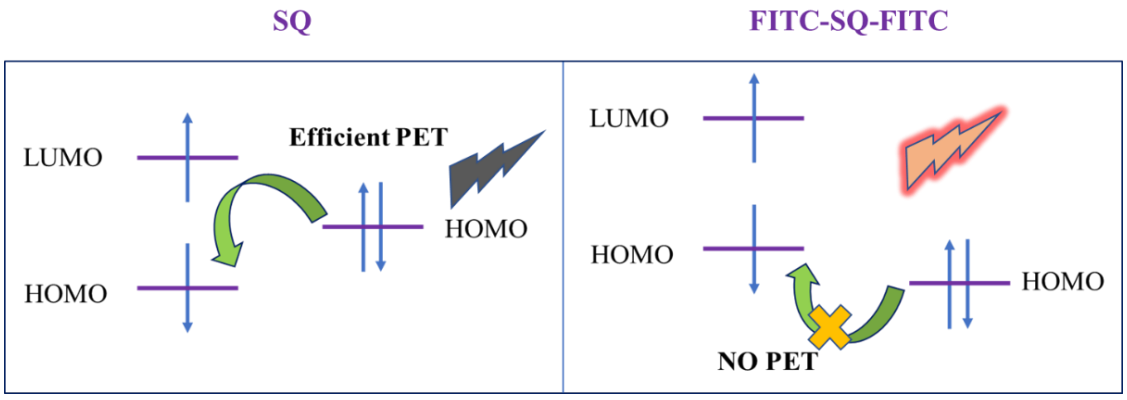

Figure 6. *Frontier orbital theory to explain the photoinduced electron transfer (PET) phenomena process in SQ and FITC-SQ-FITC.*

Table 2. summarizes the energy associated with the LUMO and Eg, in addition to the HOMO. The energy band diagram demonstrates a notable reduction in the HOMO energy level of the FITC-SQ-FITC conjugate in comparison to that of the SQ dye alone, providing additional evidence of the existence of the FITC unit. Simultaneously, it was observed that the Eg value for the conjugate was somewhat lower at 1.89 eV, in comparison to its SQ-dye counterpart with a value of 1.84 eV.

Table 2. *Physical parameters for FITC, SQ, and FITC-SQ-FITC were deduced from electrochemical and photophysical investigations.*

Compounds	HOMO (eV)	LUMO (eV)	E_g (eV)
FITC	-5.99	-3.42	2.56
SQ	-4.77	-2.92	1.84
FITC-SQ-FITC	-5.81	-3.92	1.89

The modest non-planarity in the π-conjugated molecular framework of the SQ-dye in the conjugation can be explained to the presence of the bulky FITC unit. The confirmation was

obtained through theoretical quantum chemical calculations conducted using the Gaussian G16 program. These calculations focused on the optimization of the structure, as depicted in **Figure 4**.

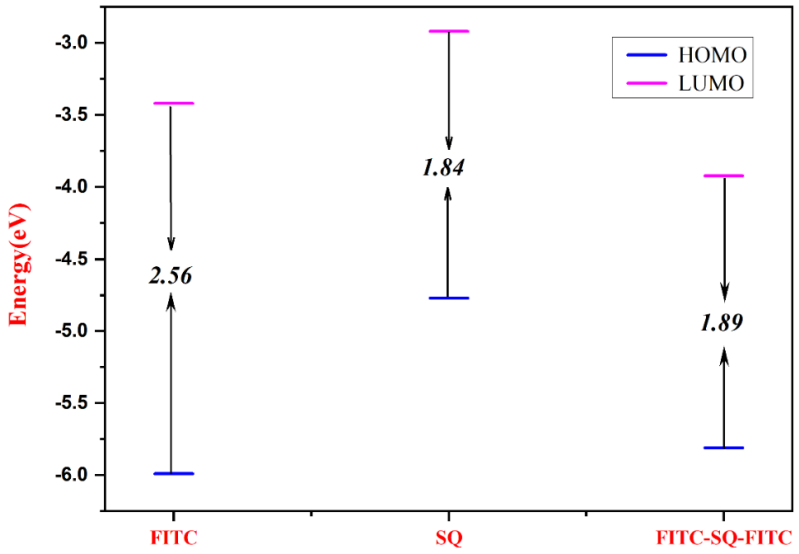

Figure 7. *Energy band diagram for FITC, SQ, and FITC-SQ-FITC.*

3.3.4 Interaction of FITC-SQ-FITC dye with BSA

The squaraine dye interaction with model proteins, including bovine serum albumin (BSA), human serum albumin (HSA), avidin, and ovalbumin, aids in understanding how the dye facilitates protein sensing. The study investigates the interactions between dyes and proteins using phosphate-buffered saline (PBS) as a buffer. This topic is of great interest in understanding ligand binding mechanisms and protein folding processes in imaging and sensing applications [31]. When studying the relationship between dyes and protein molecules, it becomes clear that noncovalent labeling of biomolecules is more effective than covalent labeling. Research has shown that BSA forms noncovalent interactions with proteins, leading to noticeable alterations in the color of the solution. As a result, using noncovalent labeling techniques avoids the need for purification procedures and reduces chemical interactions between biomolecules and dyes. This improves the usefulness of optical imaging approaches [32]. The BSA protein is composed of three distinct domains, namely I, II, and III. Each domain is further divided into two subdomains, labeled A and B. These subdomains are interconnected by a total of 17 disulfide links. BSA has three inherent fluorophores, namely tryptophan, tyrosine, and phenylalanine, which exhibit great sensitivity to

their surrounding microenvironment. Tryptophan has the greatest impact on the fluorescence of BSA compared to the other two fluorophores. BSA has two tryptophan residues, specifically Trp-212 and Trp-134[33,34]. Trp-134 is situated in the hydrophilic region on the protein's surface, while Trp-212 is positioned in the non-polar region within the protein. Trp-212 has a greater impact on the fluorescence intensity compared to Trp-134 [35,36]. **Figure 4** depicts the locations where BSA binds and the possible interactions it has with the dye.

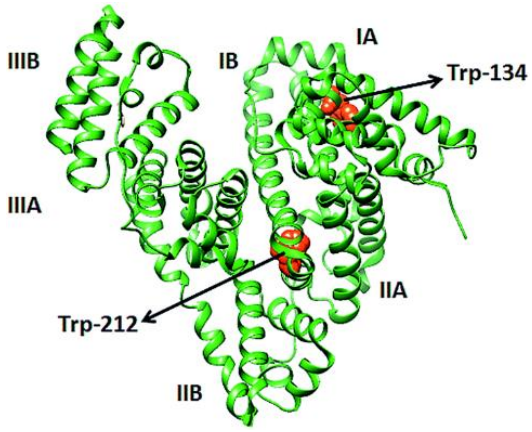

Figure 8. *BSA structure with various binding sites*. [33]

Phosphate-buffered saline (PBS), often used in imaging applications to study protein folding and ligand binding mechanisms, has been widely used as the preferred buffer to investigate the interactions between dyes and proteins. Efforts have been made to understand the interactions between the newly designed FITC-SQ-FITC as a far-red dye and protein molecules. A lot of focus has been given to the noncovalent labeling of biomolecules. Welder et al. used absorption detection techniques to investigate the noncovalent labeling of Bovine Serum Albumin (BSA) and Human Serum Albumin (HSA) with NIR squarylium dyes [37]. BSA, a globular protein commonly used as a model protein, is a valuable tool for studying dye-protein interactions. For this study, we have used the FITC-SQ-FITC dye to investigate its interactions with BSA, which serves as a representative model protein. The BSA content varied from 0 to 50 µM, though the dye concentration remained constant at 10 µM. **Figure 9.** provides a comprehensive depiction of the BSA interaction of FITC-SQ-FITC, along with the relevant techniques.

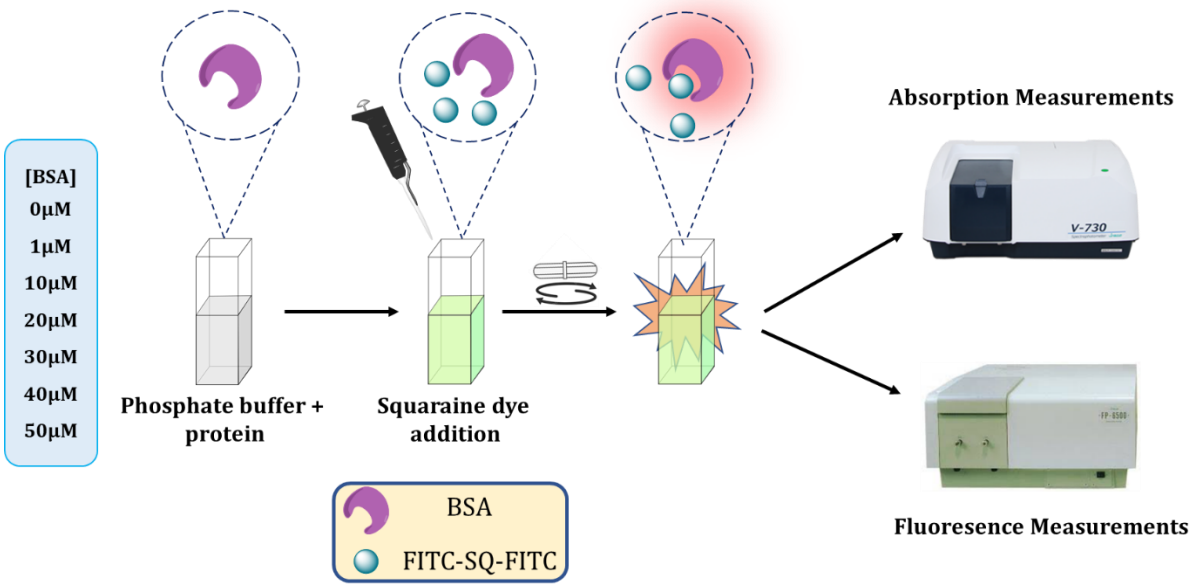

Figure 9. *Overview of FITC-SQ-FITC and BSA interaction.*

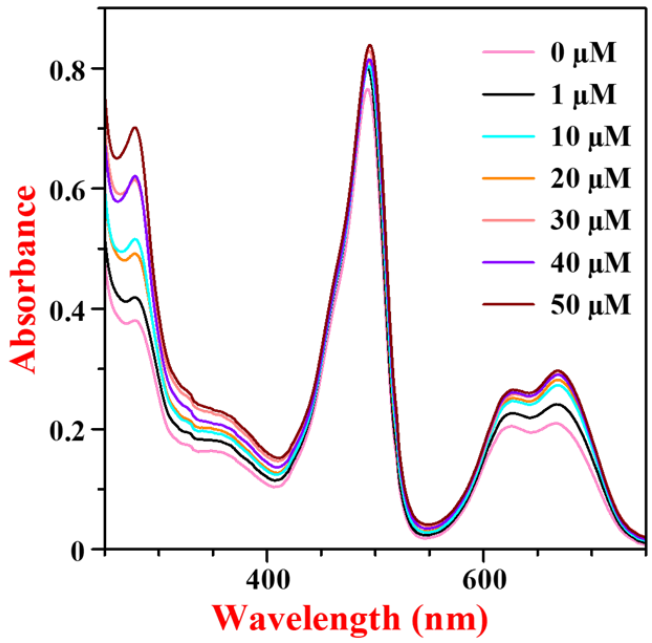

Figure 10. *The electronic absorption spectra of FITC-SQ-FITC in 0.1 M PBS were measured at various concentrations of BSA while keeping the dye concentration fixed at 10 μM.*

Figure 11. illustrates the fluorescence spectra of FITC-SQ-FITC dye at different BSA concentrations. It is interesting to note that in PBS, the fluorescence is completely quenched in the far-red wavelength region from 620 nm to 720 nm. This is in contrast to what was observed in methanol, as discussed earlier (**Figure 2**). Despite the existing PET-off state in FITC-SQ-FITC, as mentioned earlier, the fluorescence quenching remains intact in PBS, possibly because of enhanced ACQ. It is clear from the wide range of spectral features, including a vibronic shoulder at 610 nm, that exceeds the absorption peak of the monomeric dye at 660 nm.

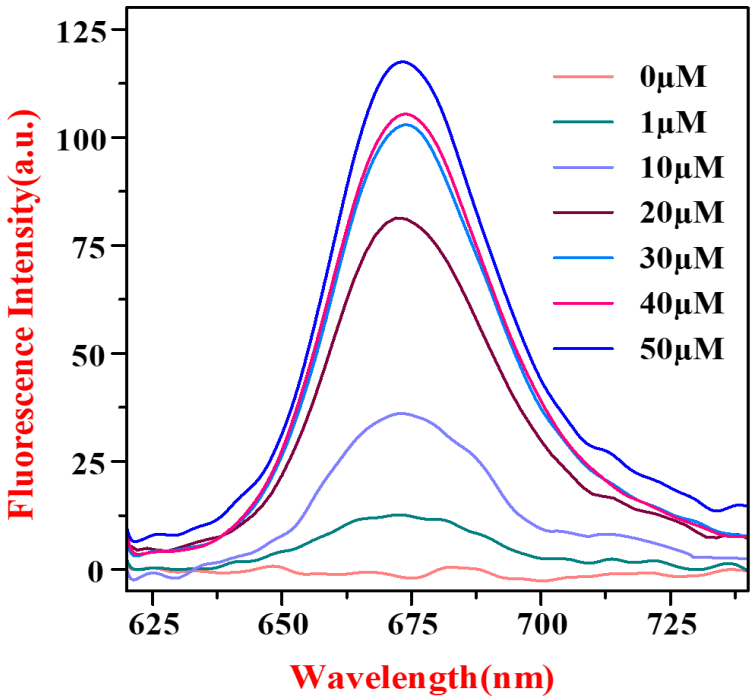

Figure 11. *The fluorescence emission spectra of FITC-SQ-FITC dye were measured at different doses of BSA while keeping the dye concentration fixed at 10 μM.*

When the amount of BSA is increased, there is only a little shift in the absorbance ratio between the vibronic shoulder and the major monomeric peak, as seen in **Figure 9**. The presence of a bulky group is responsible for the kinetics of the interaction between the dye BSA, which in turn impacts aggregation-induced emission (AIE)[38].

Simultaneously, there was a noticeable rise in the emission intensity of the squaraine sub-chromophore as the concentration of BSA increased. This indicates a complex interaction between

this molecular segment and the protein. This interaction resulted in a significant increase in fluorescence emission, increasing it by a remarkable factor of 117. This enhancement involves a significant change in the fluorescence characteristics of the dye caused by the presence of BSA. This highlights the potential importance of this interaction in biological sensing and imaging applications. The size of the BSA molecule is crucial in this occurrence as it efficiently suppresses the tendency of the FITC-SQ-FITC dye to aggregate. The prevention of aggregation is essential as it recovers the fluorescence that was before suppressed. Furthermore, the fluorescence that has been recovered becomes stronger in direct proportion to the rising concentration of BSA. This suggests that there is a relationship between the dye and the protein that depends on the concentration. The complex intermolecular interaction highlights the delicate equilibrium between protein binding and dye fluorescence, providing an essential understanding of the fundamental mechanisms that control their relationship. BSA is a protein with numerous roles. It has two active sites: site-I, which is hydrophobic, and site-II, which involves a combination of hydrophobic, hydrogen bonding, and electrostatic interactions. The molecular structure of FITC-SQ-FITC, which has a carboxylic acid group in the FITC component and a thioamide linkage in the SQ segment, indicates a specific affinity for site II of the BSA molecule. This molecular analysis enhances comprehension of the specificity and strength of the dye-protein interaction, facilitating the development of purpose-built fluorescent probes for precise protein labeling and imaging. In addition, the calculation of the apparent binding constant (K_a) using a precise mathematical framework highlights the quantitative aspect of the interaction between the dye and protein. The K_a value, calculated to be $1.1 \times 10^4\ M^{-1}$ by plotting the fluorescence change against the inverse of BSA concentration, indicates a robust and favorable binding affinity between the symmetrical FITC-SQ-FITC dye and BSA. The apparent binding constant (K_a) was estimated using an equation by plotting $(F_\infty - F_0) / (F_X - F_0)$ as a function of the inverse of BSA concentration, as depicted in **Figure 12.** This quantitative evaluation provides more evidence for the potential usefulness of the developed dye probe in accurately and effectively identifying proteins without forming chemical bonds, thereby making it easier to see them in the far-red part of the light spectrum.

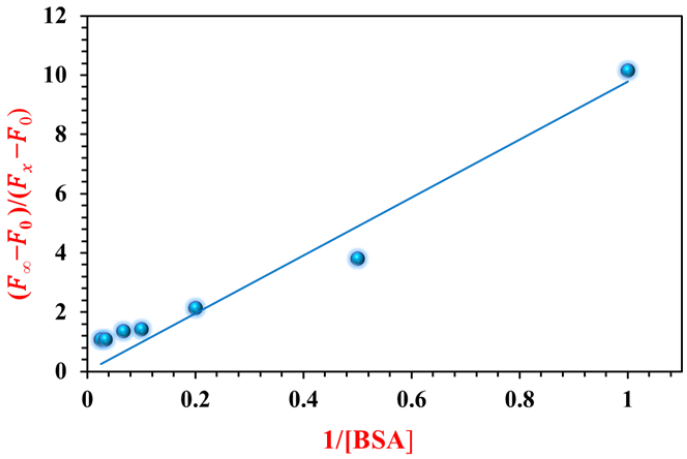

Figure 12. *The plot shows the ratio of $(F_\infty - F_0) / (F_X - F_0)$ as a function of $[BSA]^{-1}$, with a constant dye concentration of 10×10^{-6} M.*

The relationship between BSA concentration and the fluorescence intensity of symmetrical squaraine dye (FITC-SQ-FITC) is illustrated in **Figure 13**. In this study the results demonstrate a linear correlation between fluorescence intensity and BSA concentration, indicating an increase in fluorescence intensity with increasing BSA concentration up to 50 μM, after which saturation is reached. However, further addition of BSA leads to non-linear changes in emission intensity, with a less pronounced effect on fluorescence intensity beyond the saturation point at 50 μM. This behavior is attributed to non-covalent interactions between the dyes and proteins, resulting in the formation of BSA-dye conjugates. It is widely acknowledged that drugs or probes interact uniquely with proteins in a concentration-dependent manner. The key criterion for utilizing these dyes as probes is their ability to interact with proteins without disrupting their structure, as protein structure is crucial for maintaining function and activity. The location of the dye within the protein may induce conformational changes, highlighting the importance of using an optimized dye concentration (10 μM) to study the synergistic effects of dye-BSA interactions while minimizing potential structural alterations to the protein.

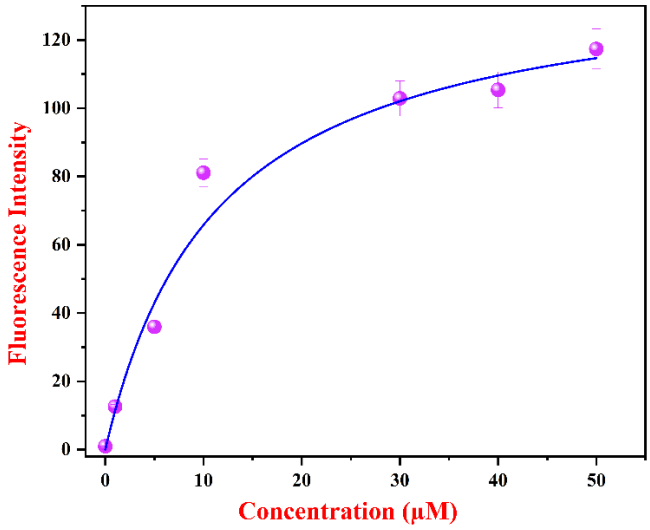

Figure 13. *The relationship between the intensity of fluorescence emission and the concentration of Bovine Serum Albumin (BSA) for FITC-SQ-FITC.*

3.4 Conclusion

This study involved the successful synthesis of amine-functionalized symmetrical squaraine (SQ) dye and a FITC-SQ-FITC dye conjugate. The structures and photophysical characteristics of these compounds were thoroughly investigated. The SQ dye, which has symmetrical properties, displayed total fluorescence quenching. This quenching is primarily triggered by photoinduced electron transfer (PET), which serves as the primary mechanism for the quenching. The addition of FITC on both ends of the SQ dye in the FITC-SQ-FITC dye conjugation resulted in decreased aggregation of both SQ and FITC components. This additionally caused an enormous 47-fold increase in far-red fluorescence emission at 674 nm in a solution of methanol. The increased far-red fluorescence is due to the combined influence of inhibiting aggregation-caused quenching (ACQ) and photoinduced electron transfer (PET) processes.

The newly designed FITC-SQ-FITC dye conjugate exhibited total suppression of far-red fluorescence in phosphate-buffered saline (PBS) as a result of intense dye aggregation, as verified by spectral absorption experiments. However, when bovine serum albumin (BSA) was present as a model protein, the conjugate exhibited a strong interaction with BSA, characterized by an

association constant of 1.1 x 10^4 M^{-1}. This interaction disrupted the aggregation of the dye and resulted in an elevation of far-red fluorescence associated with the SQ component as the concentration of BSA increased. A remarkable enhancement of fluorescence at 674 nm by a factor of 117 was found when the concentration of BSA increased by a factor of 25. This demonstrates the great potential of the FITC-SQ-FITC compound as a highly effective probe for investigating interactions between dyes and proteins in the far-red range.

In summary, the SQ dye and FITC-SQ-FITC combination created in this study show great potential as effective far-red quenching and fluorescent moieties. These findings open up possibilities for creating innovative far-red-sensitive Förster resonance energy transfer (FRET) or PET systems, which can be used in fluorescence biosensing applications. These findings enhance the progress of fluorescent probes used in the investigation of protein interactions and show potential for the development of effective biosensing platforms.

3.5 References

1. Shah, S.; Mandecki, W.; Li, J.; Gryczynski, Z.; Borejdo, J.; Gryczynski, I.; Fudala, R. FRET Study in Oligopeptide-Linked Donor-Acceptor System in PVA Matrix. *Methods Appl. Fluoresc.* **2016**, *4*, 047002, doi:10.1088/2050-6120/4/4/047002.

2. Fan, J.; Hu, M.; Zhan, P.; Peng, X. Energy Transfer Cassettes Based on Organic Fluorophores: Construction and Applications in Ratiometric Sensing. *Chem. Soc. Rev.* **2013**, *42*, 29–43, doi:10.1039/c2cs35273g.

3. Edition, T. *Principles of Fluorescence Spectroscopy*; ISBN 9780387312781.

4. Dong, Y.; Iagatti, A.; Foggi, P.; Zhao, J.; Mazzone, G.; Xu, K.; Ji, W.; Di Donato, M.; Russo, N. Bodipy-Squaraine Triads: Preparation and Study of the Intramolecular Energy Transfer, Charge Separation and Intersystem Crossing. *Dye. Pigment.* **2017**, *147*, 560–572, doi:10.1016/j.dyepig.2017.08.028.

5. De Silva, A.P.; Gunnlaugsson, T.; Rice, T.E. Recent Evolution of Luminescent Photoinduced Electron Transfer Sensors: A Review. *Analyst* **1996**, *121*, 1759–1762, doi:10.1039/an9962101759.

6. Callan, J.F.; De Silva, A.P.; Magri, D.C. Luminescent Sensors and Switches in the Early 21st Century. *Tetrahedron* **2005**, *61*, 8551–8588, doi:10.1016/j.tet.2005.05.043.

7. Lou, Z.; Li, P.; Pan, Q.; Han, K. A Reversible Fluorescent Probe for Detecting Hypochloric Acid in Living Cells and Animals: Utilizing a Novel Strategy for Effectively Modulating the Fluorescence of Selenide and Selenoxide. *Chem. Commun.* **2013**, *49*, 2445–2447, doi:10.1039/c3cc39269d.

8. Venkatesan, P.; Wu, S.P. A Turn-on Fluorescent Probe for Hypochlorous Acid Based on the Oxidation of Diphenyl Telluride. *Analyst* **2015**, *140*, 1349–1355, doi:10.1039/c4an02116a.

9. Zhu, H.; Fan, J.; Wang, J.; Mu, H.; Peng, X. An “Enhanced PET”-Based Fluorescent Probe with Ultrasensitivity for Imaging Basal and Elesclomol-Induced HClO in Cancer Cells. *J. Am. Chem. Soc.* **2014**, *136*, 12820–12823, doi:10.1021/ja505988g.

10. Sparano, B.A.; Koide, K. Fluorescent Sensors for Specific RNA: A General Paradigm Using Chemistry and Combinatorial Biology. *J. Am. Chem. Soc.* **2007**, *129*, 4785–4794, doi:10.1021/ja070111z.

11. Gao, Y.; Gu, Q.; Yang, B.; Zhang, S.; Yao, L.; Ma, Y.; Pan, Y.; Guo, Y.; Liu, H. Hybridization and De-Hybridization between the Locally-Excited (LE) State and the Charge-Transfer (CT) State: A Combined Experimental and Theoretical Study. *Phys. Chem. Chem. Phys.* **2016**, *18*, 24176–24184, doi:10.1039/c6cp02778d.

12. Kim, S.Y.; Cho, Y.J.; Lee, A.R.; Son, H.J.; Han, W.S.; Cho, D.W.; Kang, S.O. Influence of P-Conjugation Structural Changes on Intramolecular Charge Transfer and Photoinduced Electron Transfer in Donor-p-Acceptor Dyads. *Phys. Chem. Chem. Phys.* **2017**, *19*, 426–435, doi:10.1039/c6cp06566j.

13. Tanaka, K.; Miura, T.; Umezawa, N.; Urano, Y.; Kikuchi, K.; Higuchi, T.; Nagano, T. Rational Design of Fluorescein-Based Fluorescence Probes. Mechanism-Based Design of a Maximum Fluorescence Probe for Singlet Oxygen. *J. Am. Chem. Soc.* **2001**, *123*, 2530–2536, doi:10.1021/ja0035708.

14. de Silva, A.P.; Gunaratne, H.Q.N.; Gunnlaugsson, T.; Huxley, A.J.M.; McCoy, C.P.; Rademacher, J.T.; Rice, T.E. Signaling Recognition Events with Fluorescent Sensors and Switches. *Chem. Rev.* **1997**, *97*, 1515–1566, doi:10.1021/cr960386p.

15. Weller, A. No Title. *Pure Appl. Chem.* **1968**, *16*, 115–124, doi:doi:10.1351/pac196816010115.

16. Kobayashi, H.; Ogawa, M.; Alford, R.; Choyke, P.L.; Urano, Y. New Strategies for Fluorescent Probe Design in Medical Diagnostic Imaging. **2010**, 2620–2640.

17. Chen, H.; Farahat, M.S.; Law, K.; Whitten, D.G. Aggregation of Surfactant Squaraine Dyes in Aqueous Solution and Microheterogeneous Media : Correlation of Aggregation Behavior with Molecular Structure. **1996**, 2584–2594.

18. Yi, R.; Das, P.; Lin, F.; Shen, B.; Yang, Z.; Zhao, Y.; Hong, L.; He, Y.; Hu, R.; Song, J.; et al. Fluorescence Enhancement of Small Squaraine Dye and Its Two-Photon Excited Fluorescence in Long-Term near-Infrared I&II Bioimaging. *Opt. Express* **2019**, *27*,

12360, doi:10.1364/oe.27.012360.

19. Ros-lis, J. V; Garcı, B.; Jime, D.; Soto, J.; Gonzalvo, F.; Valldecabres, M.C. Squaraines as Fluoro - Chromogenic Probes for Thiol-Containing Compounds and Their Application to the Detection of Biorelevant Thiols. **2004**, 4064–4065.

20. Gassensmith, J.; Arunkumar, E.; Barr, L.; Baumes, J.M.; Kristy, M.; Johnson, J.R.; Noll, B.C.; Smith, B.D. NIH Public Access. **2010**, *129*, 15054–15059, doi:10.1021/ja075567v.Self-Assembly.

21. Engineering, O. Fluorescence Enhancement of Small Squaraine Dye and Its Two-Photon Excited Fluorescence in Long-Term near-Infrared I & II Bioimaging. **2019**, *27*, 12360–12372.

22. Editor, G.; Harriman, A.; Yu, H.; Fu, M.; Xiao, Y.; Chem, P.C.; Nastasi, F.; Puntoriero, F.; Olivier, J.; Ziessel, R.; et al. This Paper Is Published as Part of a PCCP Themed Issue on Electronic Energy Transfer Electronic Energy Transfer Transfer Switching off FRET by Analyte-Induced Decomposition of Squaraine Energy Acceptor : A Concept to Transform ' Turn off ' Chemodosimeter . **2010**, doi:10.1039/c001504k.

23. Kim, Y.S.; Liang, K.; Law, K.Y.; Whitten, D.G. An Investigation of Photocurrent Generation by Squaraine Aggregates in Monolayer-Modified SnO2 Electrodes. *J. Phys. Chem.* **1994**, *98*, 984–988, doi:10.1021/j100054a039.

24. Khazraji, A.C.; Hotchandani, S.; Das, S.; Kamat, P. V. Controlling Dye (Merocyanine-540) Aggregation on Nanostructured TiO2 Films. An Organized Assembly Approach for Enhancing the Efficiency of Photosensitization. *J. Phys. Chem. B* **1999**, *103*, 4693–4700, doi:10.1021/jp9903110.

25. Kantar, C.; Kaya, B.; Türk, M.; Şaşmaz, S. Novel Phthalocyanines Containing Guaiacol Azo Dyes: Synhthesis, Antioxidant, Antibacterial, and Anticancer Activity. *J. Struct. Chem.* **2018**, *59*, 1241–1250, doi:10.1134/S0022476618050335.

26. Morimoto, T.; Fujikawa, N.; Ogomi, Y.; Pandey, S.S.; Ma, T.; Hayase, S. Design of Far-Red Sensitizing Squaraine Dyes Aiming towards the Fine Tuning of Dye Molecular Structure. *J. Nanosci. Nanotechnol.* **2016**, *16*, 3282–3288, doi:10.1166/jnn.2016.12304.

27. Li, P.; Duan, X.; Chen, Z.; Liu, Y.; Xie, T.; Fang, L.; Li, X.; Yin, M.; Tang, B. A Near-Infrared Fluorescent Probe for Detecting Copper(II) with High Selectivity and Sensitivity and Its Biological Imaging Applications. *Chem. Commun.* **2011**, *47*, 7755–7757, doi:10.1039/c1cc11885d.

28. Yuan, L.; Lin, W.; Zhao, S.; Gao, W.; Chen, B.; He, L.; Zhu, S. A Unique Approach to Development of Near-Infrared Fluorescent Sensors for in Vivo Imaging. *J. Am. Chem. Soc.* **2012**, *134*, 13510–13523, doi:10.1021/ja305802v.

29. Wurthner, Angew Chem Int Ed, 2021 - Polymorphism in Squaraine Dye Aggregates by Self-Assembly Pathway Differentiation.Pdf.

30. Inoue, T.; Pandey, S.S.; Fujikawa, N.; Yamaguchi, Y.; Hayase, S. Synthesis and Characterization of Squaric Acid Based NIR Dyes for Their Application towards Dye-Sensitized Solar Cells. *J. Photochem. Photobiol. A Chem.* **2010**, *213*, 23–29, doi:10.1016/j.jphotochem.2010.04.015.

31. Jisha, V.S.; Arun, K.T.; Hariharan, M.; Ramaiah, D. Site-Selective Binding and Dual Mode Recognition of Serum Albumin by a Squaraine Dye. *J. Am. Chem. Soc.* **2006**, *128*, 6024—6025, doi:10.1021/ja061301x.

32. Patonay, G.; Salon, J.; Sowell, J.; Strekowski, L. Noncovalent Labeling of Biomolecules with Red and Near- Infrared Dyes. *Molecules* **2004**, *9*, 40–49, doi:10.3390/90300040.

33. Dockal, M.; Carter, D.C.; Rüker, F. Conformational Transitions of the Three Recombinant Domains of Human Serum Albumin Depending on PH*. *J. Biol. Chem.* **2000**, *275*, 3042–3050, doi:https://doi.org/10.1074/jbc.275.5.3042.

34. Zhao, X.; Liu, R.; Chi, Z.; Teng, Y.; Qin, P. New Insights into the Behavior of Bovine Serum Albumin Adsorbed onto Carbon Nanotubes: Comprehensive Spectroscopic Studies. *J. Phys. Chem. B* **2010**, *114*, 5625–5631, doi:10.1021/jp100903x.

35. Chakraborti, S.; Joshi, P.; Chakravarty, D.; Shanker, V.; Ansari, Z.A.; Singh, S.P.; Chakrabarti, P. Interaction of Polyethyleneimine-Functionalized ZnO Nanoparticles with Bovine Serum Albumin. *Langmuir* **2012**, *28*, 11142–11152, doi:10.1021/la3007603.

36. Zhao, L.; Liu, R.; Zhao, X.; Yang, B.; Gao, C.; Hao, X.; Wu, Y. New Strategy for the

Evaluation of CdTe Quantum Dot Toxicity Targeted to Bovine Serum Albumin. *Sci. Total Environ.* **2009**, *407*, 5019–5023, doi:https://doi.org/10.1016/j.scitotenv.2009.05.052.

37. Welder, F.; Paul, B.; Nakazumi, H.; Yagi, S.; Colyer, C.L. Symmetric and Asymmetric Squarylium Dyes as Noncovalent Protein Labels: A Study by Fluorimetry and Capillary Electrophoresis. *J. Chromatogr. B. Analyt. Technol. Biomed. Life Sci.* **2003**, *793*, 93—105, doi:10.1016/s1570-0232(03)00367-2.

38. Barbero, N.; Butnarasu, C.; Visentin, S.; Barolo, C. Squaraine Dyes: Interaction with Bovine Serum Albumin to Investigate Supramolecular Adducts with Aggregation-Induced Emission (AIE) Properties. *Chem. – An Asian J.* **2019**, *14*, 896–903, doi:https://doi.org/10.1002/asia.201900055.

3.6 Appendix

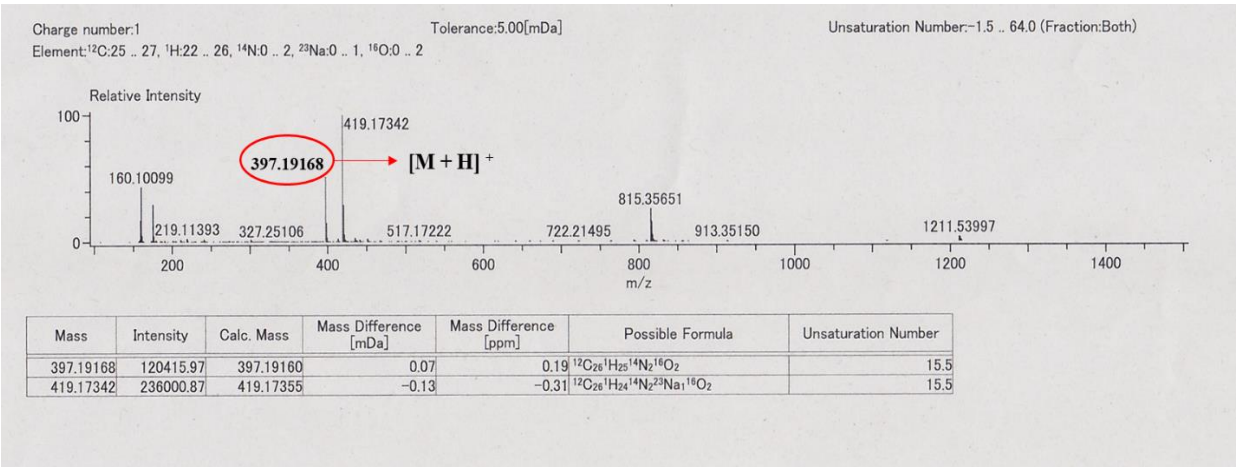

Mass	Intensity	Calc. Mass	Mass Difference [mDa]	Mass Difference [ppm]	Possible Formula	Unsaturation Number
397.19168	120415.97	397.19160	0.07	0.19	$^{12}C_{26}{}^{1}H_{25}{}^{14}N_2{}^{16}O_2$	15.5
419.17342	236000.87	419.17355	-0.13	-0.31	$^{12}C_{26}{}^{1}H_{24}{}^{14}N_2{}^{23}Na_1{}^{16}O_2$	15.5

Figure 1. *TOF mass of compound 1*

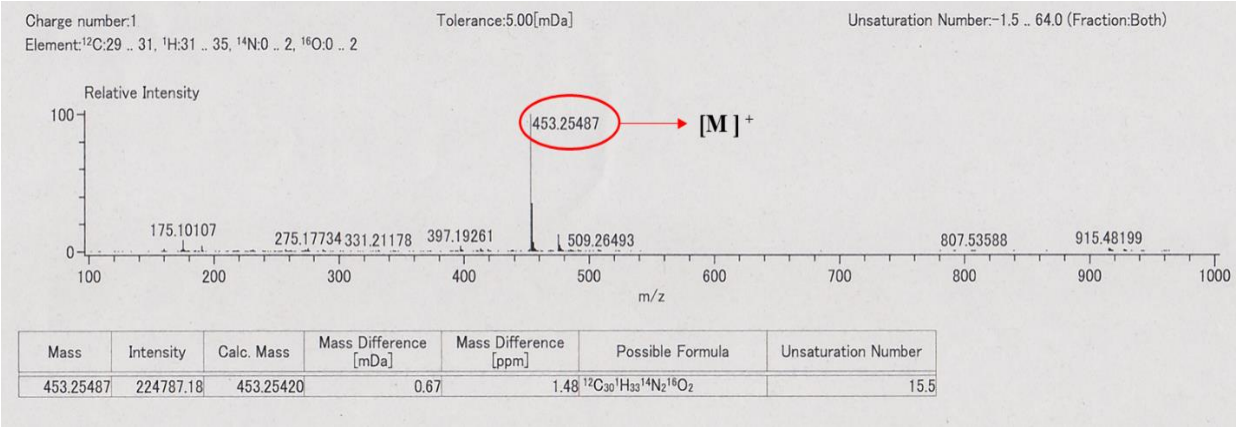

Mass	Intensity	Calc. Mass	Mass Difference [mDa]	Mass Difference [ppm]	Possible Formula	Unsaturation Number
453.25487	224787.18	453.25420	0.67	1.48	$^{12}C_{30}{}^{1}H_{33}{}^{14}N_2{}^{16}O_2$	15.5

Figure 2. *TOF mass of compound 2*

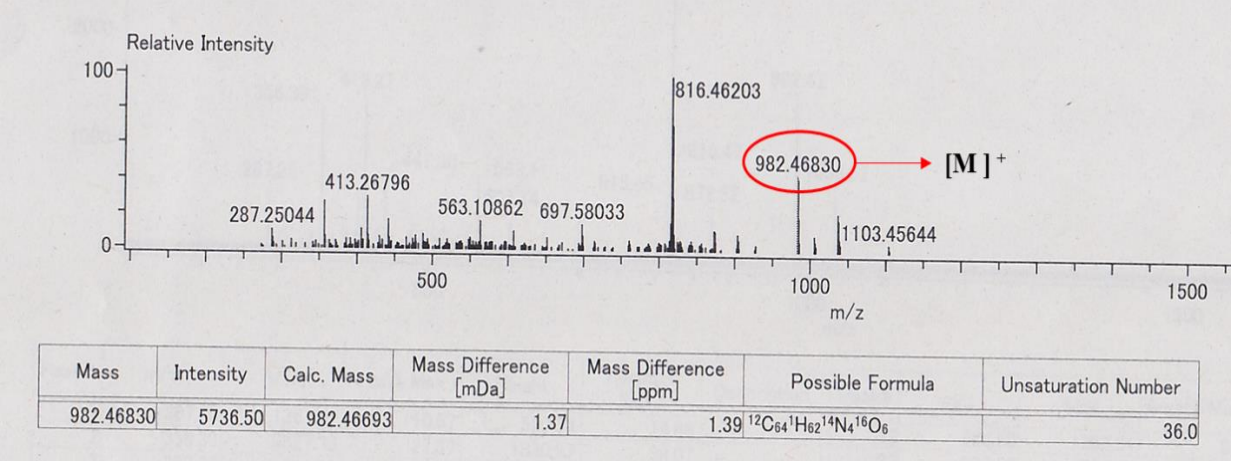

Mass	Intensity	Calc. Mass	Mass Difference [mDa]	Mass Difference [ppm]	Possible Formula	Unsaturation Number
982.46830	5736.50	982.46693	1.37	1.39	$^{12}C_{64}{}^{1}H_{62}{}^{14}N_{4}{}^{16}O_{6}$	36.0

Figure 3. *TOF mass of compound 3*

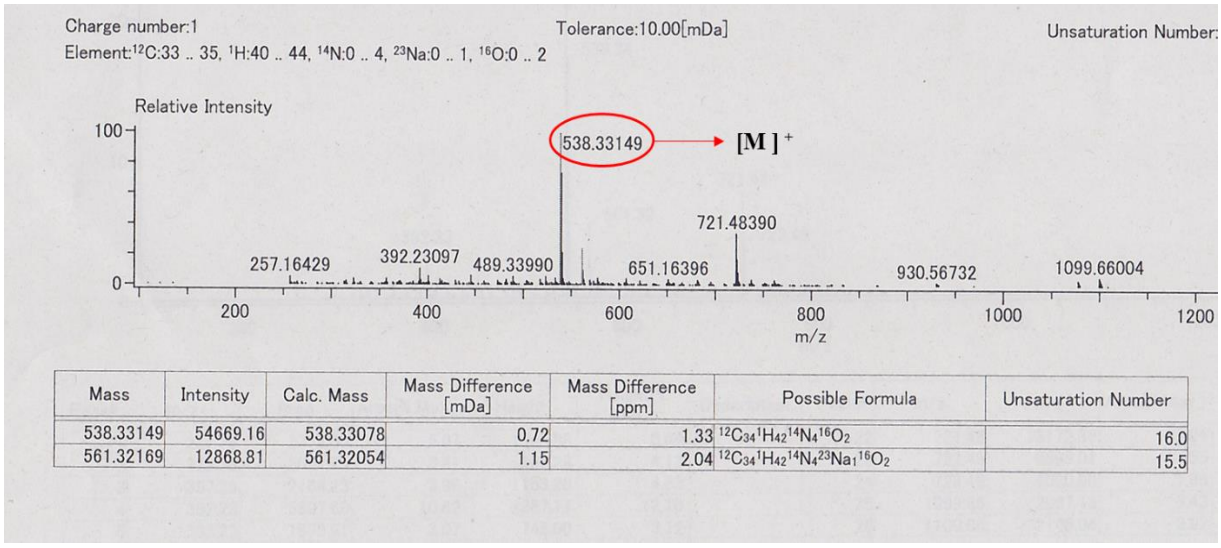

Mass	Intensity	Calc. Mass	Mass Difference [mDa]	Mass Difference [ppm]	Possible Formula	Unsaturation Number
538.33149	54669.16	538.33078	0.72	1.33	$^{12}C_{34}{}^{1}H_{42}{}^{14}N_{4}{}^{16}O_{2}$	16.0
561.32169	12868.81	561.32054	1.15	2.04	$^{12}C_{34}{}^{1}H_{42}{}^{14}N_{4}{}^{23}Na_{1}{}^{16}O_{2}$	15.5

Figure 4. *TOF mass of SQ*

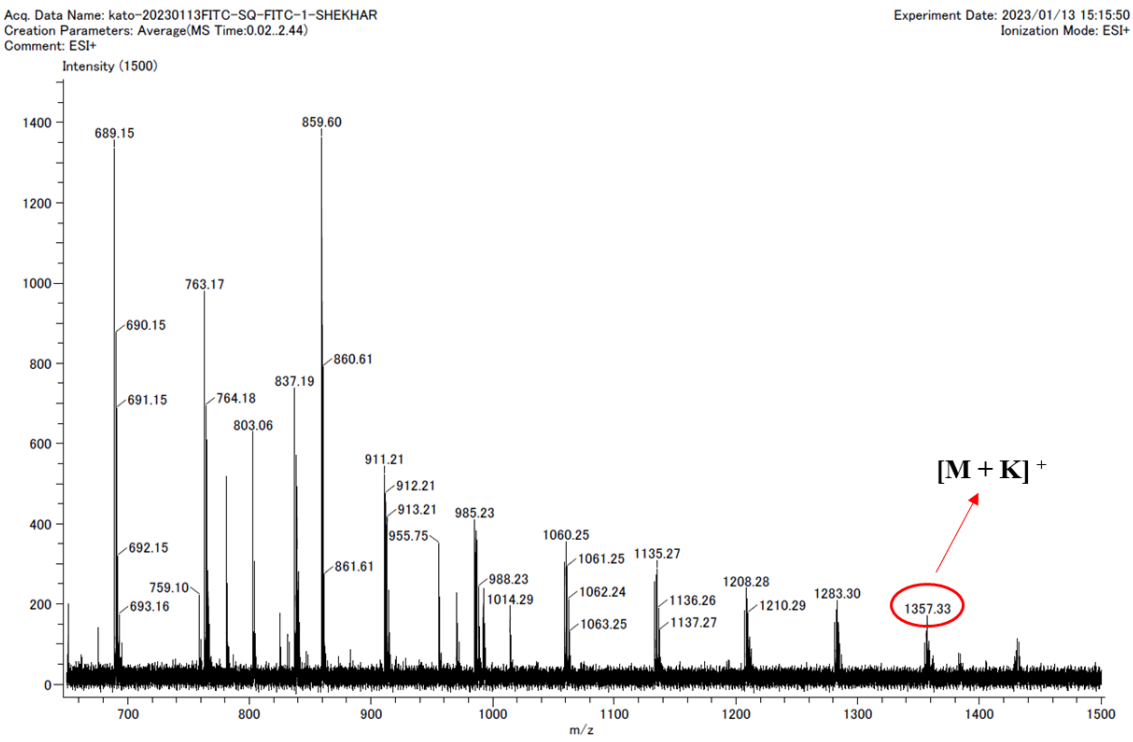

Figure 5. *TOF mass of FITC-SQ-FITC*

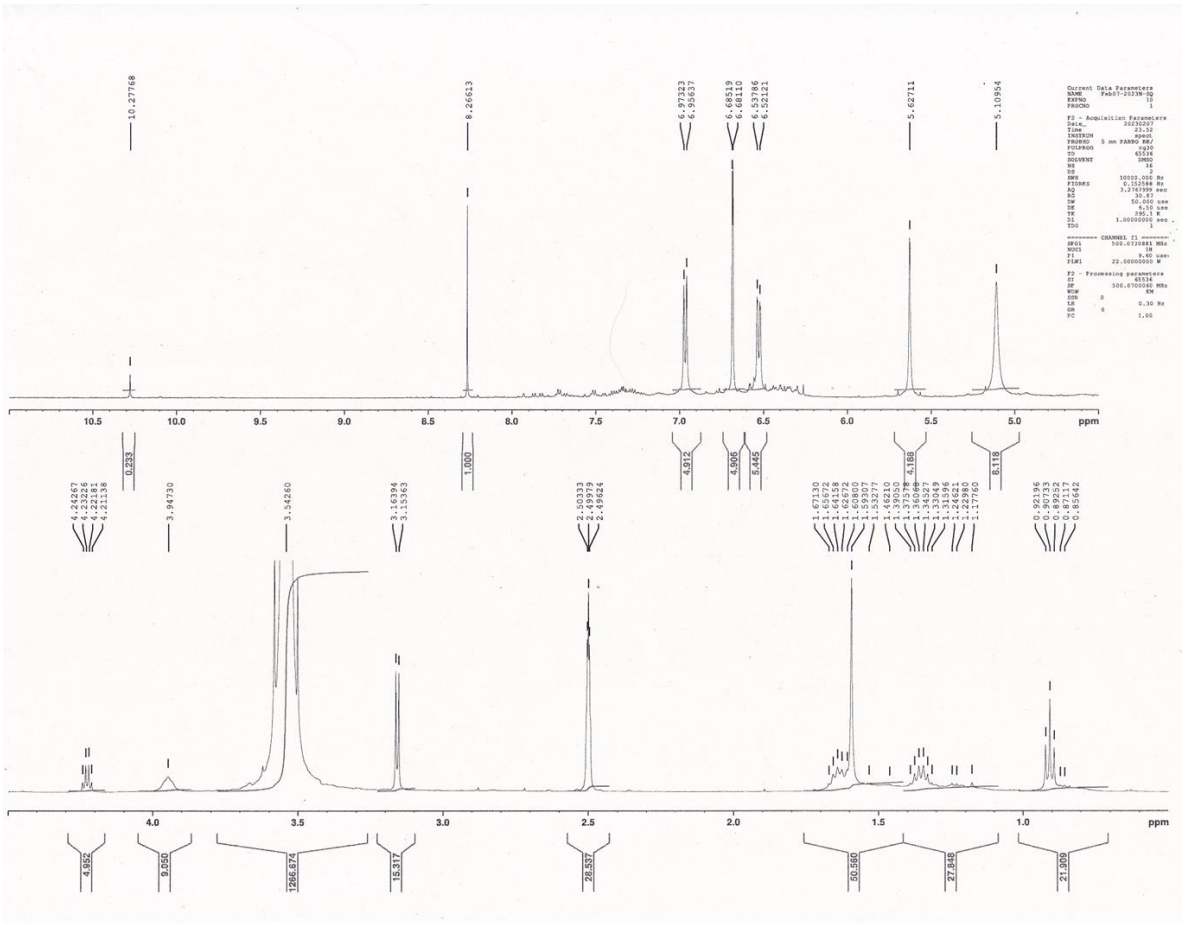

Figure 6. *^{1}H-NMR of dye SQ*

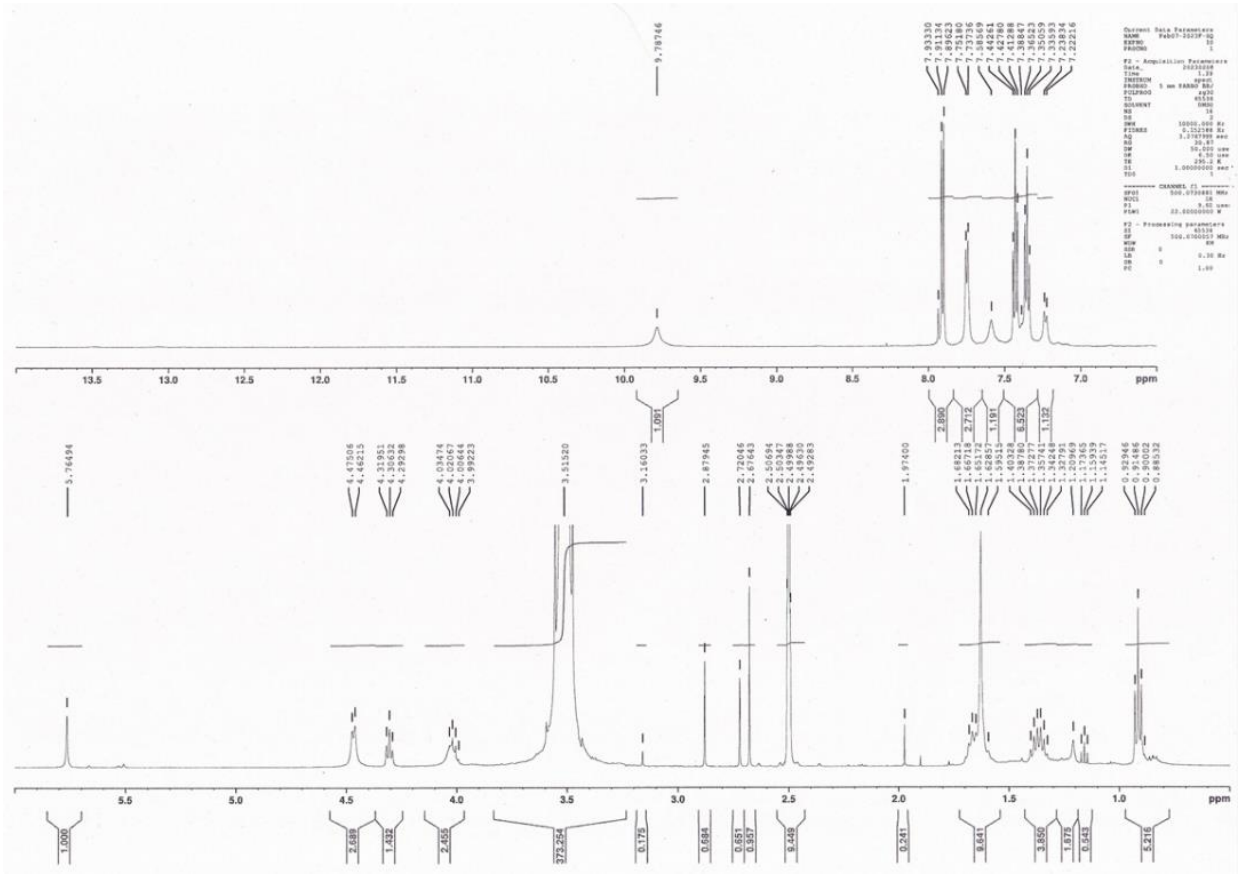

Figure 7. *^{1}H-NMR of dye FITC-SQ-FITC*

CHAPTER 4 : Design and Synthesis of Novel Squaraine-Based Fluorescent Probe for Far-Red Detection of Chymotrypsin Enzyme

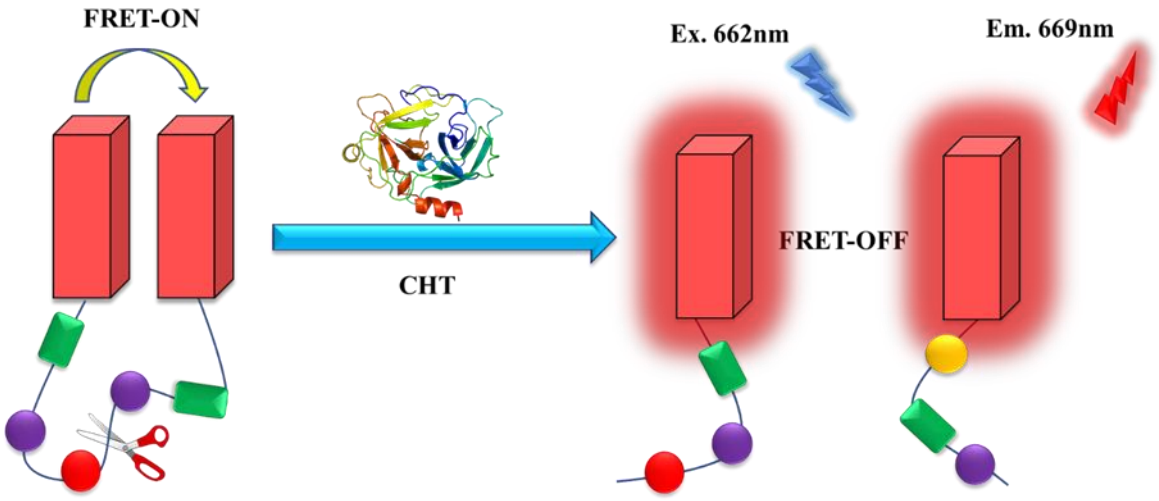

Abstract: Chymotrypsin is a prevalent serine protease that plays a significant role in various physiological processes, including digestion, hemostasis, apoptosis, signal transduction, reproduction, and the immunological response. To meet the urgent requirement for fast and affordable detection methods, we provide an innovative approach that utilizes far-red technologies and homo-Förster resonance energy transfer (FRET). The SQ-122 PC probe showcases a unique molecular structure comprising a squaraine dye (SQ), a peptide linker, and SQ moieties produced via solid-phase peptide synthesis. Our probe has shown an impressive quenching efficiency of 93.75% in a specifically designed solvent system consisting of H_2O: DMSO (7:3). Additionally, the probe has absorption and emission properties that fall within the far-red range of the electromagnetic spectrum. It is worth noting that the probe has an exceptionally low detection limit of 0.130 nM, which is unprecedented. Additionally, our approach provides unmatched specificity for chymotrypsin, guaranteeing reliable and precise detection of the enzyme. This groundbreaking research highlights the vast capabilities of far-red-based homo-FRET systems in facilitating accurate and targeted identification of chymotrypsin enzyme activity. Our research findings signify a significant improvement in enzyme sensing, which has the potential to revolutionize disease detection and dairy quality control by combining cutting-edge technology with biological diagnostics.

4.1 Introduction

Proteases are vital enzymes in the body that have been the subject of research for developing efficient and sensitive assays that can be utilized in health diagnosis, treatment, and biological studies. Proteases cleave the amide bond at particular points on the polypeptide chain, which is important for regulating several physiological processes [1,2]. The processes encompassed in this list are cell proliferation, DNA replication, apoptosis, differentiation, immunological responses, and hemostasis (coagulation). Chymotrypsin (CHT) is a serine protease that is often present in the digestive tract of mammals [3]. Chymotrypsin hydrolyzes polypeptide substrate by breaking the peptide bond on the carboxyl side of aromatic amino acids [4]. Chymotrypsin has a crucial function in controlling the breakdown, cell death, and controlled cell death of proteins obtained from food [5–7]. When the body is exposed to an excessive amount of chymotrypsin, it

triggers the production of histamine, which can lead to allergic reactions [8]. Chymotrypsin demonstrates anti-inflammatory properties in the realms of pathology and medicine. It is effective in reducing post-operative problems after cataract surgery [9]. Chymotrypsin is commonly used as a prototypical protease because it is cost-effective, readily available, and has the potential to be a biomarker. To accurately identify chymotrypsin with great sensitivity, it is crucial to create an efficient fluorescent probe.

Despite the rapid advancement of protease test methods, effective development and commercialization of immunoassays that utilize antibodies for selective binding to target proteases have been achieved. These immunoassays are efficient in accurately measuring the amounts of protease [10]. However, they are not well-suited for mapping protease activity and establishing its correlation with ailments phases, as their main emphasis is on quantifying protease content. To address this difficulty, many methods have been extensively employed, such as the utilization of appropriate peptide substrates, optical detection (absorbance/fluorescence), and the monitoring of fluorescence changes using Forster resonance energy transfer (FRET) [10,11]. The interaction between proteases and fluorogenic substrates leads to the specific cleavage of peptide bonds, resulting in a change in the fluorescence spectra of the enzymes. This forms the basis for detecting protease activity. Several highly efficient FRET reporters utilizing tiny compounds have been discovered to date [11–13]. Although these probes have demonstrated a high level of sensitivity in protease bioassays, most of them rely on a quencher-acceptor and fluorophore-donor system known as hetero-FRET. Creating a new enzyme probe presents a challenge in designing a donor-acceptor pair with optimal spectrum properties. The widespread usage of fluorescent labels is mainly limited to the visible or low wavelength spectrum [14–16], which might potentially harm tissues. Additionally, these fluorophores emit light at shorter wavelengths, which can disrupt the natural fluorescence of cells. By incorporating far-red and near-infrared (NIR) fluorophores, sensitivity is increased by reducing interference from biological autofluorescence. Additionally, this enables more effective bioimaging with improved depth penetration [17]. Fluorescent peptide-based probes are commonly used in optical imaging, and there are ongoing attempts to investigate the near-infrared imaging range of the spectrum [18]. Cyanine dyes have a longer emission wavelength,

which makes them better suited for application in tissues. Nevertheless, their main disadvantage resides in their fast photobleaching rate [19,20]. Within this particular framework, the NIR squaraine dye demonstrates exceptional physical and chemical attributes, such as very intense absorption bands, a high molar absorption coefficient, elevated quantum yield, excellent photostability, and favorable photoconductivity [21–23]. Simultaneously, the ability of squaraine dyes with a donor-acceptor-donor Zwitterionic molecular framework to absorb and emit light may be adjusted within the visible to near-infrared wavelength range by carefully choosing appropriate donor groups with different levels of π-conjugation [24]. Recently, there has been an increasing trend in using the indole heterocycle as a donor component in squaraine dyes. This phenomenon has resulted in a wide range of applications in various fields [25,26]. Saikiran et al. developed a novel sensor that can detect human neutrophil elastase by utilizing a squaraine dye-based aggregation-caused quenching mechanism. This sensor allows for real-time monitoring of enzyme activity by fluorescence [27]. This design enables the continuous monitoring of enzyme activity by measuring fluorescence variations, providing a fast and cost-efficient approach to detection.

To detect chymotrypsin in the far-red region, we have designed and synthesized a novel probe SQ-122 PC. This probe is a combination of a dye and a peptide, and it operates via the homo-Förster resonance energy transfer (homo-FRET) mechanism. The probe's design includes the integration of two far-red-sensitive squaraine dye molecules, each with a suitable peptide sequence at its ends to enable homo-FRET. When cleaved by chymotrypsin, the homo-FRET is deactivated, resulting in an enormous rise in fluorescence signal in the far-red region (**Scheme 1**). We have developed a detection method with exceptional sensitivity that can accurately identify chymotrypsin activity even at exceedingly low concentrations. In addition, the probe shows remarkable selectivity, with low interference from other proteases usually found in complicated biological materials.

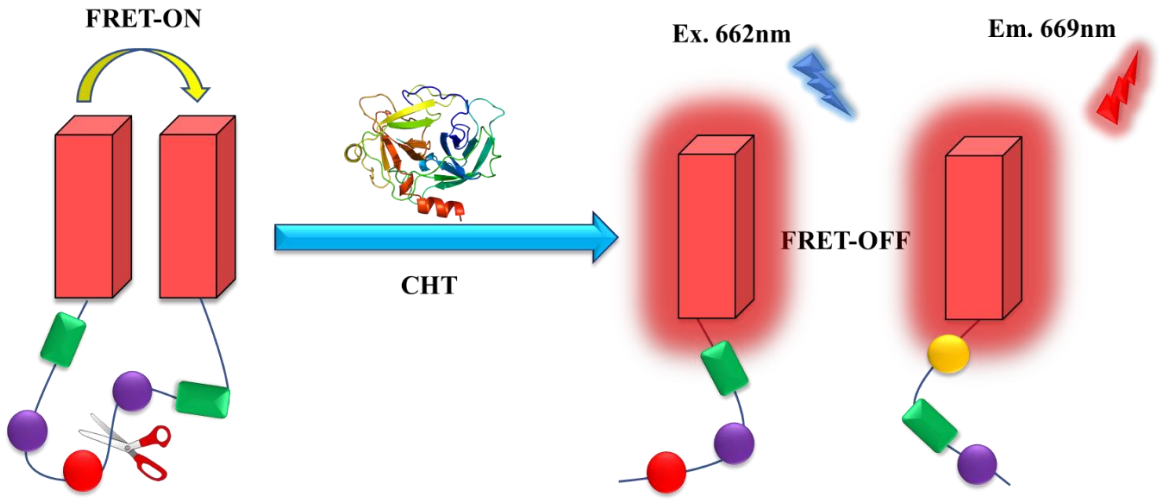

Scheme 1. *Illustrates the detection of chymotrypsin using a fluorescence switch-off/on mechanism caused by homo-FRET.*

4.2 Materials and Methods

4.2.1 Reagents and Instruments

All the chemicals, solvents, and reagents utilized for synthesis and photophysical characterization are of analytical or spectroscopic quality and are employed without any modifications. All Fmoc-protected amino acids, Rink amide MBHA resin, piperidine, O-(1H-benzotriazol-1- yl)-N,N,N',N'-tetramethyluronium hexafluorophosphate (HBTU), 1-hydrolxy-1Hbenzotriazole hydrate (HOBt·H_2O), N,N-diisopropylethylamine (DIEA), 2,2,2-trifluoroacetic acid (TFA), and 4 M HCl/Dioxane were acquired from Watanabe Chemical Industries, Ltd. α-chymotrypsin, α-trypsin, elastase pancreatic, peroxidase, bovine serum albumin, and papain were acquired from Sigma-Aldrich Co. LLC. These substances were sourced from bovine pancreas and horseradish. All solvents and other reagents were purchased from Wako Pure Chemical Industries, Ltd. The acquisition of deionized water was accomplished by the utilization of a Milli-Q Plus system, which was produced by Millipore. The synthesized unsymmetrical squaraine dye and dye intermediates underwent analysis using TOF/FAB-mass spectroscopy in

positive ion monitoring mode and nuclear magnetic resonance spectroscopy (NMR 500 MHz for 1 H NMR) to determine their structures. The electronic absorption spectra in the solution were obtained using a UV-visible-NIR spectrophotometer (JASCO V-530 UV/VIS spectrophotometer). The fluorescence emission spectra were recorded using a JASCO FP-6600 spectrophotometer, which is a fluorescence emission spectrometer. The experiment involved the use of an Xterra MS C8-5µm column (4.6 x 150 mm), manufactured by Walters, in combination with a Hitachi L-7100 instrument, to conduct analytical high-performance liquid chromatography (HPLC). The mobile phases consisted of solvent A, which was 0.1% trifluoroacetic acid (TFA) in H_2O, and solvent B, which was 0.1% TFA in acetonitrile. A linear gradient of solvent B in solvent A was utilized, ranging from 0% to 50% over a period of 15 minutes. The rate of flow was 1.0 ml per minute. The detection method utilized absorbance measurements at wavelengths of 220 nm and 662 nm. The incubation process of the samples was carried out using the EYELA SLI-400 incubator. Fluorescence microscopy (ECLIPSE Ts2-FL, Nikon) was used to obtain images of the probe SQ-122 PC with and without enzymes. The wavelength used for excitation was 580 nm.

4.2.2 SQ-122 Dye and Dye Intermediates Synthesis

4.2.2.1 Synthesis of 2,3,3-trimethyl-3H-indole-5-carboxylic acid (2)

The synthesis of 2,3,3-trimethyl-3H-indole-5-carboxylic acid was carried out using the technique described by Pandey et al. [29]. **TOF-mass**: $C_{12}H_{13}NO_2$ (calculated *m/z* = 203.0946 and measured m/z = 204.1028 $[M+H]^+$).

4.2.2.2 Synthesis of 1-butyl-5-carboxy-2,3,3-trimethyl-3H-indolium (3)

2,3,3-trimethyl-3H-indole-5-carboxylic acid (1 equivalent) and 1-iodobutane (3 equivalents) were dissolved in acetonitrile and the reaction was heated to reflux for 36 hours at 90^0C. The reaction was seen using thin-layer chromatography (TLC) with a chloroform: methanol (9:1) solvent solution. After the reaction was finished, the solvent was removed by evaporation using reduced pressure, and the result was obtained by adding a sufficient amount of ether, causing it

to precipitate. The solid was subjected to filtration and subsequent drying, resulting in a yield of 81%. **TOF-mass** (measured 260.17 $[M]^+$; calculated 260.16451).

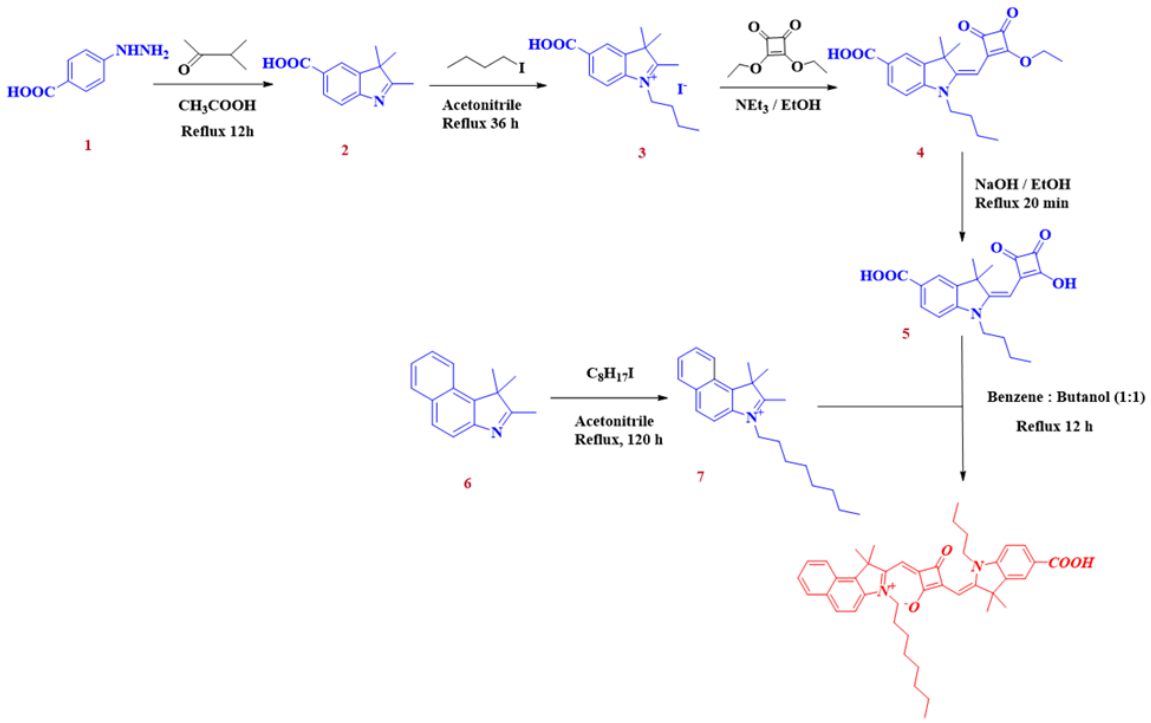

Scheme 2. *Scheme for synthesis for unsymmetrical squaraine dye SQ-122.*

4.2.2.3 Synthesis of semi squaraine ester (4)

1-Butyl-5-carboxy-2,3,3-trimethyl-3H-indolium (5 g; 19 mmol), diethoxy squarate (3.4 g; 20 mmol), and trimethylamine (2 ml) were dissolved in ethanol in a round bottom flask equipped with a condenser. Subsequently, the combination underwent reflux for a duration of 1 hour. The advancement of the reaction was observed through the use of thin-layer chromatography (TLC). After the reaction completed as shown by thin-layer chromatography (TLC), the solvent was evaporated using reduced pressure. The crude substance was subsequently refined using silica gel column chromatography, resulting in a yield of 60%. **TOF-Mass** (measured 384.81 $[M+H]^+$ and 406.16 $[M+Na]^+$; calculated 383.18327 $[M+H]^+$).

4.2.2.4 Synthesis of 1,1,2-trimethyl-3-octyl-1H-benzo[e]indol-3-ium (7)

In a round-bottomed flask equipped with a condenser, 5 g (equivalent to 1 mole) of 1,1,2-trimethyl-1H-benzo[e]indole (6) and 17.2 g (equivalent to 3 moles) of 1-iodoctane were dissolved in 50 ml of acetonitrile. The reaction mixture underwent reflux for a duration of 120 hours. The reaction was monitored using thin-layer chromatography (TLC) using an eluting solvent mixture of Hexane and Ethyl acetate in a 1:1 ratio. Once the reaction was finished, as confirmed by thin-layer chromatography (TLC), the solvent was removed by evaporation using a vacuum. The product was precipitated using hexane, and the resulting solid was filtered and dried under a vacuum. **TOF-Mass** (322.25 measured $[M+H]^+$; calculated 322.25293 $[M+H]^+$)

4.2.2.5 Synthesis of Unsymmetrical Squaraine Dye (SQ122)

A round bottom flask was used to dissolve 1 g (2.6 mmol) of semi-squaraine ester in 30 ml of ethanol. 0.6 cc of a 40% NaOH solution was added to the reaction mixture, which was then heated to 100^0C and refluxed for 30 minutes. The progress of the reaction was observed using thin-layer chromatography (TLC). After the reaction was completed, the mixture was cooled and 1.2 ml of hydrochloric acid with a concentration of 20% was added. After being cooled, the solvent was removed by evaporation using decreased pressure. To the resulting residue, 1,1,2-trimethyl-3-octyl-1H-benzo[e]indol-3-ium (676.72 mg; 2.1 mmol) and a mixture of benzene and butanol in a 1:1 ratio were added. The combination was thereafter subjected to reflux at a temperature of 1100C for a duration of 12 hours. The progress of the reaction was observed using thin-layer chromatography (TLC) and high-performance liquid chromatography (HPLC). Following the reaction, the solvent was evaporated and the crude product was purified using silica gel column chromatography, resulting in a yield of 60%. **TOF-Mass** (measured 659.39 $[M+H]^+$; 658.37706 calculated). **^{1}H NMR** (500 MHz, $CDCl_3$): δ /ppm = 8.22 (d, 1H, CH_{arom}); 8.12 (d, 1H,CH_{arom}); 8.0 (s,1H, CH_{arom}); 7.9(t,1H, CH_{arom}); 7.61 (t,1H,CH_{arom}); 7.48 (t,1H,CH_{arom}); 7.35 (d,1H,CH_{arom}); 6.16 (s,1H,C$H_{methine}$); 6.03 (s,1H, C$H_{methine}$); 4.21 (t,2H,N-C$H_{methylene}$); 3.97 (t,2H,N-C$H_{methylene}$); 2.96 (s,6H,CH_{methyl}); 2.89 (s,6H, CH_{methyl}) ; 1.90-1.77 (m, 4H,$CH_{methylene}$) ; 1.51-1.25 (m,12H, $CH_{methylene}$); 1.0 (t, 3H, CH_{methyl}); 0.86 (t, 3H, CH_{methyl}) and **^{13}C NMR** (500 MHz, $CDCl_3$) : δ /ppm = 181.52, 176.20, 173.99, 170.22, 167.85, 147.19,

141.99, 139.15, 135.39, 131.16, 129.88, 129.74, 128.53, 127.54, 124.87, 124.01, 123.80, 122.72, 110.35, 108.21, 87.80, 87.35, 51.83, 48.32, 44.28, 43.43, 31.71, 29.31, 29.13, 29.01, 27.60, 27.31, 27.01, 26.58, 22.59, 20.38, 14.06 and 13.89 confirms the identity of the synthesized product.

4.2.3 Synthesis of Peptide Sequence by Solid Phase Peptide Synthesis

Fmoc-Lys (Boc)OH was bound onto Rink Amide MBHA resin with a substitution rate of 0.41 mmol/g of resin. The loading process was carried out using Fmoc/piperidine methods on a scale of 0.432 mmol. HBTU and HOBT.H_2O were utilized as activating agents. Afterwards, Fmoc-β-Ala-OH, Fmoc-Ala-OH, Fmoc-Phe-OH, Fmoc-Ala-OH, and Fmoc-β-Ala-OH were attached. A small quantity of the resin-bound peptide was treated with a mixture of TFA, Triisopropylsilane, and H_2O at a ratio of 95:2.5:2.5. The peptide was then detached from the resin in the cleavage cocktail. The peptide was precipitated using ether in an ice bath. The crude peptide was purified using High Performance Liquid Chromatography (HPLC). The substrate that had been purified underwent analysis using high-resolution mass spectrometry (HR-MS) with electrospray ionization time-of-flight mass spectrometry (ESI-TOF-MS). The measured TOF mass is 799.42 $[M+H]^+$, while the computed mass is 798.40646.

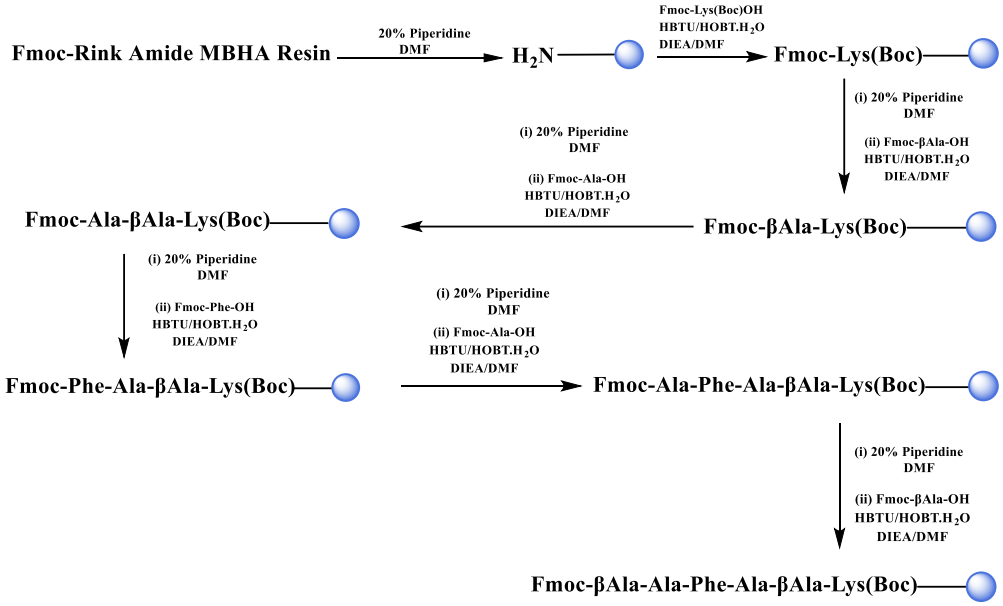

Scheme 3. *Scheme for the synthesis of peptide sequence Fmoc-βAla-Ala-Phe-βAla-Lys (Boc)-Resin.*

4.2.4 Synthesis of Dye Peptide Conjugate (SQ-122 PC)

Solid-phase peptide synthesis was used to synthesize the fluorescent probe SQ-122 PC, as indicated in **Scheme 2**. The synthesis of the resin-supported peptide (Fmoc-βAla-Ala-Phe-βAla-Lys (Boc)-Resin) began with the Fmoc group being deprotected by 20% piperidine treatment, and the Boc group being removed by subjecting it to HCl/Dioxane (2M) for 10 minutes. After deprotection, the elongated peptide was coupled with SQ-122 using HOBt/HBTU as a coupling reagent at a molar ratio of 2.2:1. After that, a cleavage cocktail of TFA/Triisopropylsilane/H_2O in a ratio of 95: 2.5: 2.5 was used to separate the resin-supported peptide from the resin. Following cleavage, the dye-peptide conjugate was precipitated using ether in an ice bath and then purified further employing silica gel column chromatography utilizing a solvent system composed of methanol: chloroform (9:1). A good yield of the dye-peptide conjugate was obtained using this purification method. A characteristic dark reddish colour was observed by the resultant compound, signifying the conjugate successful synthesis. Time of Flight (TOF)-Mass spectrometry analysis was used to verify the successful synthesis, which showed 1858.10 [$M+H^+$] and 1880.07 [$M+Na^+$] (calculated 1857.07137) as measured values. This analytical validation demonstrates the efficacy of the synthetic approach used in the conjugation process and validates the accurate synthesis of the dye-peptide conjugate.

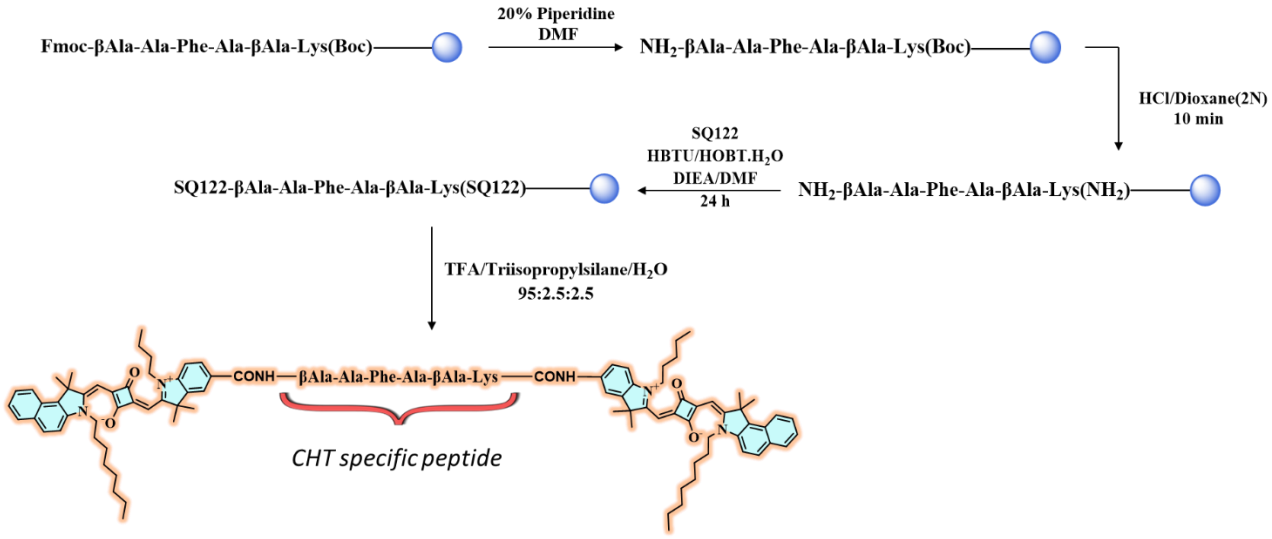

Scheme 2. *The scheme for synthesizing the dye-peptide conjugate SQ122-PC.*

4.2.3 Spectroscopic Measurements

A highly purified solution of SQ-122 PC (100 μM) in DMSO was prepared and subsequently diluted with H_2O (pH 7.2, 30% DMSO) for use. The α-chymotrypsin bovine pancreatic stock solution had a concentration of 100μM in PBS (pH 7.2, 0.1M) and was utilized after being diluted. Similarly, the concentration of the stock solution for other enzymes was 100μM in PBS (pH 7.2, 0.1M). The fluorescence response of SQ-122 PC (at a concentration of 5 μM) to CHT was assessed in an aqueous solution (pH 7.2, including 30% DMSO) using the following procedure. The reaction mixture, consisting of a probe and an enzyme, was incubated at a temperature of 37°C. The total volume of the mixture was 3 ml. The fluorescence response at a wavelength of 669 nm was measured using excitation and emission slit widths of 10 nm. Measurements were taken after 5 minutes and then every 10 minutes for a total duration of 60 minutes. The chymotrypsin concentration in the cuvette ranged from 0.025nM to 25nM, with increments of 0.025nM. The volume of the reaction mixture was modified to get a final concentration of the probe at 5 μM. To compare variations in fluorescence intensity, a baseline intensity called F_0 was determined by measuring the fluorescence of SQ-122 PC at a concentration of 5 μM in a solution of H_2O (30% DMSO) at a wavelength of 669 nm. The standard measurement was used as a reference to evaluate the fluorescence response of SQ-122 PC to chymotrypsin under specific conditions. This measurement provided a quantitative basis for examining the interaction between the enzyme and the probe.

4.2.4 Evaluation of the Detection Limit in Chymotrypsin Assays

The probe (SQ-122 PC) was diluted to a concentration of 5μM in H_2O using 30% DMSO. The concentrations of chymotrypsin varied from 0.025 nM to 0.5 nM. The fluorescence recovery of each substrate was evaluated after 60 minutes by incubation at a temperature of 37 degrees Celsius, using the emission maxima of 669 nm. The detection limit for chymotrypsin was found with the following formula [29]:

$$\mathbf{LOD = 3.3\ (SD)/S}$$

SD represents the standard deviation of the sample, whereas S specifies the slope derived from the linear portion of the calibration curve fitting.

4.2.5 Fluorescence Quenching Efficiency

The calculation of fluorescence quenching efficiency was performed using the following formula [30]:

$$\text{Fluorescence quenching efficiency (\%)} = [\mathbf{1} - (\boldsymbol{F_{PC}/F_{dye}})] \times \mathbf{100}$$

F_{PC} represents the emission intensity of SQ-122 PC, while F_{dye} is the emission intensity of the SQ-122 dye at the same concentration in H_2O (30%).

4.3 Results and Discussion

Two squaraine dye molecules are firmly attached to both ends of the peptide terminals in the recently proposed peptide-dye conjugation. Squaraine dye was chosen as the model dye due to its far-red fluorescence emission and its good interactions with commonly used model proteins, such as human serum albumin and bovine serum albumin [28,31–33]. The behavior of the squaraine dye in aqueous settings is mostly determined by its chain length, which affects aggregation formation. In particular, shorter chain lengths are more likely to produce J-aggregates as well as H-aggregates. On the other hand, longer alkyl chain substitutions like octyl and dodecyl have been shown to oppose this aggregation by causing steric hindrance [34]. Consequently, a benzo[e]indole squaraine dye (SQ-122) has been synthesized, as depicted in Figure 1(a), with an octyl chain substituting the benzo indole ring N-terminal. Chymotrypsin, a serine protease from the super-family, is known to disrupt peptide bonds on the C-terminal side of amide linkages that have aromatic side chains, such as tyrosine (Tyr), phenylalanine (Phe), tryptophan (Trp), and others. We synthesized a specific tripeptide Ala-Phe-Ala and incorporated β-Alanine (β-Ala) as a spacer to facilitate the access of the chymotrypsin enzyme to the selected probe. Conversely, the attachment of the terminal squaraine dye to the side chain necessitated the incorporation of lysine (Lys).

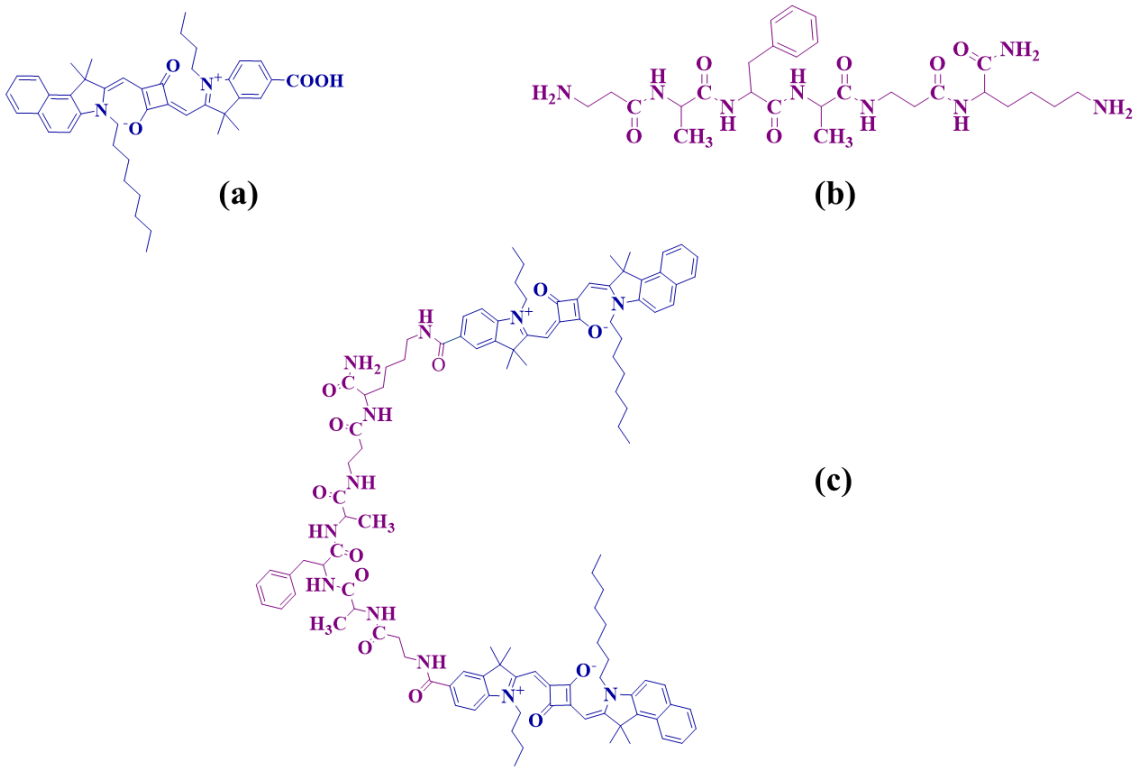

Figure 1. *Chemical structure of unsymmetrical squaraine dye (SQ-122) (a), chymotrypsin enzyme specific peptide (b) dye-peptide conjugate probe (SQ-122 PC) (c)*

4.3.1 Photophysical Characterization of Dye and the Probe

The electronic absorption spectra of SQ-122 in dimethyl sulfoxide (DMSO) solution show a vibrionic shoulder at 620 nm and a distinct electronic absorption peak with an absorption maximum (λ_{abs}) at 667 nm. On the other hand, the emission spectra of SQ-122 has a fluorescence emission peak at 682 nm, which leads to a relatively small difference in wavelength (Stokes shift) of 15 nm. The low Stokes shift seen in SQ-type molecules suggests that the structural arrangements of the dye ground and excited states are highly similar [35]. Table 1. presents the molar extinction coefficients (ε), Stoke shifts (Δ), absorption maxima (λ_{abs}), emission maxima (λ_{em}), and molar extinction coefficients (ε) of SQ-122 standalone dye and SQ-122 PC at a concentration of 5 μM in DMSO and H_2O (with 30% DMSO). This data provides a clear explanation of the optical characteristics of SQ-122, emphasizing the dye consistent chemical

structure in many states and showcasing its potential for use in fluorescence-based detection and imaging methods.

Table 1. *The photophysical characteristics of SQ-122 and SQ-122 PC in DMSO H_2O (30% DMSO).*

	DMSO				**H_20 (30% DMSO)**			
	λ_{abs}	λ_{em}	Δ	ε ($dm^3\ mol^{-1}\ cm^{-1}$)	λ_{abs}	λ_{em}	Δ	ε ($dm^3\ mol^{-1}\ cm^{-1}$)
SQ-122	667 nm	682 nm	15 nm	1.85×10^5	659 nm	669 nm	10	0.62×10^5
SQ-122 PC	667 nm	682 nm	15 nm	1.95×10^5	662 nm	669 nm	7	0.68×10^5

For Förster resonance energy transfer (FRET) to occur, there must be a significant overlap between the excitation spectra of the acceptor and the emission spectrum of the donor. In the context of homo-FRET, energy transfer takes place between two identical fluorophores, as long as there is an overlap between their excitation and emission spectra [36]. Figure 2 (a) clearly shows that the excitation (absorption spectrum) and emission spectrum of the SQ-122 fluorophore overlap due to the extremely small stokes shift. Thus, SQ-122 can be recognized as an appropriate fluorophore for the development of the homo-FRET probe. In addition, homo-FRET refers to the transfer of energy between identical fluorophores, without affecting the spectral properties of the fluorophore and the probe [37].

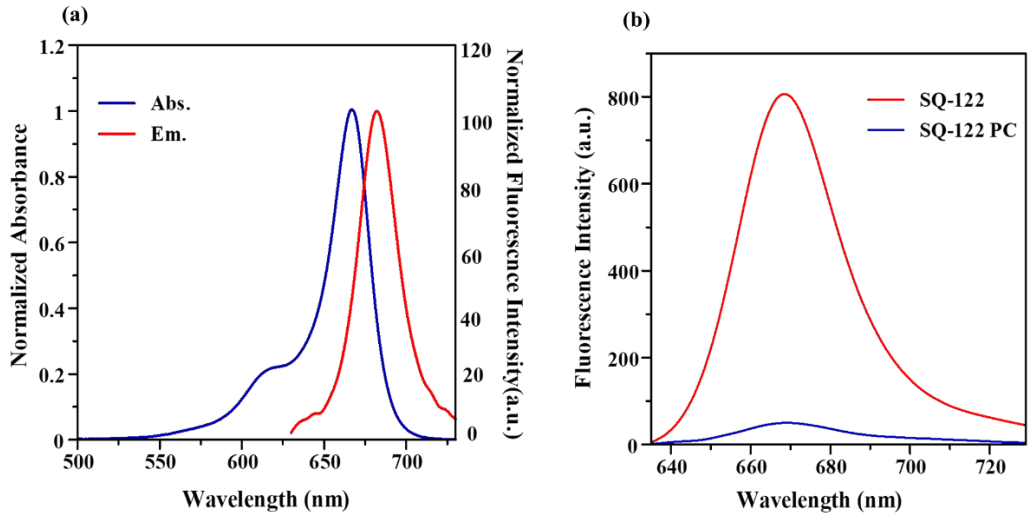

Figure 2. *(a) Spectra of normalized absorbance and normalized fluorescence intensity of SQ-122 in DMSO at a concentration of 5µM. (b) The fluorescence emission spectra of SQ-122 (5µM) and the probe, SQ-122 PC (5µM), were measured in H_2O with 30% DMSO as a co-solvent. The instrumental configuration for the excitation and emission involved setting the slit width at 10 nm for both.*

The absorption spectra displayed in Figure 3(a) reveal that both SQ-122 and the probe SQ-122 PC exhibit an absorption peak at the absorption maximum (λ_{max}) of 669 nm in DMSO. This indicates that the addition of peptides does not modify the fundamental spectral characteristics of the dye molecule. However, when the SQ-122 PC is in a medium containing H_2O (30% DMSO), its absorption spectra (shown in Figure 3(b)) display a distinct peak at 616 nm and a displaced peak at 662 nm, indicating the presence of dye aggregation. The aggregation tendencies observed in squaraine dyes, which result in either blue-shifted H-aggregates or red-shifted J-aggregates, are controlled by their flat molecular structure and ambient variables [38]. The quantum yield of the dye was measured to be 0.16%.

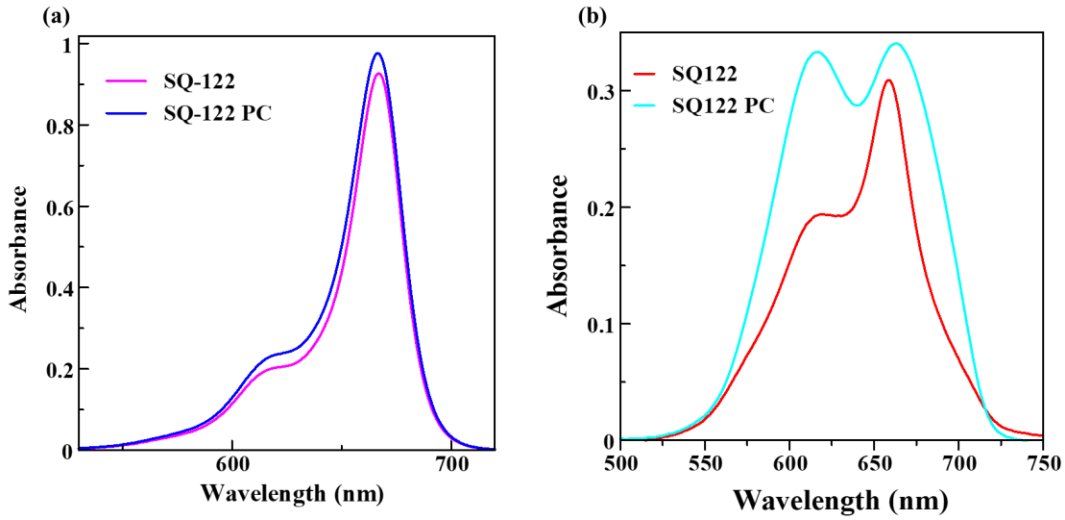

Figure 3. *Electronic absorption spectra of SQ-122 and SQ-122 PC were measured in two different solvents: (a) 5μM solution of DMSO and (b) 5μM solution of H_2O (30% DMSO).*

Remarkably, when both SQ-122 PC and pure dye SQ-122 are present in a solution with the same concentration (5 μM) and solvent (H_2O, 30% DMSO), the fluorescence intensity of SQ-122 PC is noticeably reduced compared to that of the pure dye SQ-122. Based on the finding, it can be concluded that fluorescence quenching occurs when SQ-122 is connected to the investigated peptide (SQ 122- PC), as depicted in Figure 2(b). The observed quenching effect indicates the presence of Förster Resonance Energy Transfer (FRET) within the probe labeled with the same dye, which can be attributed to the small difference in energy levels (Stokes shift) of the system. In these cases, there is often a phenomenon called FRET-mediated quenching, which occurs due to a significant overlap between the absorption and emission spectra of the dye. This aligns with the empirical observations found in this study. The fluorescence quenching efficiency in H_2O (30% DMSO) was determined to be 93.75% based on the peak fluorescence intensities of the dye alone (SQ-122) and the dye-peptide conjugate (SQ-122 PC).

4.3.2 Enzymatic Hydrolysis of SQ-122 PC with Chymotrypsin

Figure 2(b) demonstrates that the SQ-122 PC probe exhibits a diminished fluorescence as a result of the homo-FRET quenching phenomenon. After incubation with chymotrypsin, a significant rise

in fluorescence at 669 nm is detected. Various doses of chymotrypsin, ranging from 0 to 25 nM, were mixed with 5 μM of SQ-122 PC in H_2O (30% DMSO). The mixture was

then incubated for 60 minutes. The inclusion of the chymotrypsin enzyme resulted in a significant restoration of the quenched fluorescence of the dye, as depicted in **Figure 4(a)**. The significant increase in the fluorescent signal can be attributed to the enzymatic breakdown of the SQ-122 PC, which causes the separation of FRET pairs and thus leads to an increase in fluorescence intensity. When the enzyme acts on the peptide, it breaks it down, which interrupts the transmission of energy between two squaraine dyes. This interruption causes a detectable change in the intensity of fluorescence. An increase in the intensity of fluorescence can be seen at the specific wavelength where the fluorophore emits light, which is directly linked to the amount of activity of the enzyme. The fluorescence signal increased by a factor of eight when 25 nM of chymotrypsin was added, compared to when the enzyme was absent. Additionally, the fluorescence signal increased by a factor of three when 5 nM of chymotrypsin was added, as shown in **Figure 3(b).** In addition, the inclusion of 0.5 nM of chymotrypsin results in a doubling of the fluorescent signal within 60 minutes, as depicted in **Figure 5**. The symbol F_0 represents the initial fluorescence intensity when the enzyme is not present, while F represents the fluorescence intensity at a specified time point after the enzyme is added.

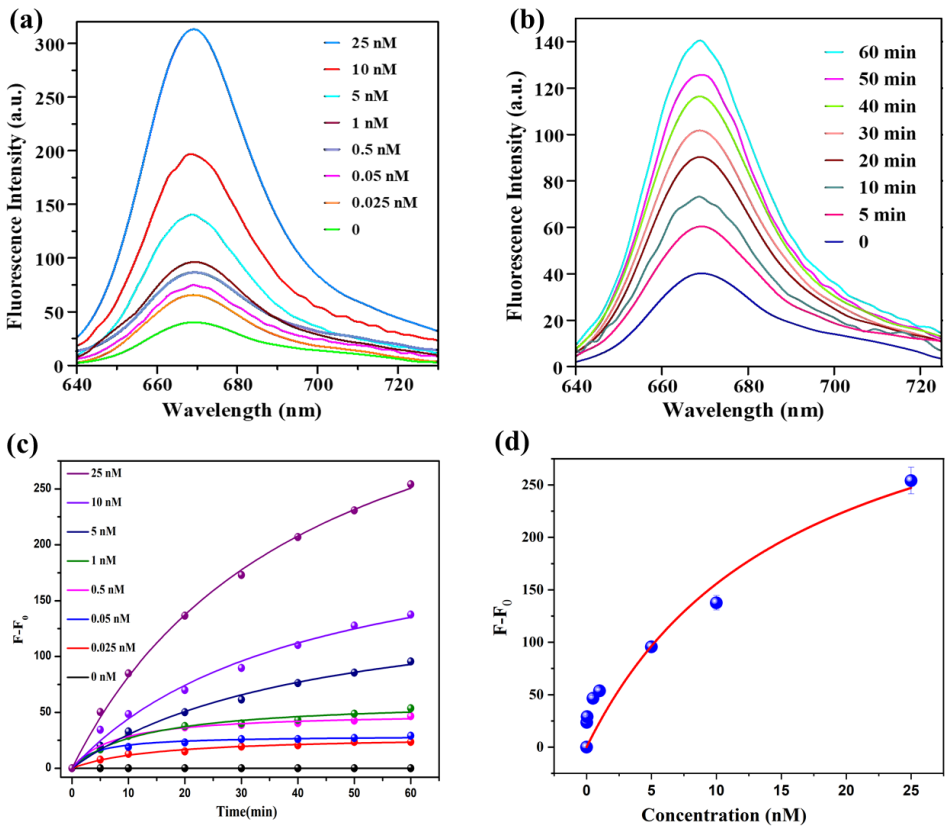

Figure 4. *(a) Concentration-dependent fluorescence spectra of SQ-122 PC (5μM) in H_2O (30%DMSO) at 37°C for 60 min with the addition of 0 to 25 nM of chymotrypsin. (b)Time-dependent fluorescence spectra of SQ-122 PC (5μM) in H_2O (30%DMSO) at 37°C for 60 min with the addition of 5 nM of chymotrypsin. (c) Plot of difference in fluorescence intensity ($F-F_0$) vs time. (d) Plot of difference in fluorescence intensity ($F-F_0$) vs concentration of enzyme.*

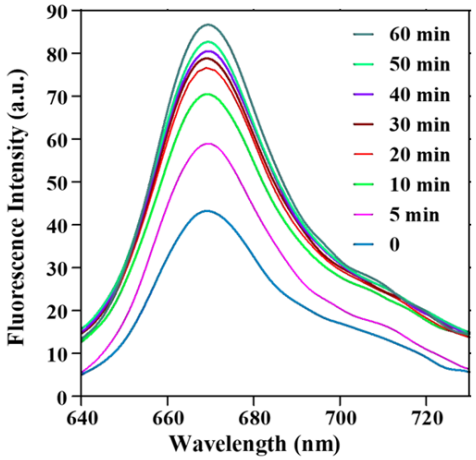

Figure 5. *Time-dependent fluorescence spectra of SQ-122 PC, probe towards chymotrypsin. The concentration of chymotrypsin is 0.5nM.*

4.3.3 Fluorescence Microscopy Images

Our study investigated the fluorescence characteristics of SQ-122 PC under various conditions using fluorescence microscopy [39,40], with a specific focus on the effect of chymotrypsin. We conducted a comparison of fluorescence images acquired for SQ-122 PC under two different conditions, as shown in Figure 6. (a)(b). Under condition (a), the fluorescence intensity of SQ-122 PC is insignificant when there is no enzyme present. Nevertheless, following pre-incubation with chymotrypsin (condition b), we observed a substantial augmentation in fluorescence emission. This increase in the fluorescence signal indicates the presence of FRET off, which signifies a modification in the energy transfer dynamics within the dye-peptide combination.

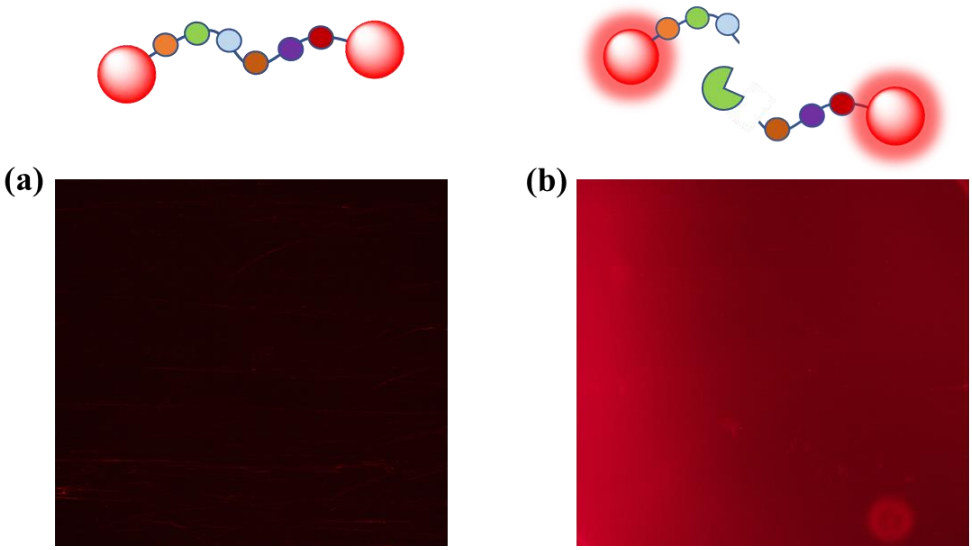

Figure 6. *Fluorescence microscopy images were taken of (a) SQ-122 PC (5μM) in H_2O (30% DMSO) and (b) SQ-122 PC (5μM) in H_2O (30% DMSO) that had been pre-incubated with 25 nM of chymotrypsin at 37°C for 60 min.*

4.3.4 Validation of the Peptide Cleavage by Chymotrypsin

A comprehensive investigation was undertaken to investigate the effects of chymotrypsin (CHT) on the enzymatic hydrolysis of the SQ-122 PC probe and its subsequent impact on emission spectral features. This work utilized high-performance liquid chromatography (HPLC) and high-resolution mass spectrometry (HRMS). Figure 7 illustrates the HPLC peaks observed for SQ-122 PC both before and after pre-incubation with CHT in a solution containing 30% DMSO in water,

at 30 minutes and 60 minutes. The m/z 1858.08 peak represents the $[M+H]^+$ ion of SQ-122 PC, indicating its molecular ion. The presence of a single peak indicates the probe's exceptional purity. On the other hand, the HRMS spectrum obtained by analyzing the reaction mixture of probe SQ-122 PC with CHT shows a significant peak at m/z=948.52 $[M+H]^+$ and 929.54 $[M+H]^+$ (Figure 10). This indicates that the substrate underwent hydrolysis, resulting in the emergence of two asymmetrical fragments formed by fragmenting the Phe-Ala peptide bond. The HPLC chromatogram revealed the presence of the SQ-122 PC and its subsequent reaction products with retention time of 26.26 min, 22.19 min, and 19.51 min, respectively. The appearance of additional peaks at 22.19 min/22.16 min and 19.51 min/19.48 min (shown in Figure 7(b)(c)) indicates the creation of two asymmetrical fragments, SQ122 - βAla-Ala-Phe and Ala- βAla-Lys-SQ122, as a result of chymotrypsin's enzymatic activity. The thorough examination using High-Performance Liquid Chromatography (HPLC) and High-Resolution Mass Spectrometry (HRMS) not only verifies the effectiveness of the probe in identifying substrates but also offers essential information on the exact locations where the probe is cleaved and the resulting fragments that are produced when it interacts with the target enzyme. These discoveries not only improve our understanding of how enzymes work but also provide a basis for creating advanced techniques to detect enzymes and customized molecular tools for various analytical and diagnostic purposes [41].

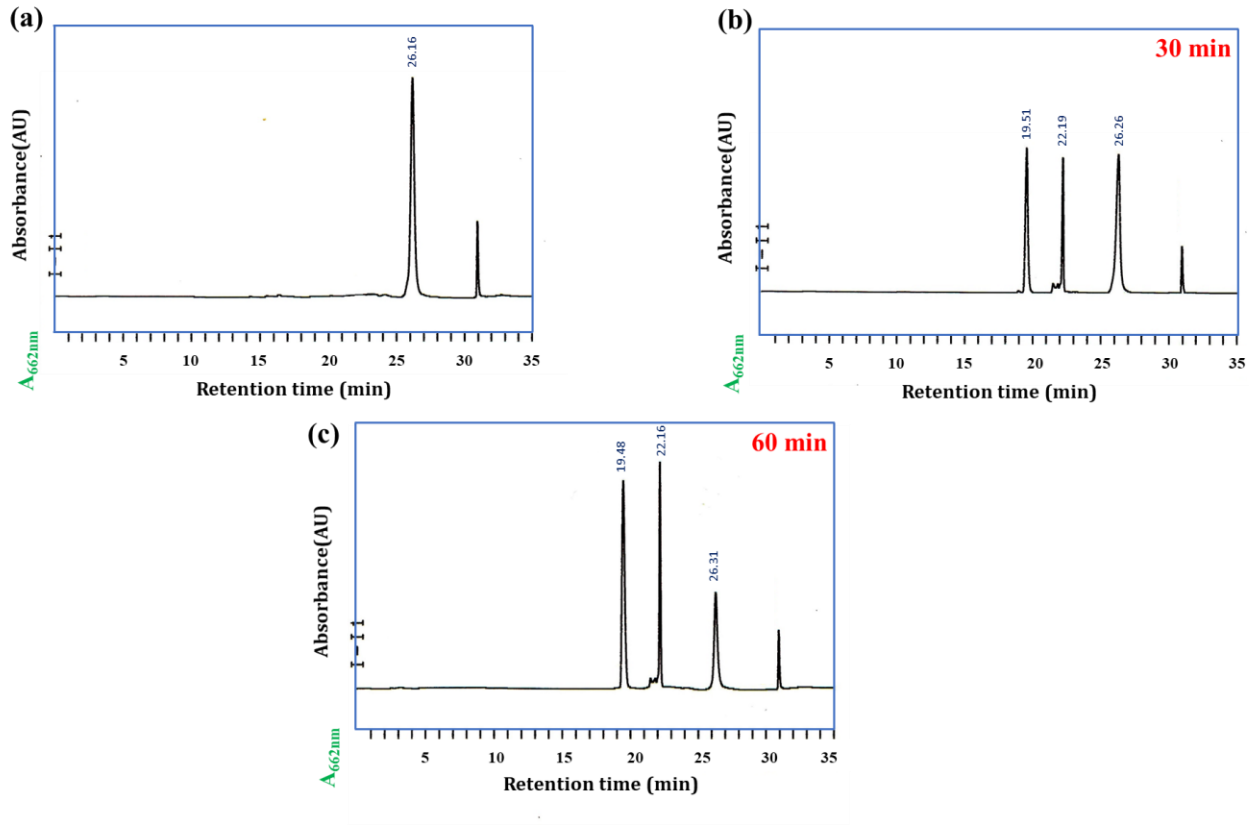

Figure 7. *HPLC chromatogram that confirms the enzymatic cleavage of SQ-122 PC with chymotrypsin. (a) SQ-122 PC (10uM) in H_2O with 30% DMSO (0 min). (b) SQ-122 PC and chymotrypsin (10 nM) in H_2O (30% DMSO) incubated at 37^0C for 30 min. (c) SQ-122 PC and chymotrypsin (10 nM) in H_2O (30% DMSO) incubated at 37^0C for 60 min. The mobile phase was acetonitrile/water, and the flow rate was 1.0 mL/min.*

4.3.5 Enzyme Selectivity of the Probe SQ-122 PC

The selectivity studies of chymotrypsin in the presence of different enzymes involve investigating the enzyme's ability to selectively recognize and cleave specific substrates in the presence of other enzymes. Chymotrypsin, papain, elastase pancreatic, peroxidase from horseradish, trypsin, and BSA (each enzyme at an amount of 25 nM) were introduced into a solution of the probe in H_20 (with 30% DMSO) at a concentration of 5μM. The mixture was then kept at an ambient temperature of 37°C for a duration of 60 minutes. Figure 8 demonstrates that the emission intensity at 669 nm showed little fluctuations in the presence of possible competing enzymes. Nevertheless,

a notable surge in emission intensity was detected after the introduction of chymotrypsin. Nevertheless, there was a notable rise in emission intensity after the use of chymotrypsin. This significant alteration highlights the probe's remarkable selectivity for chymotrypsin, demonstrating its capacity to specifically interact with and react to the presence of this specific enzyme among other competing enzymes.

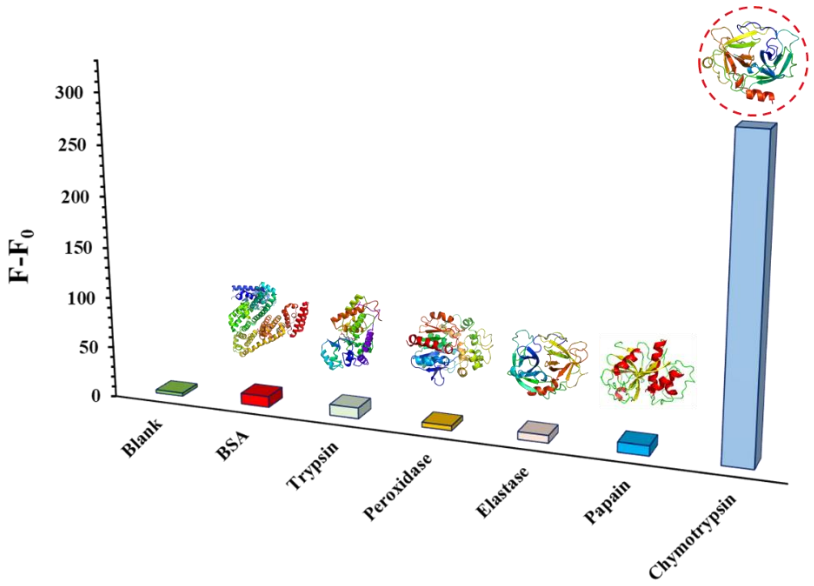

Figure 8. *Fluorescence response (F/F_0) of the probe towards various possible species (chymotrypsin, papain, pancreatic elastase, peroxidase from horseradish, trypsin, and BSA) at a concentration of 25 nM.*

4.3.6 Sensitivity of the SQ-122 PC Probe for Chymotrypsin

To assess the responsiveness of SQ-122 PC, various doses of chymotrypsin (0, 0.025 nM, 0.05 nM, 0.1 nM, 0.25 nM, and 0.5 nM) were added to SQ-122 PC solutions (5 μM) in H_2O (30% DMSO) at a temperature of 37°C for a duration of 60 minutes. Afterward, the fluorescent emission at a wavelength of 669 nm was measured. Figure 7(b) depicts a linear graph that shows the variation in fluorescence intensities of each sample concerning their respective enzyme concentrations. The equation for linear regression is y = 42.15081x + 24.8361, with an R-squared value of 0.91098. The analysis demonstrated an impressive limit of detection (LOD) of 130 pM for chymotrypsin, showcasing the assay outstanding sensitivity. Compared to probes used in previous studies, the SQ-122 PC probe stands out as a remarkably efficient and effective tool for detecting chymotrypsin.

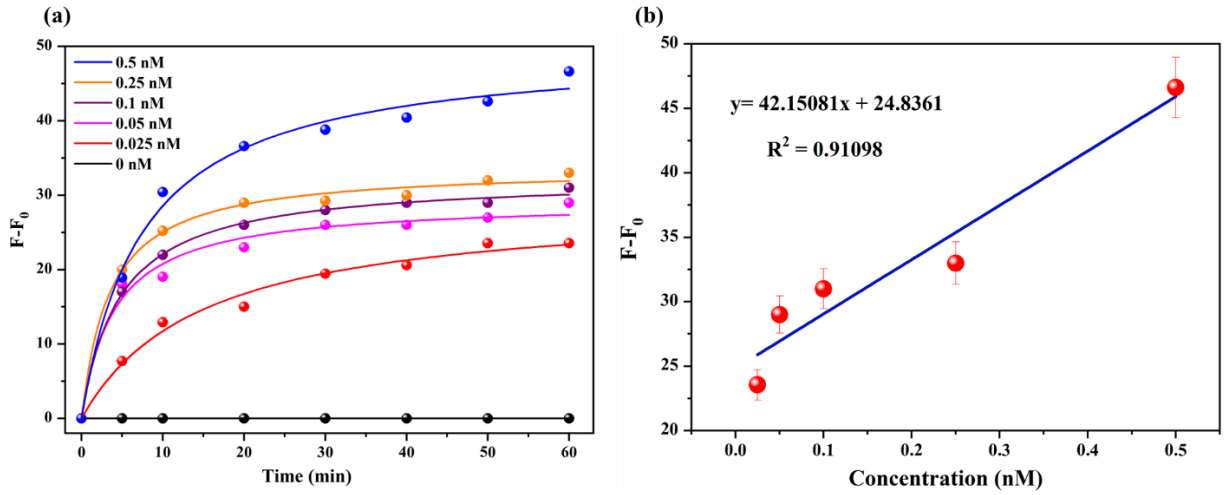

Figure 9. *(a) The difference in fluorescence intensity with time with the addition of 0, 0.025, 0.05, 0.1,0.25, and 0.5 nM of chymotrypsin in 5μM of probe in H_2O (30%DMSO) incubated at 37°C for 60 min. (b) Linear correction curve of difference in fluorescence intensity at 669 nm against chymotrypsin concentration.*

Table 2. provides a comprehensive evaluation of the performance of SQ-122 PC in detecting chymotrypsin, concerning other techniques reported in the literature. Our results show that our method has comparable or even better limits of detection (LOD) compared to existing approaches. Additionally, our method has the advantage of being able to detect in the far-red spectral region, which sets it apart from conventional techniques.

Table 2. Comparison of SQ-122 PC with previously reported work for CHT detection.

Methods	Probe	$\lambda_{ex}/\lambda_{em}$(nm)	Far-red	LOD	Reference
Turn-on fluorescence	Probe	450/515	No	50 ng/ml	[42]
Ratiometric Fluorescent	NI	385/450 and 550	No	0.34 nM	[43]
Turn-on fluorescence	CyB	670/695	Yes	0.5 nM	[44]
Turn-on fluorescence	$PPESO_3$	440/520	No	6 pM	[45]
Turn-on fluorescence	**SQ-122 PC**	**662/669**	**Yes**	**0.13 nM**	**This work**

4.4 Conclusions

In conclusion, we have successfully and effectively synthesized a novel far-red fluorescent probe based on squaraine dye that exhibits very high sensitivity in the far-red wavelength range for the specific detection of chymotrypsin activity. The activation of Förster resonance energy transfer (FRET) in the probe resulted in a reduction of fluorescence intensity. Nevertheless, when the probe was exposed to the enzyme, there was a significant increase in fluorescence emission in the far-red region as a result of FRET-off. The probe exhibited exceptional sensitivity, with an impressively low detection limit of 0.130 nM. Additionally, it demonstrated excellent selectivity for chymotrypsin even in the presence of other competitive enzymes. The research's implications go beyond its immediate conclusions, offering a flexible foundation for creating far-red probes that are specifically designed to detect particular enzyme activities. This would improve the capabilities of biochemical analysis and diagnostic techniques.

4.5 References

1. Turk, B. Targeting Proteases: Successes, Failures and Future Prospects. *Nat. Rev. Drug Discov.* **2006**, *5*, 785–799, doi:10.1038/nrd2092.

2. Kos, J. Proteases: Role and Function in Cancer. *Int. J. Mol. Sci.* 2022, *23*.

3. Banerjee, D.; Pal, S.K. Conformational Dynamics at the Active Site of α-Chymotrypsin and Enzymatic Activity. *Langmuir* **2008**, *24*, 8163–8168, doi:10.1021/la8010184.

4. Welzel, P.B. Investigation of Adsorption-Induced Structural Changes of Proteins at Solid/Liquid Interfaces by Differential Scanning Calorimetry. *Thermochim. Acta* **2002**, *382*, 175–188, doi:https://doi.org/10.1016/S0040-6031(01)00728-6.

5. Chen, Q.; Zhang, J.; Zhao, K.; Li, W.; Miao, Q.; Sun, Y.; Zhao, X.; Wei, T.; Yang, F. Lysosomal Chymotrypsin Induces Mitochondrial Fission in Apoptotic Cells by Proteolytic Activation of Calcineurin. *Protein Cell* **2014**, *5*, 643–647, doi:10.1007/s13238-014-0085-5.

6. Rauh, R.; Diakov, A.; Tzschoppe, A.; Korbmacher, J.; Azad, A.K.; Cuppens, H.; Cassiman, J.-J.; Dötsch, J.; Sticht, H.; Korbmacher, C. A Mutation of the Epithelial Sodium Channel Associated with Atypical Cystic Fibrosis Increases Channel Open Probability and Reduces Na+ Self Inhibition. *J. Physiol.* **2010**, *588*, 1211–1225, doi:https://doi.org/10.1113/jphysiol.2009.180224.

7. Wang, S.; Li, P.; Zhang, T.; Wang, S.; Copeland, L. Trypsin and Chymotrypsin Are Necessary for in Vitro Enzymatic Digestion of Rice Starch. *RSC Adv.* **2017**, *7*, 3660–3666, doi:10.1039/C6RA24816K.

8. Chymotrypsin and Anaphylactic Shock: Continuing Issue. *React. Wkly.* **2017**, 2.

9. Barraquer, J.; Rutllán, J. Alpha-Chymotrypsin in Cataract Surgery. *Postgrad. Med.* **1964**, *35*, 57–62, doi:10.1080/00325481.1964.11694979.

10. Grahn, S.; Ullmann, D.; Jakubke, H.-D. Design and Synthesis of Fluorogenic Trypsin Peptide Substrates Based on Resonance Energy Transfer. *Anal. Biochem.* **1998**, *265*, 225 – 231, doi:10.1006/abio.1998.2902.

11. Sun, H.; Panicker, R.C.; Yao, S.Q. Activity Based Fingerprinting of Proteases Using FRET Peptides. In Proceedings of the Biopolymers - Peptide Science Section; 2007; Vol. 88, pp. 141–149.

12. Alhadrami, H.A.; Hassan, A.M.; Chinnappan, R.; Al-Hadrami, H.; Abdulaal, W.H.; Azhar, E.I.; Zourob, M. Peptide Substrate Screening for the Diagnosis of SARS-CoV-2 Using Fluorescence Resonance Energy Transfer (FRET) Assay. *Mikrochim. Acta* **2021**, *188*, 137, doi:10.1007/s00604-021-04766-5.

13. Zhang, J.; Chai, X.; He, X.-P.; Kim, H.-J.; Yoon, J.; Tian, H. Fluorogenic Probes for Disease-Relevant Enzymes. *Chem. Soc. Rev.* **2019**, *48*, 683–722, doi:10.1039/C7CS00907K.

14. Mineno, T.; Ueno, T.; Urano, Y.; Kojima, H.; Nagano, T. Creation of Superior Carboxyfluorescein Dyes by Blocking Donor-Excited Photoinduced Electron Transfer. *Org. Lett.* **2006**, *8*, 5963–5966, doi:10.1021/ol0623926.

15. Dong, Y.; Iagatti, A.; Foggi, P.; Zhao, J.; Mazzone, G.; Xu, K.; Ji, W.; Di Donato, M.; Russo, N. Bodipy-Squaraine Triads: Preparation and Study of the Intramolecular Energy Transfer, Charge Separation and Intersystem Crossing. *Dye. Pigment.* **2017**, *147*, 560–572, doi:10.1016/j.dyepig.2017.08.028.

16. Duke, R.M.; Veale, E.B.; Pfeffer, F.M.; Kruger, P.E.; Gunnlaugsson, T. Colorimetric and Fluorescent Anion Sensors: An Overview of Recent Developments in the Use of 1,8-Naphthalimide-Based Chemosensors. *Chem. Soc. Rev.* **2010**, *39*, 3936–3953, doi:10.1039/b910560n.

17. Gong, Y.-J.; Zhang, X.-B.; Mao, G.-J.; Su, L.; Meng, H.-M.; Tan, W.; Feng, S.; Zhang, G. A Unique Approach toward Near-Infrared Fluorescent Probes for Bioimaging with Remarkably Enhanced Contrast. *Chem. Sci.* **2016**, *7*, 2275–2285, doi:10.1039/C5SC04014K.

18. Chin, J.; Kim, H.-J. Near-Infrared Fluorescent Probes for Peptidases. *Coord. Chem. Rev.* **2018**, *354*, 169–181, doi:https://doi.org/10.1016/j.ccr.2017.07.009.

19. Kassab, K. Photophysical and Photosensitizing Properties of Selected Cyanines. *J.*

Photochem. Photobiol. B Biol. **2002**, *68*, 15–22, doi:https://doi.org/10.1016/S1011-1344(02)00325-1.

20. Matikonda, S.S.; Helmerich, D.A.; Meub, M.; Beliu, G.; Kollmannsberger, P.; Greer, A.; Sauer, M.; Schnermann, M.J. Defining the Basis of Cyanine Phototruncation Enables a New Approach to Single-Molecule Localization Microscopy. *ACS Cent. Sci.* **2021**, *7*, 1144–1155, doi:10.1021/acscentsci.1c00483.

21. Gross, S.; Piwnica-Worms, D. Molecular Imaging Strategies for Drug Discovery and Development. *Curr. Opin. Chem. Biol.* **2006**, *10*, 334–342, doi:10.1016/j.cbpa.2006.06.028.

22. Gayathri Devi, D.; Cibin, T.R.; Ramaiah, D.; Abraham, A. Bis(3,5-Diiodo-2,4,6-Trihydroxyphenyl)Squaraine: A Novel Candidate in Photodynamic Therapy for Skin Cancer Models in Vivo. *J. Photochem. Photobiol. B.* **2008**, *92*, 153–159, doi:10.1016/j.jphotobiol.2008.06.002.

23. Oswald, B.; Lehmann, F.; Simon, L.; Terpetschnig, E.; Wolfbeis, O.S. Red Laser-Induced Fluorescence Energy Transfer in an Immunosystem. *Anal. Biochem.* **2000**, *280*, 272–277, doi:10.1006/abio.2000.4553.

24. Ilina, K.; MacCuaig, W.M.; Laramie, M.; Jeouty, J.N.; McNally, L.R.; Henary, M. Squaraine Dyes: Molecular Design for Different Applications and Remaining Challenges. *Bioconjug. Chem.* **2020**, *31*, 194–213, doi:10.1021/acs.bioconjchem.9b00482.

25. Yadav, Y.; Owens, E.; Nomura, S.; Fukuda, T.; Baek, Y.; Kashiwagi, S.; Choi, H.S.; Henary, M. Ultrabright and Serum-Stable Squaraine Dyes. *J. Med. Chem.* **2020**, *63*, 9436–9445, doi:10.1021/acs.jmedchem.0c00617.

26. He, Y.; Mei, J.; Zhou, M.; Zhang, Y.; Liang, Q.; Xu, S.; Li, Z. Colorimetric and Fluorescent Probe for Highly Selective and Sensitive Recognition of Cu2+ and Fe3+ Based on Asymmetric Squaraine Dye. *Inorg. Chem. Commun.* **2022**, *142*, 109592, doi:https://doi.org/10.1016/j.inoche.2022.109592.

27. Saikiran, M.; Sato, D.; Pandey, S.S.; Hayase, S.; Kato, T. Efficient near Infrared Fluorescence Detection of Elastase Enzyme Using Peptide-Bound Unsymmetrical

Squaraine Dye. *Bioorg. Med. Chem. Lett.* **2017**, *27*, 4024–4029, doi:10.1016/j.bmcl.2017.07.057.

28. Saikiran, M.; Pandey, S.S.; Hayase, S.; Kato, T. Photophysical Characterization and BSA Interaction of Direct Ring Carboxy Functionalized Symmetrical Squaraine Dyes. *J. Phys. Conf. Ser.* **2017**, *924*, 12006, doi:10.1088/1742-6596/924/1/012006.

29. Piovarci, I.; Hianik, T.; Ivanov, I.N. Detection of Chymotrypsin by Optical and Acoustic Methods. *Biosensors* **2021**, *11*, doi:10.3390/bios11030063.

30. Liu, Y.; Zhang, D.; Ding, J.; Hayat, K.; Yang, X.; Zhan, X.; Zhang, D.; Lu, Y.; Zhou, P. A Facile Aptasensor for Instantaneous Determination of Cadmium Ions Based on Fluorescence Amplification Effect of MOPS on FAM-Labeled Aptamer. *Biosensors* **2021**, *11*, doi:10.3390/bios11050133.

31. Gupta, S.; Yamawaki, Y.; Pradhan, S.; Pandey, S.S.; Kato, T. Design and Synthesis of Novel Squaraine Dye with Highly Enhanced Far-Red Fluorescence and Its Interaction with a Model Protein. *Phys. status solidi* **2023**, *220*, 2300226, doi:https://doi.org/10.1002/pssa.202300226.

32. Jisha, V.S.; Arun, K.T.; Hariharan, M.; Ramaiah, D. Site-Selective Interactions: Squaraine Dye-Serum Albumin Complexes with Enhanced Fluorescence and Triplet Yields. *J. Phys. Chem. B* **2010**, *114*, 5912–5919, doi:10.1021/jp100369x.

33. Jiang, Q.; Chen, Z.; Huang, Y.; Gao, Q.; Luo, C.; Mehdi, M.; Xu, Y.; Li, H.; Sun, S. A Bovine Serum Albumin and Squaraine Dye Assembly Fluorescent Probe for Pepsin Detection. *Microchem. J.* **2023**, *186*, 108361, doi:https://doi.org/10.1016/j.microc.2022.108361.

34. Mavileti, S.K.; Bila, G.; Utka, V.; Bila, E.; Kato, T.; Bilyy, R.; Pandey, S.S. Photophysical Characterization and Biointeractions of NIR Squaraine Dyes for in Vitro and in Vivo Bioimaging. *ACS Appl. bio Mater.* **2024**, *7*, 416–428, doi:10.1021/acsabm.3c00997.

35. Marchena, M.J.; de Miguel, G.; Cohen, B.; Organero, J.A.; Pandey, S.; Hayase, S.; Douhal, A. Real-Time Photodynamics of Squaraine-Based Dye-Sensitized Solar Cells with Iodide and Cobalt Electrolytes. *J. Phys. Chem. C* **2013**, *117*, 11906–11919,

doi:10.1021/jp401399j.

36. Shrestha, D.; Jenei, A.; Nagy, P.; Vereb, G.; Szöllősi, J. Understanding FRET as a Research Tool for Cellular Studies. *Int. J. Mol. Sci.* **2015**, *16*, 6718–6756, doi:10.3390/ijms16046718.

37. Bader, A.N.; Hofman, E.G.; Voortman, J.; en Henegouwen, P.M.P. van B.; Gerritsen, H.C. Homo-FRET Imaging Enables Quantification of Protein Cluster Sizes with Subcellular Resolution. *Biophys. J.* **2009**, *97*, 2613–2622, doi:10.1016/j.bpj.2009.07.059.

38. Hu, L.; Yan, Z.; Xu, H. Advances in Synthesis and Application of Near-Infrared Absorbing Squaraine Dyes. *RSC Adv.* **2013**, *3*, 7667–7676, doi:10.1039/C3RA23048A.

39. Lee, A.I.; Brody, J.P. Single-Molecule Enzymology of Chymotrypsin Using Water-in-Oil Emulsion. *Biophys. J.* **2005**, *88*, 4303–4311, doi:10.1529/biophysj.104.055053.

40. Efimova, A.S.; Ustimova, M.A.; Chmelyuk, N.S.; Abakumov, M.A.; Fedorov, Y. V; Fedorova, O.A. Specific Fluorescent Probes for Imaging DNA in Cell-Free Solution and in Mitochondria in Living Cells. *Biosensors* **2023**, *13*, doi:10.3390/bios13070734.

41. Yuan, M.; Wu, Y.; Zhao, C.; Chen, Z.; Su, L.; Yang, H.; Song, J. Activated Molecular Probes for Enzyme Recognition and Detection. *Theranostics* **2022**, *12*, 1459–1485, doi:10.7150/thno.66676.

42. Wu, L.; Yang, S.-H.; Xiong, H.; Yang, J.-Q.; Guo, J.; Yang, W.-C.; Yang, G.-F. Nonpeptide-Based Small-Molecule Probe for Fluorogenic and Chromogenic Detection of Chymotrypsin. *Anal. Chem.* **2017**, *89*, 3687–3693, doi:10.1021/acs.analchem.6b05115.

43. Chen, Y.; Cao, J.; Jiang, X.; Pan, Z.; Fu, N. A Sensitive Ratiometric Fluorescence Probe for Chymotrypsin Activity and Inhibitor Screening. *Sensors Actuators B Chem.* **2018**, *273*, 204–210, doi:https://doi.org/10.1016/j.snb.2018.06.021.

44. Mu, S.; Xu, Y.; Zhang, Y.; Guo, X.; Li, J.; Wang, Y.; Liu, X.; Zhang, H. A Non-Peptide NIR Fluorescent Probe for Detection of Chymotrypsin and Its Imaging Application. *J. Mater. Chem. B* **2019**, *7*, 2974–2980, doi:10.1039/C9TB00085B.

45. Fan, H.; Jiang, X.; Zhang, T.; Jin, Q. Peptide-Induced Fluorescence Quenching of

Conjugated Polyelectrolyte for Label-Free, Ultrasensitive and Selective Assay of Protease Activity. *Biosens. Bioelectron.* **2012**, *34*, 221–226, doi:https://doi.org/10.1016/j.bios.2012.02.006.

4.6 Appendix

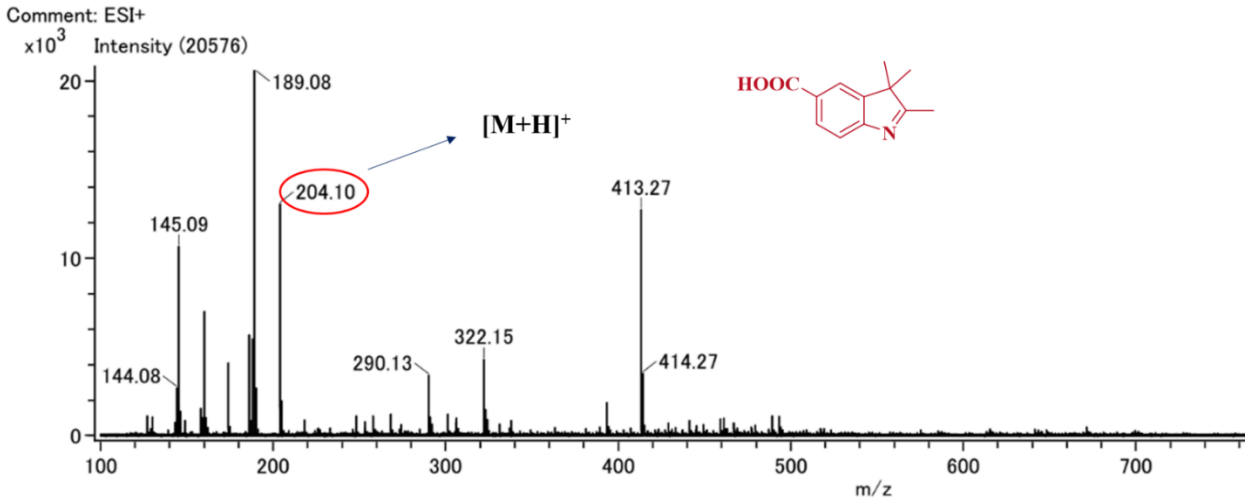

Figure 1. *TOF-mass of 2,3,3-trimethyl-3H-indole-5-carboxylic acid (2).*

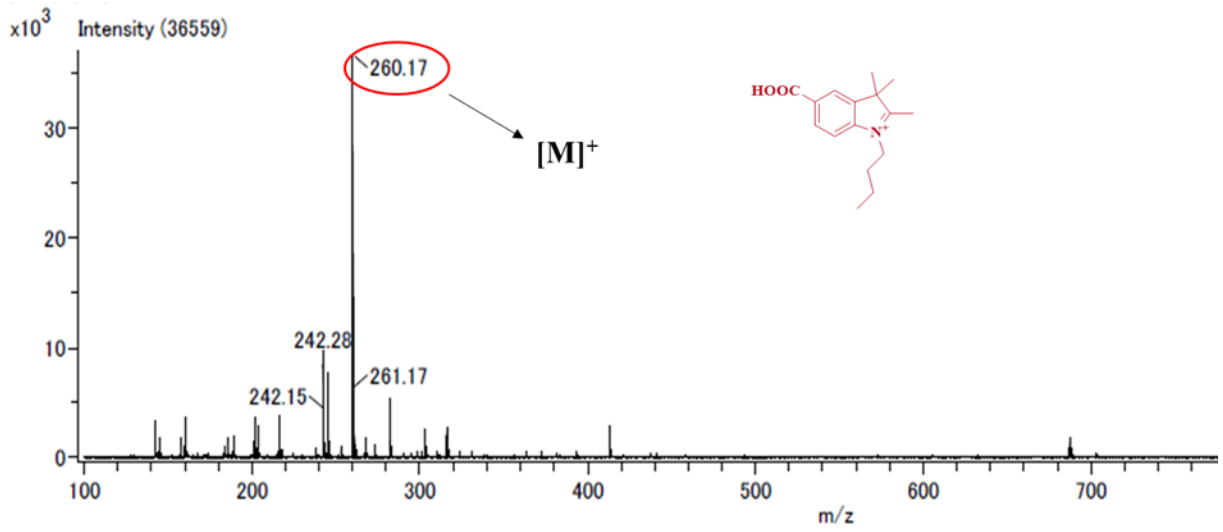

Figure 2. *TOF-mass of 1-butyl-5-carboxy-2,3,3-trimethyl-3H-indolium (3).*

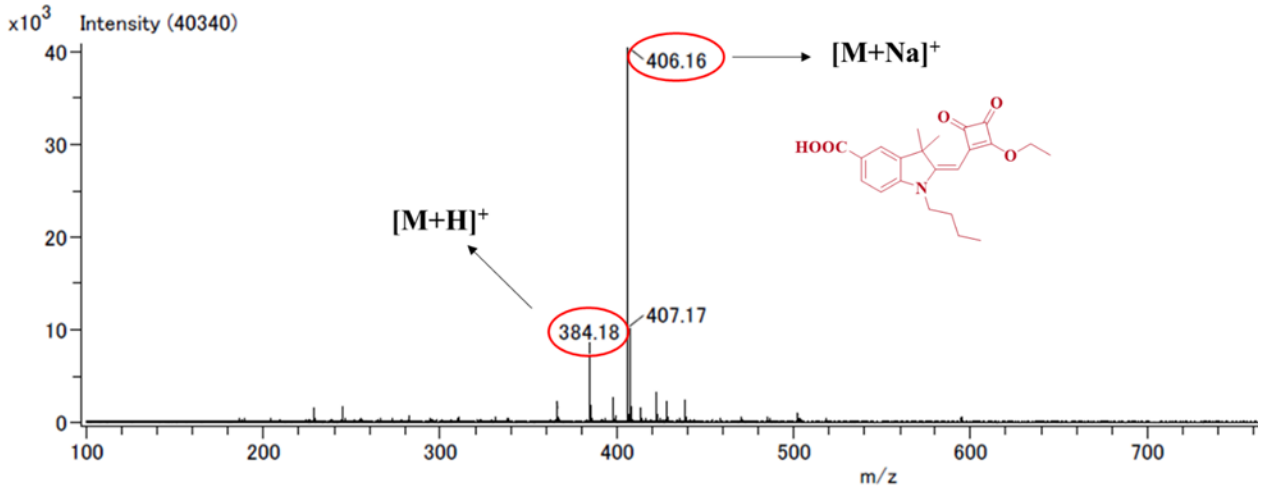

Figure 3. *TOF-mass of (E)-1-butyl-2-((2-ethoxy-3,4-dioxocyclobut-1-en-1-yl)methylene)-3,3-dimethylindoline-5-carboxylic acid (semi squaraine ester) (4)*

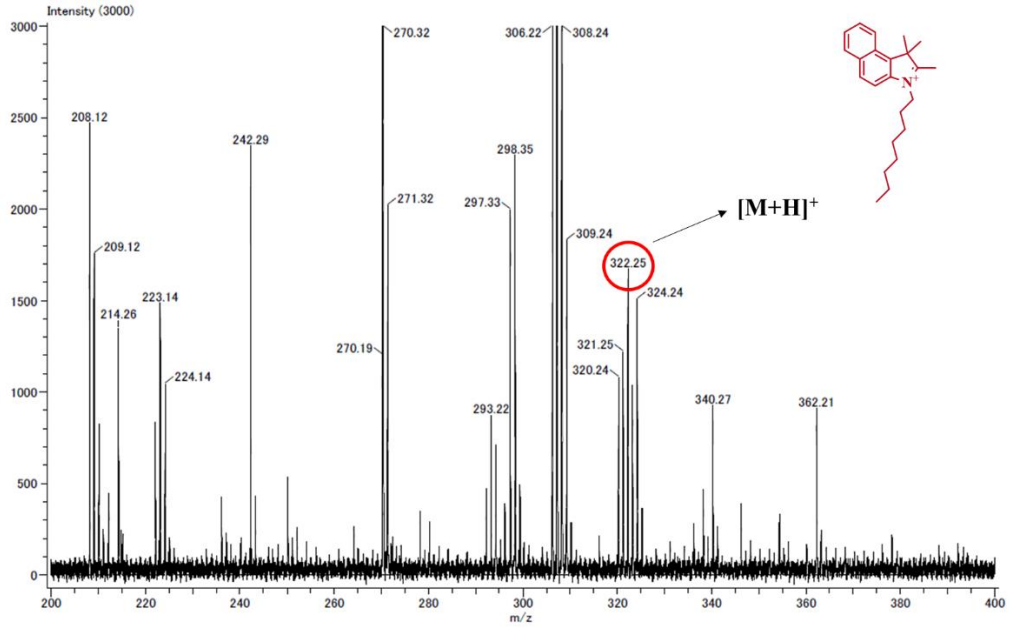

Figure 4. *TOF-mass of 1,1,2-trimethyl-3-octyl-1H-benzo[e]indol-3-ium (7).*

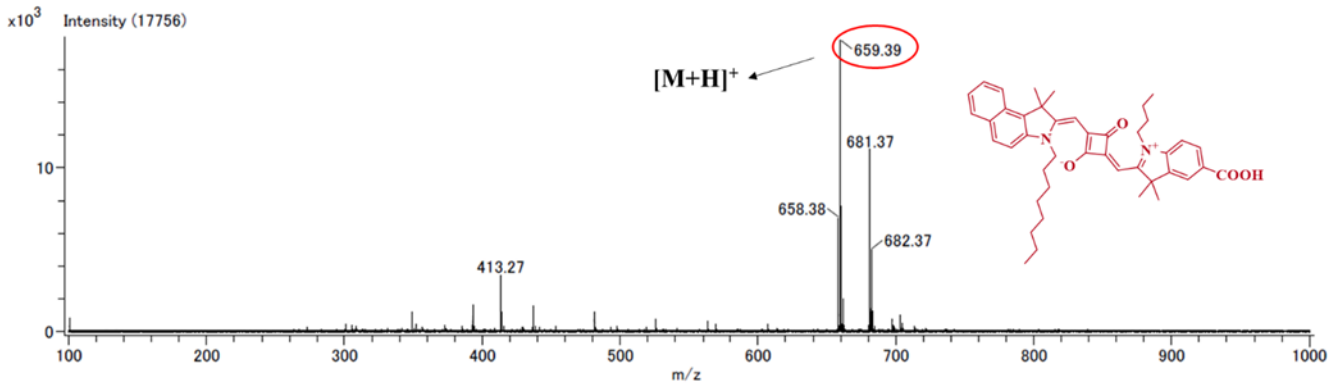

Figure 5. *TOF-mass of* ***SQ-122***.

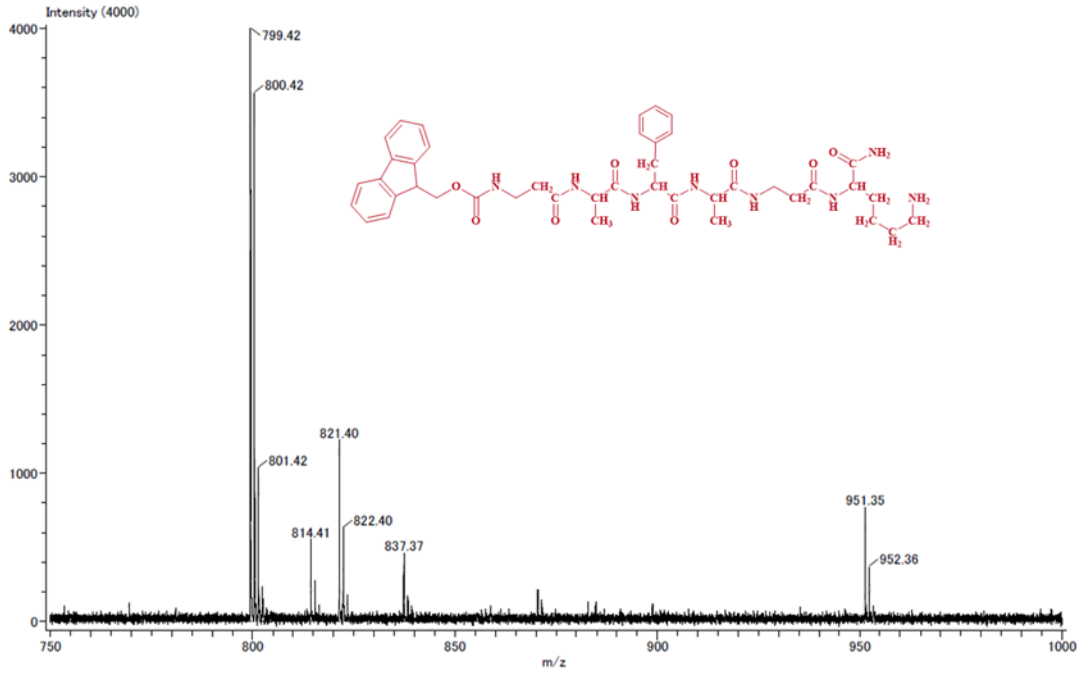

Figure 6. *TOF-Mass of Fmoc-βAla-Ala-Phe-βAla-Lys-NH₂*

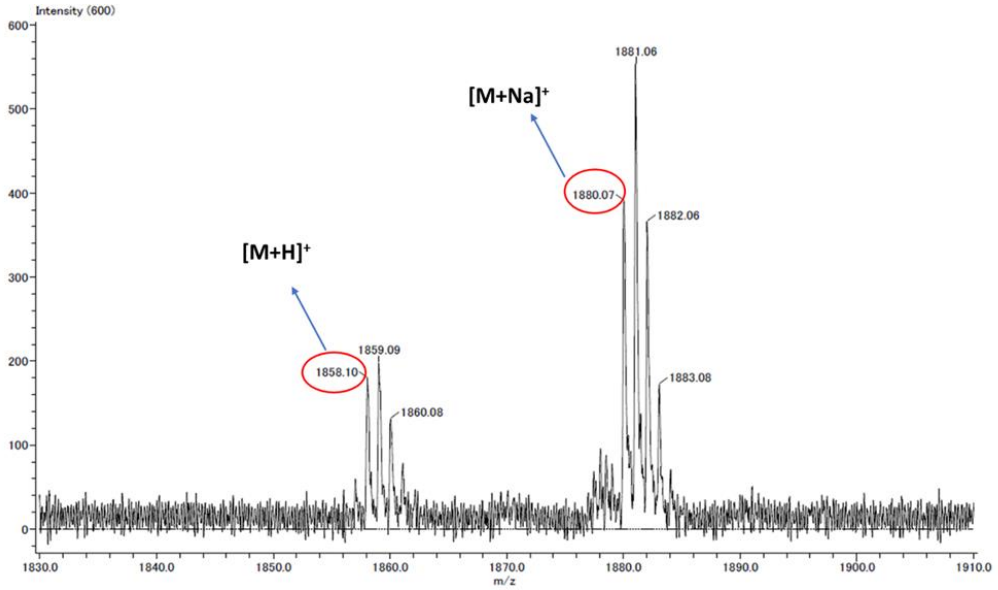

Figure 7. *TOF-Mass of* ***SQ-122 PC***

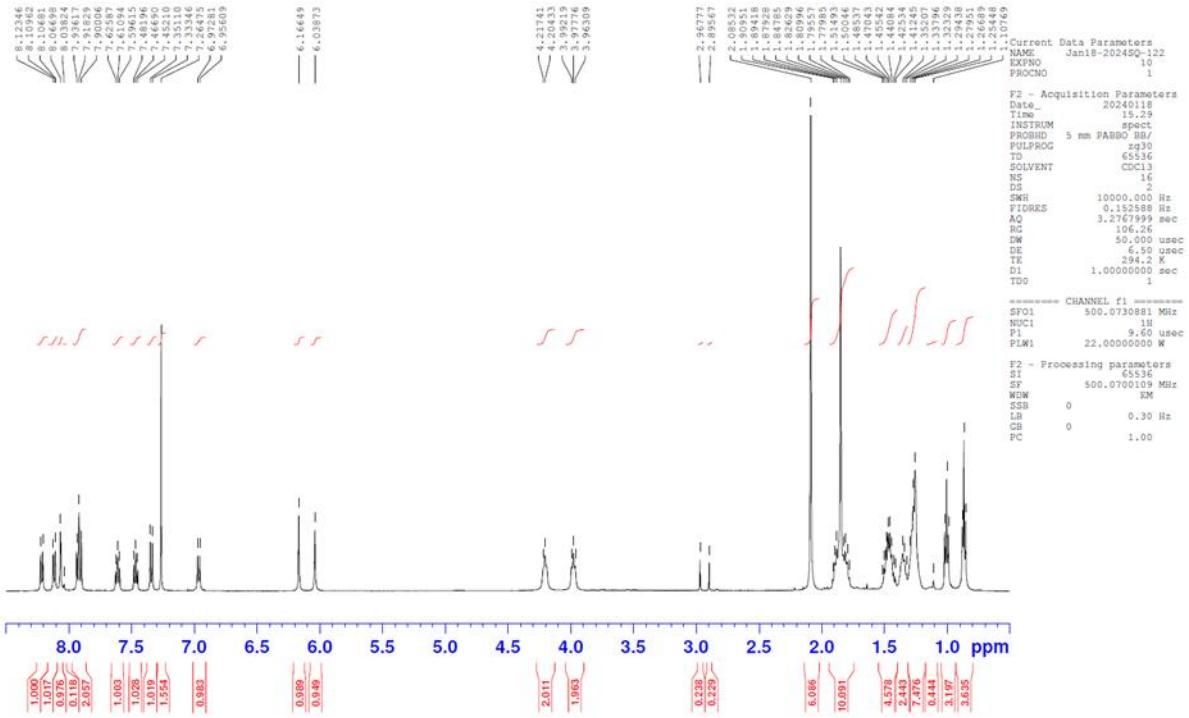

Figure 8. *^{1}H NMR of* ***SQ-122.***

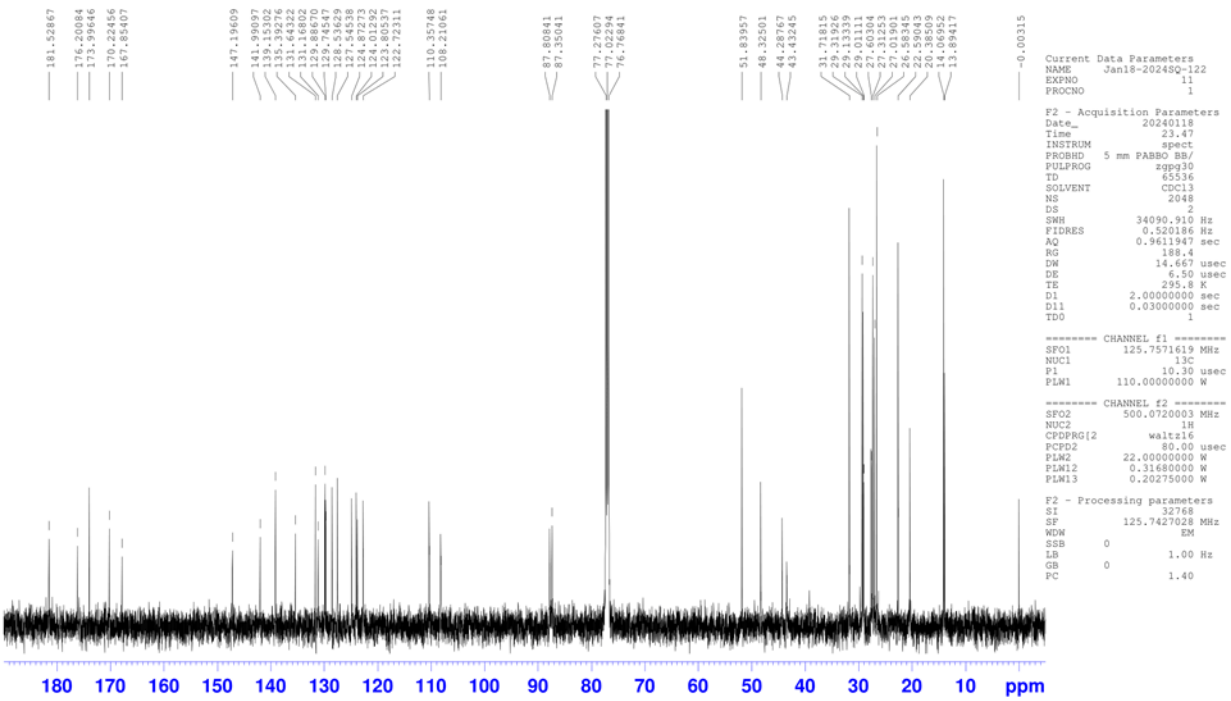

Figure 9. *^{13}C NMR of* ***SQ-122***.

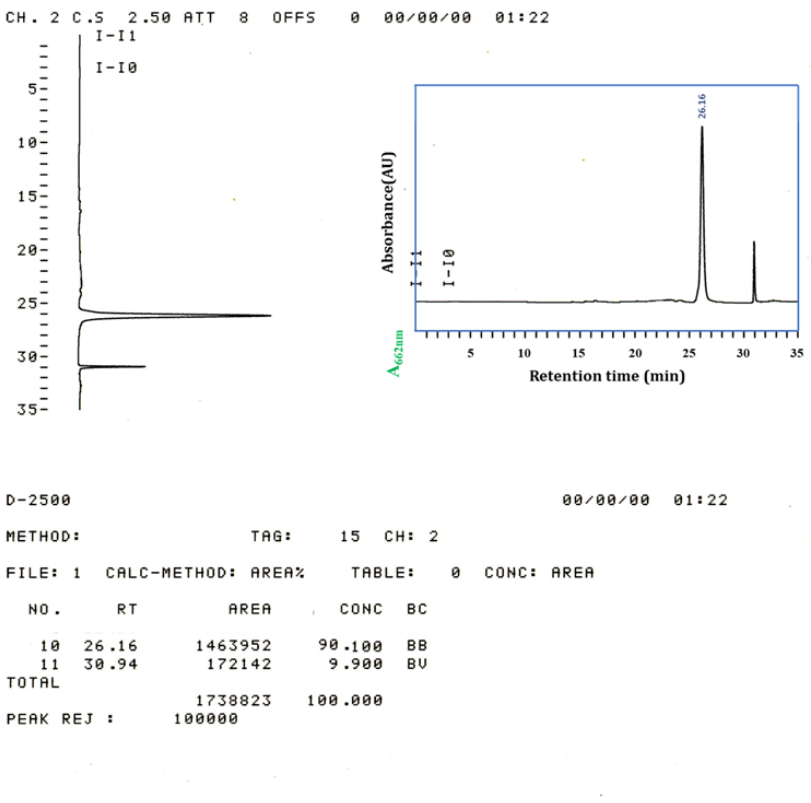

Figure 10. *HPLC of the probe SQ-122 PC.*

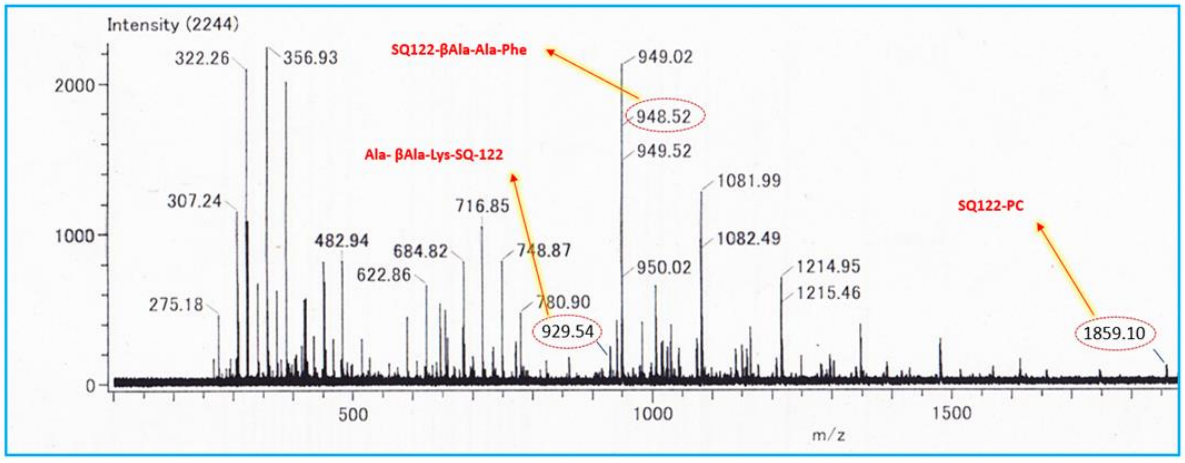

Figure 11. *TOF-MS of SQ-122 PC after enzymatic cleavage of the probe. The concentration of enzyme was 10nM in 10μM of probe in H_2O (30% DMSO) incubated at 37°C for 60 min.*

CHAPTER 5: CONCLUSION & PROSPECTS

5.1 General Conclusion

Fluorescence-based methods are extremely sensitive and adaptable analytical tools that may be modified to detect different targets utilizing a variety of fluorescent materials and mechanisms. These materials can be used either separately or jointly to develop very sensitive detection systems. These systems are based on mechanisms that include the transfer of charge (such as photoinduced electron transfer) or the transmission of energy (such as fluorescence resonance energy transfer). Frequently, the objects being detected are biologically significant substances, such as ions, small molecules, proteins, and DNA. Developing fluorescence-based detection systems that are specifically designed for these targets allows for the precise monitoring of crucial physiological processes, and disease states, and the understanding of the pharmacodynamics and pharmacokinetics of different drugs in therapeutic drug monitoring practices. These areas have been gaining more attention over time. **Chapter 1** contains an extensive review of the current techniques used in POCT devices. After Chapter 1, we outline the current obstacles in this field, which also serve as the goals of this thesis.

In **Chapter 3**, the study of successfully synthesized amine-functionalized symmetrical squaraine (SQ) dye and FITC-SQ-FITC dye conjugate. These compounds were studied for their structures and photophysical properties. Symmetrical SQ dye quenched fluorescence completely. This quenching is caused by photoinduced electron transfer (PET). Linking FITC to both ends of the SQ dye in the FITC-SQ-FITC dye conjugation reduced SQ and FITC aggregation. This also increased far-red fluorescence emission at 674 nm in methanol by 47-fold. Inhibiting aggregation-caused quenching (ACQ) and photoinduced electron transfer (PET) increases far-red fluorescence. Spectral absorption examinations showed that severe dye aggregation in the newly proposed FITC-SQ-FITC dye conjugation completely suppressed far-red fluorescence in phosphate-buffered saline (PBS). As a model protein, bovine serum albumin (BSA) interacted strongly with the conjugate, having an association constant of 1.1×10^4 M^{-1}. This interaction disturbed dye aggregation and increased SQ component far-red fluorescence as BSA concentration rise. When BSA content was increased by 25, fluorescence at 674 nm rose by 117. This shows that the FITC-SQ-FITC triad is a powerful far-red probe for dye-protein interactions.

In **Chapter 4**, a novel FRET-based far-red fluorescent probe based on squaraine dye that exhibits very high sensitivity in the far-red wavelength range for the specific detection of chymotrypsin activity was synthesized. The probe consists of squaraine dye (SQ-122) conjugated with chymotrypsin-specific peptide (Ala-Phe-Ala) and β-Ala as a spacer to facilitate the access of the chymotrypsin enzyme. To link the terminal squaraine dye to the side chain, it was essential to include lysine (Lys) in the structure. The intensity of fluorescence was reduced upon activation of Förster resonance energy transfer (FRET) in the probe. However, when the probe came into interaction with the enzyme, there was a notable rise in fluorescence emission in the far-red area due to FRET-off. The probe demonstrated remarkable sensitivity, achieving an incredibly low detection limit of 0.130 nM. Furthermore, it exhibited exceptional specificity for chymotrypsin, even when other competing enzymes were present. The impact of the research extends beyond its immediate conclusions, providing a versatile basis for developing far-red probes that are specifically tailored to detect certain enzyme activity. Implementing this would enhance the proficiency of biochemical analysis and diagnostic techniques.

5.2 Future Prospects

In the future, I plan to further develop a near-infrared region Förster resonance energy transfer (NIR FRET) system for protein-based chips. This system will be used to identify disorders that are linked to the activity of proteases. Commercialized immunoassay approaches, which involve the specific binding of proteases with antibodies, have been developed and can provide quantitative estimates. They are unsuitable for detecting disorders linked to proteases. Consequently, there has been significant focus on the use of optical-based fluorescence detection with appropriate peptide substrates. There is significant focus and opportunity to address challenges such as detecting multiple analytes, increasing sensing capacity, and reducing signal-to-noise ratio. This can be achieved by using near-infrared (NIR) fluorophores that do not have auto-fluorescence from biological samples. To develop efficient and adaptable point-of-care testing devices, it is important to utilize fluorescent peptide substrates labeled with NIR fluorophores due to their high sensitivity and compatibility with high throughput mapping. To address the limitations mentioned above, there is a growing need for the use of fluorophores that emit in the near-infrared (NIR) wavelength range. These fluorophores offer increased sensitivity due to their lower levels of auto-fluorescence

and ability to penetrate deep into tissues.

Although there have been advancements in the development of high-performance NIR fluorescent dyes, increasing their water solubility is still difficult due to their massive and flat hydrophobic π-conjugate structures. This limited water solubility often leads to aggregation in aqueous environments, resulting in fluorescence quenching that hampers their use for in vivo applications, particularly in enzyme detection and imaging. To address this issue, a squaraine fluorophore and quencher dyes conjugated with an oligo (ethylene glycol) moiety can exhibit good water solubility in aqueous medium. My future goal is to design water-soluble NIR squaraine fluorophore and quencher dye and incorporate it into a peptide selective to a specific target enzyme. This approach used to synthesize the probe may yield valuable insights when developing alternative water-soluble squaraine-based fluorophores that could be employed as effective NIR bio probes in challenging physiological circumstances.

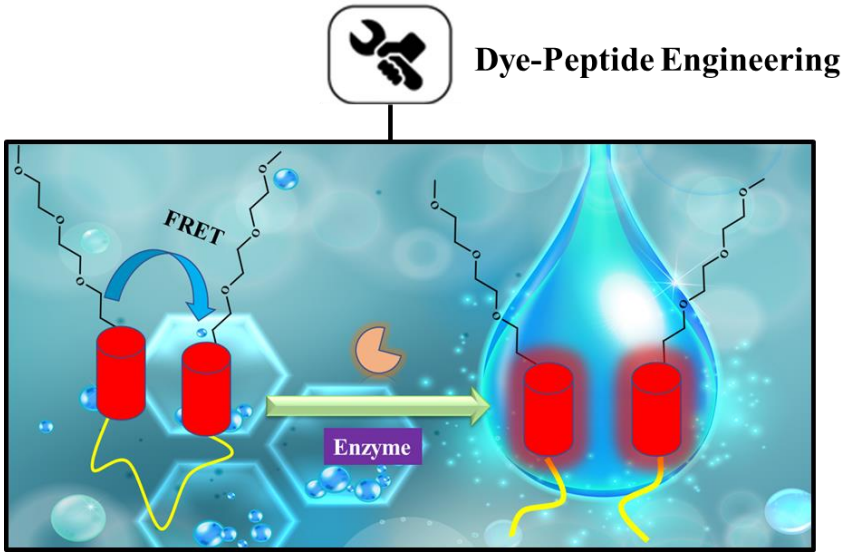

Figure 1. *Design strategy for water-soluble NIR squaraine probes for enhanced enzyme detection.*

ACHIEVEMENTS

(A) Publications

1. **Shekhar Gupta,** Priyanka, Sai Kiran Mavileti, Shyam S. Pandey, and Tamaki Kato ***"Design and Synthesis of Novel Squaraine Based Far-Red Fluorescent Probe for Detection of Chymotrypsin"*** *Molecules.2024; 29 6 1282***.**
2. **Shekhar Gupta**, Yuki Yamawaki, Safalmani Pradhan, Shyam S. Pandey, and Tamaki Kato ***"Design and Synthesis of Novel Squaraine Dye with Highly Enhanced Far-Red Fluorescence and its Interaction with a Model Protein"*** *Phys. Status Solidi A,220: 2300226*
3. Priyanka Balyan, Galyna Bila, Sai Kiran Mavileti, Evgenia Bila, Nazar Negrych, **Shekhar Gupta**, Linjun Tang, Rostyslav Bilyy, Shyam S. Pandey, and Tamaki Kato ***"A Biocompatible NIR-Squaraine Dye and Dye Antibody-Conjugate for Versatile Long-Term In Vivo Fluorescence Bioimaging"*** RSC ***Mater. Adv.***, 2024,**5**, 3940-3949
4. Priyanka, **Shekhar Gupta**, Sai Kiran Mavileti, Shyam S. Pandey, and Tamaki Kato ***"NIR-Sensitive Squaraine Dye-Peptide Conjugate for Trypsin Fluorogenic Detection"*** *Biosensors (Under Review)*
5. Sai Kiran Mavileti, Galyna Bila, Valentyn Utka, Rostyslav Bilyy, Evgenia Bila, **Shekhar Gupta**, Priyanka Balyan, Tamaki Kato, Rostyslav Bilyy and Shyam Pandey ***"Squaraine-Peptide Conjugates as Efficient Reporters of Neutrophil Extracellular Traps Mediated Chronic Inflammation"*** *ACS Applied Materials & Interfaces (Under Review)*

(B) National and International Conferences

1. **Shekhar Gupta**, Priyanka, Sai Kiran Mavileti, Shyam S. Pandey and Tamaki Kato ***"Near-Infrared Fluorescent Detection of Protease Activity Using Peptide-Bound Squaraine Dye";*** The 104th CSJ Annual Meeting 18th -21st March (2024), organized by Chemical Society of Japan, Tokyo, Japan (Oral).

2. **Shekhar Gupta**, Priyanka, Sai Kiran Mavileti, Shyam S. Pandey and Tamaki Kato ***"Near-Infrared Fluorescent Squaraine-Peptide Conjugates for Enhanced Detection of Chymotrypsin Activity"***; International Conference on New Materials for Industry and Medicine (NMIM'24") organized by PG & Research Department of Chemistry, PSGR Krishnammal College for Women, India (Oral).
3. **Shekhar Gupta**, Priyanka, Shyam S. Pandey, and Tamaki Kato ***"Design of a Novel PET Controlled NIR-Sensitive Unsymmetrical Squaraine dye and its interaction with BSA"***; 11th International Symposium on Applied Engineering and Science 20th -21st Nov (2023), Universiti Putra Malaysia, Malaysia.
4. **Shekhar Gupta,** Priyanka, Shyam S. Pandey, and Tamaki Kato ***"Photophysical Investigations of Novel Unsymmetrical Squaraine dyes and their interaction with Bovine Serum Albumin"***; 60th Kyushu Area Joint Meeting of the Chemistry-Related Societies, Kitakyushu International Conference Hall, 1st JULY (2023), Kokura, 3-9-30, Japan.
5. **Shekhar Gupta,** Yuki Yamawaki, Safalmani Pradhan, Shyam S. Pandey, and Tamaki Kato ***"Design and Synthesis of FITC-Flanked Novel Squaraine Dye and its Interaction with Bovine Serum Albumin as a Model Protein"***; 13th International Conference on Nano-Molecular Electronics (ICNME), December 12th -14th (2022), Tokyo Institute of Technology, Tokyo, Japan.
6. Priyanka, Galyan Bila, Sai Kiran Mavileti, Evgenia Bila, Linjun Tang, Nazar Negrych, **Shekhar Gupta**, Rostyslav Bilyl, Shyam S. Pandey and Tamaki Kato ***"Functionalized Symmetrical Squaraine Dye for Long-term in-vivo Fluorescence Bioimaging"***; The 16th IEEE International Conference on Nano/Molecular Medicine & Engineering 5th -8th December 2023, Okinawa, Japan.
7. Sushma Thapa, **Shekhar Gupta**, Safalmani Pradhan, and Shyam S. Pandey ***"Synthesis and Characterization of Novel Sensitive Dye Probe for Metal Ion Sensing"***; 33rd Annual Meeting of The Material Research Society of Japan 14th to 16th Nov (2023).
8. Priyanka, Galyan Bila, Sai Kiran Mavileti, Evgenia Bila, Linjun Tang, Nazar Negrych, **Shekhar Gupta**, Rostyslav Bilyl, Shyam S. Pandey and Tamaki Kato ***"Long-term in vivo Fluorescence Bioimaging using Functionalized Symmetrical Squaraine Dye"***;

11th International Symposium on Applied Engineering and Science 20th -21st Nov (2023), Universiti Putra Malaysia, Malaysia.

9. Priyanka, Galyan Bila, Sai Kiran Mavileti, Evgenia Bila, Linjun Tang, Nazar Negrych, **Shekhar Gupta**, Rostyslav Bilyl, Shyam S. Pandey and Tamaki Kato ***"Novel NIR Squaraine Dye for Long-term in vivo Fluorescence Bioimaging"***; 60th Kyushu Area Joint Meeting of the Chemistry-Related Societies, Kitakyushu International Conference Hall, 1st JULY 2023, Kokura, 3-9-30, Japan.
10. Sai Kiran Maviletti, Tetsuya Narimatsu, **Shekhar Gupta**, Shyam S. Pandey, and Tamaki Kato ***"Fluorescence Detection of Elastase Enzyme by Novel Peptide-Squaraine Dye Conjugate"***;13th International Conference on Nano-Molecular Electronics (ICNME), December 12th -14th (2022), Tokyo Institute of Technology, Tokyo, Japan.

(C) AWARDS

- Recipient of Best Poster Award (*Gold in Biomedical Sciences Category*) in "11th International Symposium on Applied Engineering and Science (2023)", Malaysia ***"Design of a Novel PET-Controlled NIR-Sensitive Unsymmetrical Squaraine dye and its interaction with BSA"***.